NORTHWESTERN UNIVERSITY

Characterization of the Neuronal Networks of the Subiculum and Their Contribution to Epileptiform Activity In Vitro

A DISSERTATION

SUBMITTED TO THE GRADUATE SCHOOL
IN PARTIAL FULFILLMENT OF THE REQUIREMENTS

for the degree

DOCTOR OF PHILOSOPHY

Field of Neuroscience

By
Michael Patrick Fiske

EVANSTON, ILLINOIS

March 2021

Abstract

The exchange of information in the brain is accomplished through sequences of action potentials that result from the integration of local microcircuits. Unraveling the connectivity of the neurons that constitute these microcircuits and how they contribute to network activity is vital for understanding how information is relayed through the brain and how certain diseases arise when these circuits are disrupted. Despite its prominent role as the main output region of the hippocampus, the local microcircuits of the subiculum remain understudied. Much of the work on the subiculum has focused on the excitable properties of the constituent pyramidal neurons, which are typically classified as either burst-spiking or regular firing. However, the regional synaptic connectivity of the region has not been studied in an objective, quantitative way. Additionally, recent evidence from human epileptic tissue has emerged demonstrating that the subiculum can generate certain types of network activity that are closely associated with temporal lobe epilepsy. Closer analysis of subicular pyramidal neurons found changes in expression of the KCC2 transporter in a subset of neurons, a potentially epileptogenic change that might explain the ability of the subiculum to generate epileptiform activity.

In this thesis, I have first evaluated the connectivity between pyramidal neurons using an objective classification method. I have found that the pyramidal neurons in this region are connected in a non-random fashion, and the putative synapses mediating these synaptic connections favor the basal dendrites of the post-synaptic neuron. Additionally, this excitatory network is capable of generating epileptiform-like activity when inhibitory signaling is impaired, a potential property that highlights the ictogenic potential of the region. The second half of this thesis is focused on modeling the changes in KCC2 transporter expression in a manner that restricts the changes to the subiculum. When KCC2 activity is inhibited, synchronous bursting

events begin that are reminiscent of interictal activity observed in patients and animal models of TLE. These events are pharmacologically similar to interictal events and are originated by parvalbumin interneurons. In summary, my thesis work has enhanced our knowledge of how pyramidal neurons in the subiculum are connected at the level of individual neurons and has corroborated the idea that impaired KCC2 function might be a key epileptogenic step towards the progression of TLE.

Acknowledgments

First and foremost, I would like to express my unending gratitude to my advisor, Gianmaria Maccaferri. From the first day of my rotation in his lab, I knew it would be a positive environment where I could pursue research that interested me under the guidance of an advisor who truly wanted me to succeed. I have never had a mentor who so clearly cared not only about my scientific growth, but also my happiness in the lab. I'll never forget his excitement when I showed him my first synaptically connected paired recording, and I am continually impressed that his level of excitement for new data has never waned. I come to lab every day excited and enthusiastic in large part due to Gianmaria's optimism and love of science, traits he has undoubtedly bestowed upon me. Wherever my career takes me, I will proudly say that I am a Maccaferri lab alum.

I am also thankful for both members of the Maccaferri lab: Max Anstötz and Sun Kyong Lee. A lab is only as good as its members, and I could not ask for two better people to be surrounded by every day. Max is one of the most talented, patient, and genuine human beings I have ever met. He is a jack of all trades who has helped me immensely in too many ways to mention. Words can't sufficiently capture what your friendship over these years has meant, and I will greatly miss our lengthy discussions about computers and the never ending supply of candy you provided. I don't think I have ever seen Sun Kyong in a bad mood, and I will miss her wonderful sense of humor and work ethic.

I would also like to thank the members of my thesis committee, Drs. Al George, Gordon Shepherd, and Geoff Swanson. Your feedback during each one of my committee meetings pushed me to continually improve my project and made me a better scientist in the end. Thank you for your dedication to my committee. I also must extend my gratitude for Dr. Savio Chan.

My time in your lab provided a wonderful stepping-stone to the NUIN program and it was where I fell in love with electrophysiology. Thank you for that opportunity, and for letting a brand new technician learn to patch. I am also grateful to the Neurobiology of Information Storage Training program for having me as a trainee during my PhD training. Each retreat was a fantastic learning experience, both in how to effectively communicate my science and think critically about different topics in neuroscience.

A special thank you to Daniel Hegeman, Stephanie Valtierra, Takuma Sonoda and Brittany Hopkins, wonderful friends who I met during my time in NUIN.

Lastly, I would like to thank my family, and especially my Mom. You sacrificed so much for me growing up to make me the man that I am today. You have given me a life full of love and support that I could never thank you enough for. Finally, I would like to thank my wife, Natalie. You mean the world to me, and I never would have been able to finish this without your patience, wisdom, and love. Your encouragement was always unending, and I am so thankful to have had your company during this journey.

"Any man could, if he were so inclined, be the sculptor of his own brain."

-Santiago Ramón y Cajal, Advice for a Young Investigator, 1897

Table of Contents

List of Figures

Contributions

The following important contributions were made by individuals other than Michael Fiske and Gianmaria Maccaferri.

Chapter 2

-*Max Anstötz* performed anatomical reconstructions of filled pyramidal cell pairs and identification of putative synapses using neurolucida and the scholl analyses for the pyramidal cell axon and dendrites. He also performed and designed the data analysis method for calculating apical/basal dendrite and putative synapse overlap density.

-*Leah Welty* designed the statistical model to assess how potential run-down of synaptic connections between pyramidal neurons would influence our expected connectivity between type I and type II cells.

Chapter 3

-*Max Anstötz* contributed to the PV-Cre::ChR2 and PV-Cre::ArchT recordings where we excited or inhibited PV+ interneurons while recording from pyramidal neurons to assess the effect on VU0463271 induced activity. He also performed all of the histological analysis validating the PV-Cre line, for the KCC2 transporter in the PV-Cre::TdTomato line, the reconstructions of filled PV+ interneurons, and the analysis of putative synaptic locations in interneuron-pyramidal cell pairs. He performed the calcium imaging experiments in the Thy1-Cre::GCaMP6 line and contributed to the experiments where we assessed the synaptic connections between PV+ interneurons and pyramidal neurons.

Chapter 1. General Introduction

The functional unit of the brain – neuronal microcircuits

At only 3 pounds in size, the brain is thought to be the most complex biological organ to have ever evolved, and its constituent cells, called neurons, have fascinated scientists for centuries. Every behavior carried out by an animal is the result of the coordinated activity of numerous interconnected neurons, numbering around 100 billion in the human brain (Grillner and Graybiel, 2006). To communicate, neurons relay information to neighboring neurons through transient changes in their electrical voltage (Kandel et al., 2012). This voltage change, termed an action potential, travels down the signal sending domain of the neuron, a structure called the axon. At the end of the axon is a junction between the neuron and its neighbor, a minute gap called a synapse. When the action potential reaches the synapse, chemical signals conveyed by molecules called neurotransmitters induce a subsequent voltage change in the neighboring neuron that travels along the dendrite, or the signal receiving domain. Combining numerous synaptically integrated neurons forms the functional unit of the brain, a microcircuit. Each circuit is unique, and its properties are the result of a variety of characteristics, such as the different cell types incorporated in the network, the ion channels expressed at the synapses, and the pattern of connectivity between neurons (Kandel et al., 2012). The diversity of these microcircuits reflects the countless functions they are involved in, from the lifting of a finger to solving complex arithmetic problems. Aberrations in neuronal circuitry are increasingly becoming recognized as important contributors to different diseases as well. Studying how these different components combine to generate complex functions is essential for enhancing our overall knowledge of the proper functioning of the brain and how these circuits can be disrupted in disease states. My thesis work is dedicated to understanding the

microcircuitry of a region of the brain called the subiculum and the contribution of this neuronal network to temporal lobe epilepsy (TLE), a disease that is thought to result from dysfunctional neuronal networks (Noebels et al., 2012). The goal of this introduction is to highlight important features of the subiculum, provide background on TLE, and explain how the subiculum is thought to be involved in the disease.

The role of the subiculum in hippocampal function

The limbic system is a set of interconnected brain structures that is responsible for some of the most amazing and complex functions of the brain, including our emotional response, memory formation, and ability to learn. The hippocampal formation is a key component of the limbic and is anatomically composed of the dentate gyrus, the hippocampus proper, and the subiculum, with most anatomists including the presubiculum, parasubiculum, and entorhinal cortex as well (Amaral and Lavenex, 2007). Coordinated firing between synaptically connected neurons within these regions is thought to be the basis for episodic memory and spatial navigation (Squire et al., 2004; O'Keefe and Nadel, 1978; Buzsáki and Moser, 2013). Elucidating the properties of the neurons within each of these regions and the microcircuits they establish has occupied scientists for decades.

The best-known circuit within the hippocampal formation is the tri-synaptic circuit, a feed-forward excitatory loop consisting of synaptic connections between three regions: the entorhinal cortex, the dentate gyrus, and the hippocampus proper (Andersen et al., 2000; Amaral and Lavenex, 2007). Put simply, information coming from layer II of the entorhinal cortex is first received by the granule cells of the dentate gyrus via the perforant path (Andersen et al., 1971). This synapse has been studied in great detail, including the seminal discovery of long-term

potentiation by Bliss and Lomo in 1973 (Bliss and Lomo, 1973). Signaling continues with the dentate gyrus projecting excitatory inputs onto the pyramidal cells in the cornu amonus 3 (CA3) region. These axons, known as the mossy fibers owing to the moss-like appearance conferred by their large boutons, make powerful excitatory synapses, and under certain circumstances, a single granule cell is sufficient to elicit action potentials in a post-synaptic CA3 pyramidal neuron (Amaral et al., 2007; Jonas et al., 1993; Urban et al., 2001). Next, CA3 pyramidal neurons project to the proximal apical and basal dendrites of CA1 pyramidal neurons by way of the Schaffer collaterals (Szirmai et al., 2012). Finally, CA1 pyramidal neurons project onwards to the entorhinal cortex, completing the loop (Amaral and Lavenex, 2007). However, a majority of CA1 inputs pass through an intermediate structure, the subiculum.

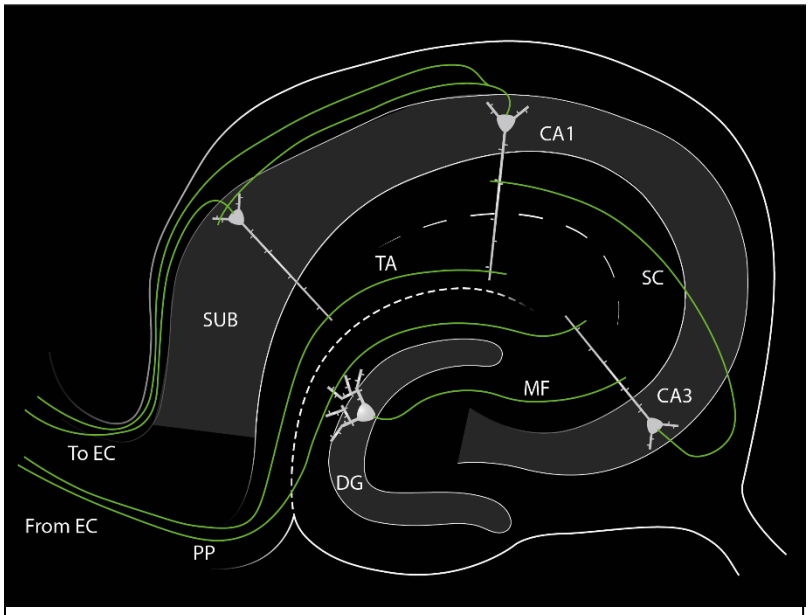

Figure 1.1: Anatomy of the tri-synaptic circuit
A diagram depicting the major components of the tri-synaptic circuit. Information arrives in the hippocampus from the entorhinal cortex (EC) via the perforant path (PP), which targets dentate gyrus (DG) granule cells. Another major input is through the temporoammonic pathway, which directly targets CA1 neurons. Granule cell axons, known as mossy fibers (MF), innervate CA3 apical dendrites. CA3 axons, known as Schaffer collaterals (SC), project towards CA1 pyramidal neurons. Information then leaves the hippocampus either through 1) direct projections from CA1 to the EC or 2) through the subiculum (SUB) acting as an intermediate stop.

The subiculum, a name that comes from the Latin word for support, is a critical contributor to the hippocampal network circuitry. While CA1 does project to extra-hippocampal areas, a majority of CA1 efferents terminate on pyramidal cells of the subiculum. This, in combination with the subiculum's extensive cortical and sub-cortical

projections, position the subiculum as the main hippocampal output (Amaral and Witter, 1989, Amaral, 1993, Naber et al., 2001). Tracer experiments revealed that axons from CA1 target the subiculum in a nested-loop pattern, where proximal (bordering CA3) CA1 pyramidal cells project to distal subiculum and distal CA1 neurons synapse on proximal subicular neurons (Tamamaki and Nojyo., 1995; Gigg, 2006). In addition to CA1, neurons from the entorhinal cortex also innervate subicular pyramidal neurons via layer III. In contrast to the well-organized layers of other hippocampal regions, the subiculum lacks a distinct organizational pattern, making it less accessible to anatomical study. Indeed, compared to other regions of the hippocampal formation, the neuronal circuits of the subiculum remain surprisingly unexplored despite its privileged position as a crucial regulator of information flow out of the hippocampus. Elucidating the properties of subicular microcircuits could provide a more complete picture of normal hippocampal function.

Structure and function of the subiculum

Anatomically, the subiculum and the hippocampus proper are distinct. Pyramidal neurons within the CA regions are located within a compact layer termed the stratum pyramidale (Amaral and Lavenex, 2007). Consequently, the basal and apical dendrites of pyramidal neurons here are localized to specific compartments. Deep from the pyramidal layer is the stratum oriens, which contains the basal dendrites of pyramidal neurons (Amaral and Lavenex, 2007). Directly superficial from the pyramidal cell layer is the stratum radiatum, which hosts the initial segments of pyramidal neuron apical dendrites. Moving towards the hippocampal fissure, the final layer is the stratum lacunosum-moleculare, where the apical dendrites of pyramidal neurons terminate. The subiculum is most notably characterized by the transition from a dense layer of pyramidal

neurons to a more loosely packed arrangement of cell bodies. It also consists of a polymorphic layer, located closer to the alveus, which is continuous with the stratum oriens of CA1, and a molecular layer, which is an extension of the radiatum and molecular layer of CA1 (Amaral and Lavenex, 2007). Recent immunohistochemical studies have also divided the pyramidal cells in the subiculum on a proximo-distal axis according to the expression of several molecular markers (Ishihara and Fukuda, 2016). An expansive examination of the genetic, anatomical, and electrophysiological properties of pyramidal neurons in the dorsal subiculum by Cerembrowski et al further supports this division (Cembrowski et al., 2018a; Cembrowski et al., 2018b).

The position of the subiculum as the main hippocampal output is reflected by its dizzying array of cortical and subcortical connections, which can be described along two main axes: proximal-distal and dorsal-ventral (Aggleton and Christiansen, 2015; Naber and Witter, 1998; Kim and Spruston, 2012). The proximal subiculum is biased in reciprocal connections to the

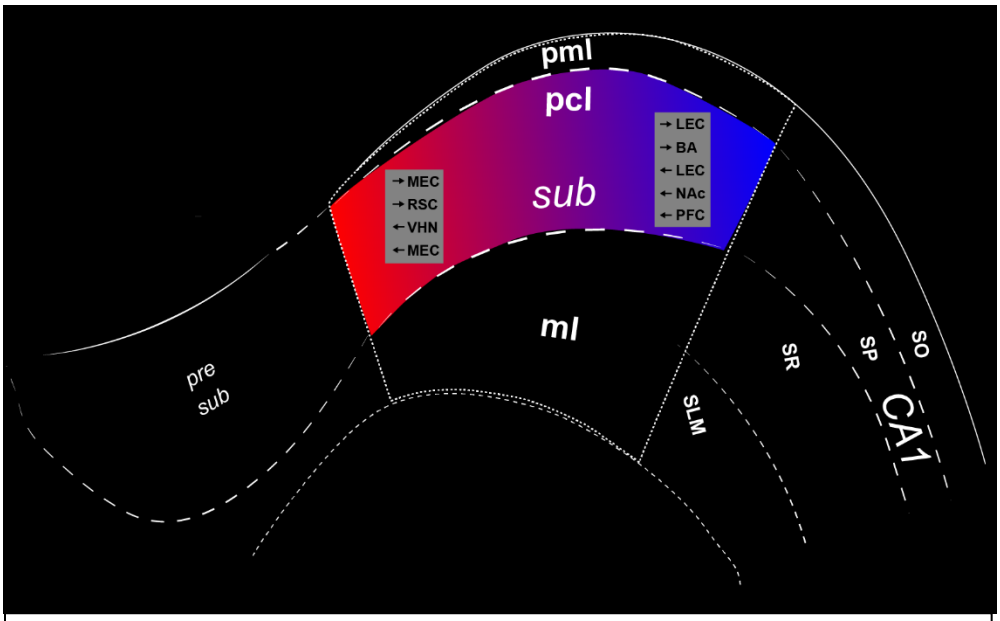

Figure 1.2: Anatomy and projection targets of distal and proximal subiculum
A diagram depicting the proximal (shaded blue) and distal (shaded red) subiculum and their long range projection targets and inputs. Outputs are indicated by a forward arrow, and inputs are indicated by a backward arrow. MEC: medical entorhinal cortex, RSC: retrosplenial cortex, VHN: ventromedial hypothalamic nucleus, LEC: lateral entorhinal cortex, BA: basolateral amygdala, NAc: nucleus accumbens, PFC: prefrontal cortex.

amygdala, lateral entorhinal cortex, olfactory cortex, and nucleus accumbens. Pyramidal neurons in the distal subiculum tend to favor projections to medial entorhinal cortex, presubiculum, retrosplenial cortex, and ventromedial hypothalamus (Witter, 2006; Ding, 2013; Namura et al., 1994). Thalamic connections are most prevalent in the middle of the proximodistal axis (Witter, 2006). Although more attention has been given to projection patterns along the proximodistal axis, differences along the dorsoventral axis are evident as well. Anterograde tracers injected into the ventral subiculum heavily label the hypothalamus and amygdala (Canteras et al., 1992; Groenewegen et al., 1987). Additionally, some nNOS positive pyramidal neurons in the subiculum send back projections to CA1, and evidence exists of subiculum axon collaterals targeting of newborn granule cells (Greene and Totterdell 1997; Greene et al. 1997; Seress et al., 2002; Deshpande et al., 2013). In contrast to CA1 where a single axon collateral can target several regions, projections from the subiculum are typically focused to a single area (Kim and Spruston. 2012).

The wide range of the subiculum's downstream targets hint at the different physiological functions in which this structure is involved. Although it can be crudely described as a simple relay point, a closer look reveals a more complex role in numerous physiological processes. The first insight into the subiculum's function came from ibotinic acid lesion studies. Damage to either the hippocampus proper or the subiculum resulted in impaired acquisition of spatial memory, with a combined lesion leading to an even more severe deficit, suggesting the subiculum contributes to spatial learning in a hippocampus independent manner (Schenk and Morris, 1985; Morris et al., 1990). A recent study using DREADDs to specifically silence proximal or distal subicular pyramidal cells provided more insight onto the exact areas involved in spatial memory. Silencing distal subiculum inhibited the encoding of spatial memories but did not prevent the animal from

retrieving previously formed memories (Cerembrowski et al., 2018). Accumulating evidence points to a segregation of functions between the dorsal and ventral subiculum as well. Broadly, the dorsal segment of the subiculum is primarily concerned with spatial navigation and memory. Massive projections from the dorsal subiculum innervate the lateral mammillary nuclei and the anterior thalamic complex, two locations which contain navigation-related neurons (Cenquizca and Swanson, 2007, Dong et al., 2009). Place cells within the dorsal subiculum tend to be have larger fields than their CA1 counterparts, and these fields tend to scale to fit the size of the environment (Barnes et al., 1990; Sharp, 1997; Sharp, 1999; Kim et al., 2012). As a major efferent target of CA1 and numerous cortical areas, it is quite possible that the subiculum's job is to encode complex spatial relationships (O'Mara et al., 2009). Tetrode recordings from freely moving rats in a multi-arm maze showed some cells in the dorsal subiculum seem to encode the direction of travel within an environment (Olson et al., 2017). Ventral subiculum, on the other hand, appears to play key roles in regulating the hypothalamic-pituitary-adrenal axis (Lowry, 2002). The ventral subiculum inhibits hormone release from the hypothalamus, as ibotenic acid lesions of the ventral subiculum prolonged the glucocorticoid stress response in rats (Herman et al., 1998). Muscimol injections to the ventral subiculum prior to training diminished contextual fear conditioning in rats, pointing to another role in the emotional response to fear (Biedenkapp and Rudy, 2009).

Subicular pyramidal cell subtypes

Similar to the neighboring CA subfields, the primary principal cell of the subiculum is the pyramidal neuron (reviewed in Spruston, 2008). Named after the shape of their triangular soma, each pyramidal neuron is characterized by two spine-laden dendritic domains. The first is a collection of relatively short basal dendrites, emanating from the base of the neuron. The second

domain features a large apical dendrite extending from the apex of the neuron with secondary dendrites branching off the main trunk at various angles. Typically, the single apical dendrite terminates in a tuft of dendrites, although the apical dendrite can bifurcate early on, resulting in twin apical dendrites with tufts of their own. The axon of pyramidal neurons, which can reach several centimeters in length, most commonly extends from the base of the soma, branching extensively. It forms excitatory glutamatergic synapses both locally and in far-away brain regions (Harris et al., 2001).

The seemingly homogenous morphological features of pyramidal neurons in the subiculum might give the impression that they share physiological similarities. However, a closer look at the firing properties of the cells in this region quickly dispels this notion. Patch clamp experiments on subiculum pyramidal neurons repeatedly reveal two distinct responses to current injection (Behr et al., 1996; Harris et al., 2001; Harris and Stewart, 2001a; Knopp et al., 2005; Mattia et al., 1997; Menendez de la Prida, 2006; Menendez de la Prida et al., 2003; Staff et al., 2000; Stewart and Wong, 1993; Taube, 1993; Wellmer et al., 2002; Graves et al., 2012; Böhm et al. 2017). One group responds to a sustained suprathreshold current injection, most commonly

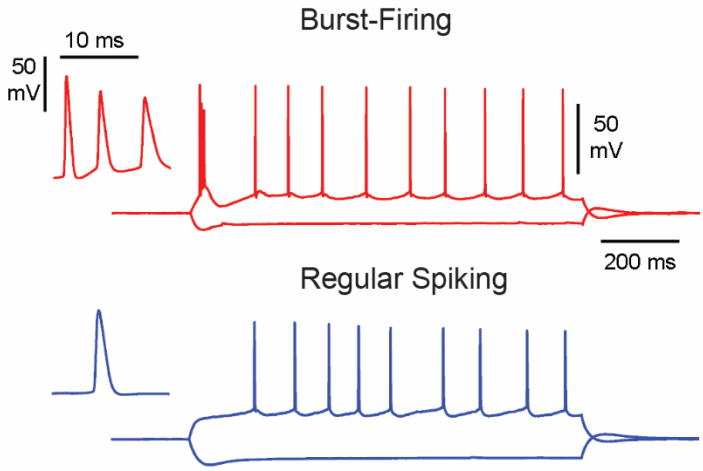

Figure 1.3: Examples of subicular pyramidal neuron firing patterns
Firing pattern of a burst-firing (top, red) and regular spiking (bottom, blue) pyramidal neuron in response to 1 s long, suprathreshold current injection. Note the initial burst of action potentials fired by the bursting neuron while the regular spiking neuron is characterized by single spikes. There is a notable voltage sag in both neurons during a -150 pA hyperpolarizing current injection. Inset is an enlarged view of the first spike event in both cells.

1s, with a string of regularly spaced action potentials and are thus commonly called “regular spiking” neurons (Staff et al., 2000; Harris et al., 2001; Metz et al., 2005; Jarsky et al., 2008). The other group fires a burst of two or more action potentials upon current injection onset, followed by either more bursts or a series of single action potentials (Jarsky et al., 2008; Staff et al., 2000; Stewart 1997). Work by Nelson Spruston’s group using different calcium channel blockers demonstrated that bursting in subicular pyramidal neurons results from a high voltage activated calcium tail current (Jung et al., 2001). Further divisions within the regular spiking and bursting classifications are also hypothesized to exist. For example, pyramidal neurons from rats that fired two separate bursts or more during current injection were classified as “strong bursters” compared to “weak bursters” (Staff et al. 2000; Menendez de la Prida et al. 2003). Additionally, the presence of spike adaptation has been used to subdivide regular spiking cells (“tonic” vs “adapting”) (Menendez de la Prida et al., 2003). Sampling of the genetic profiles of pyramidal neurons in this region using single cell RNA-seq supports potential divisions, revealing 8 potential subclasses of pyramidal cells (Cerembrowski et al., 2018). Regular spiking and bursting neurons are also roughly distributed along a proximal to distal axis, with regular spiking neurons predominating near the CA1 border and bursting cells becoming more common moving towards the entorhinal cortex (Kim and Spruston., 2012).

However, the electrophysiological criteria used to classify neurons in the subiculum has not been consistent across studies. The number of spikes required to be grouped in the bursting class has varied. One early study using sharp electrode recordings from the subiculum in rats defined a burst as 2-4 spikes (Mason et al., 1993). A second analysis of firing properties of rat subiculum also using sharp electrodes set the burst definition as 3-5 spikes (Taube et al., 1993). Another study using sharp electrodes defined a burst as 2-3 spikes but performed current injection

while holding cells at -70 to -80 mV, more hyperpolarized than other previous studies (Greene et al., 1997). Whole cell-patch clamp recordings of the rat and mouse subiculum have also used variable spike amounts, varying from 2+ to 3+ spikes constituting a burst (Kim and Spruston, 2012; Menendez de la Prida et al., 2003). Other studies evaluate the spike frequency of the first two action potentials elicited by a current injection to determine bursting vs regular spiking classification, but even these values are not uniform. One study set 200 hz as the minimum frequency for classification as a bursting neuron while others use >125 or >100 hz (Staff et al., 2000; Graves et al., 2012). Further complicating comparison is the current injection protocol used to assess firing type. The total amount of current injected has not been uniform across studies. Some studies use a single current injection amount while others calculate the threshold current injection level and add a set percentage to that value (Graves et al., 2012). Additionally, the length of current injection has ranged from 0.5s, 1s, or 2s long. The heterogenous criteria used to classify neurons as burst firing or regular spiking has made comparison across studies difficult. A quantitative, objective approach is needed for classification of subicular pyramidal neurons, as it would assist in comparison of data across studies.

Temporal lobe epilepsy – a disorder of neuronal circuits

Epilepsy is defined as a neurological disorder in which a patient experiences recurrent seizures resulting from excessive and synchronous discharge of neurons. Its prevalence is striking, with estimates of up to 1% of the worldwide population afflicted by epilepsy (Hauser and Hesdorffer, 1990). Seizures, the primary manifestation of epilepsy, are acute neurological events resulting from hypersynchronous activity of neurons and are often characterized by alterations in sensation, consciousness, or cognition (Martin et al., 2006; Engel 2006). Physical tremors or convulsion can

also be present. Epilepsies can be classified broadly into focal epilepsy, where seizures originate from specific brain regions, and idiopathic generalized epilepsies, where no clear underlying origin can be determined (Engel, 2001).

With over 40 million cases worldwide, TLE is one of the most common neurological disorders and the most common type of focal epilepsy. This complex condition is characterized by recurrent seizures originating in the temporal lobe, most often in the hippocampus (Noebels et al., 2012). The disease is typically described as progressing in stages. The first stage involves an unidentified acute injury or insult that initiates the often silent physiological and molecular changes that will lead to TLE. While the exact trigger for developing TLE is unknown, some suspected precipitating events include stroke, febrile seizures, traumatic brain injury, and previous incidence of status epilepticus. The second phase is the latent phase, a period of variable length where alterations are occurring at the cellular level, but seizures are not present. Many documented histopathological features have been found to occur during this period, including apoptosis in hippocampal subregions, ectopic granule cell production and mossy fiber sprouting, and astrocytosis (Greenfield et al., 2008; Blümcke et al., 2009). A better understanding of the numerous different changes occurring during this stage is essential for disentangling causative changes from unrelated epiphenomena. The third stage is the chronic state in which recurrent seizures emerge. The gradual process by which the brain becomes epileptic is termed epileptogenesis. The process of epileptogenesis is poorly understood, and therapies to halt these pathological changes are hindered by a lack of understanding of the disease process. No cure currently exists, and clinical treatments typically center on pharmacological suppression of seizures with anti-epileptic drugs (Avoli et al., 2005). Unfortunately, a large percentage of TLE patients exhibit pharmacoresistance, and their seizures become intractable and recurrent. It is at this point that surgical resection of the

brain region where the seizures originate often becomes necessary, despite the high risk of memory impairment.

A link between the subiculum and temporal lobe epilepsy

Although a somewhat crude approach to treating epilepsy, surgical resection has provided an unprecedented opportunity to study human epileptic tissue. One important finding from resected tissue is dramatic levels of sclerosis of the CA1 and CA3 regions in patients with severe TLE (Wieser, 2004). However, since seizures still originate in the hippocampus of patients with hippocampal sclerosis, the question remained as to what structure initiates seizures. The potential of many different regions to initiate seizures has been investigated. However, an intriguing line of evidence emerged in 2001 that implicated the subiculum in generating spontaneous activity linked to TLE. Richard Miles's group obtained live temporal lobe tissue from 11 patients undergoing surgery for intractable epilepsy that included the hippocampus (Cohen et al., 2002). When his group recorded extracellularly from 10 locations in the hippocampal formation, they observed the subiculum alone generating network discharges while all other neighboring regions (EC, CA1, CA3, DG) remained silent. Additionally, these discharges matched the frequency of inter-ictal events recorded from scalp EEGs. These findings were further confirmed by complementary work done by Joachim Behr's group (Wozny et al., 2005), although there was some disagreement over the degree of hippocampal sclerosis necessary before rhythmic activity was detectable in the subiculum (Wozny et al., 2003). Interestingly, while a majority of pyramidal neurons in the subiculum were hyperpolarized during these inter-ictal like events, a subset of pyramidal neurons depolarized instead (Cohen et al., 2002). Mile's group also reported that interneurons fired before these inter-ictal events, suggesting this activity results from a mixture of glutamatergic and

depolarizing GABAergic signaling. Pharmacologically antagonizing either GABA or glutamate receptors extinguishes inter-ictal like activity in these slices.

In addition to inter-ictal like events, ictal like events can be triggered in the subiculum in tissue from epileptic patients. Although the use of these convulsants is not physiological, it allows for the study of mechanisms of ictogenesis in human tissue. During the transition from inter-ictal to ictal states in these conditions, a type of population discharge called a pre-ictal discharge appears. It co-exists with inter-ictal events and appears to be the result of glutamatergic signaling (Huberfeld et al., 2011). Pre-ictal discharges occur immediately preceding an ictal-like event, and likely result from NMDA receptor dependent plasticity. Pre-ictal discharges are also observed in animal models of TLE using pilocarpine treated rats (Fujita et al., 2014), and the subiculum is one area showing the earliest seizure activity in these models (Toyoda et al., 2013). The accumulating evidence of the subiculum's involvement in generating inter-ictal, pre-ictal, and ictal events has provided impetus to study how the local microcircuits of this understudied region contribute to these network events.

The KCC2 down-regulation hypothesis

As described in the last section, significant data exists suggesting that the subiculum can generate network events that are intimately linked to epilepsy, but the mechanism underlying this activity has not yet been explained. One intriguing line of evidence points to disruptions in chloride homeostasis in pyramidal cells located in the epileptic focus. Neuronal chloride levels are controlled by a class of transporter proteins termed cation-chloride cotransporters (Chamma et al., 2012; Payne et al., 2003). The KCC2 transporter is the predominant chloride extruding transporter in neurons, and it couples chloride export to the K+ gradient, resulting in a lowering of the

intracellular chloride concentration (Karadsheh et al., 2001). The counterpart of KCC2 is the NKCC1 transporter, which takes advantage of the inwardly directed Na+ gradient to import chloride into the cell. The antagonistic activity of these chloride transporters sets the intracellular chloride level of a neuron. The concentration of chloride inside and outside of the cell determines the equilibrium potential of the chloride ion (E_{Cl}), or the membrane potential at which the net flow of ions across the membrane is balanced. This value can be calculated using the Nernst equation. When the membrane potential is not at this value, chloride will flow through open $GABA_A$ channels until this potential is reached. Thus, because $GABA_A$ receptors are primarily permeable to chloride (and to a lesser extent, bicarbonate ions, P_{HCO3}/P_{CL} 0.18-0.6) (Bormann et al., 1987), the amplitude and direction of the voltage change resulting from $GABA_A$ receptor activation is strongly influenced by the intracellular chloride level (Wright et al., 2011).

One of the best examples of the physiological impact of chloride transporter expression levels on the equilibrium potential of GABA receptor activation occurs during development. During embryonic and early post-natal life, NKCC1 is the predominant chloride transporter expressed in neurons of the developing brain, resulting in relatively high intracellular chloride levels (~20-40 mM) and a more depolarized E_{Cl} value (Suli Sato et al., 2017; Ben-Ari, 2002). Over time, KCC2 expression begins to increase, decreasing chloride levels inside neurons and driving the E_{Cl} value to more hyperpolarized potentials. Thus,

$$E_{ion} = \frac{RT}{zF} \ln \frac{[ion]_{out}}{[ion]_{in}}$$

Figure 1.4: The Nernst equation
The equilibrium potential for an ion (E_{ion}) can be calculated using the Nernst equation if the concentration of the ion outside ($[ion]_{out}$) and inside ($[ion]_{in}$) is known. In this equation, R is the universal gas constant (8.31 J K^{-1} mol^{-1}). T is the temperature in °K. z is the valence of the ion (-1 for chloride). F is the Faraday constant (96485 C mol^{-1}).

in a majority of adult neurons, GABAergic signaling is inhibitory, driving neurons further way from the threshold potential for firing an action potential (Hübner et al., 2013).

Changes in KCC2 expression in pyramidal cells located within the epileptic focus are one potential mechanism that might explain the emergence of pathological network activity in TLE. Early experiments using human tissue from epileptic patients revealed two populations of pyramidal neurons in the subiculum of epileptic patients (Cohen et al., 2002). The first population (~80%) exhibited hyperpolarizing responses during spontaneous field events. The second population (~20%) fired action potentials during the spontaneous events, and local electrical stimulation induced depolarizing or excitatory responses in the presence of AMPA and NMDA receptor antagonists. Indeed, recordings from interneurons showed that they discharged before pyramidal neurons during these inter-ictal like bursts, suggesting that excitatory GABAergic signaling might be what drives these events. Recent work from Mossimo Avoli's lab using

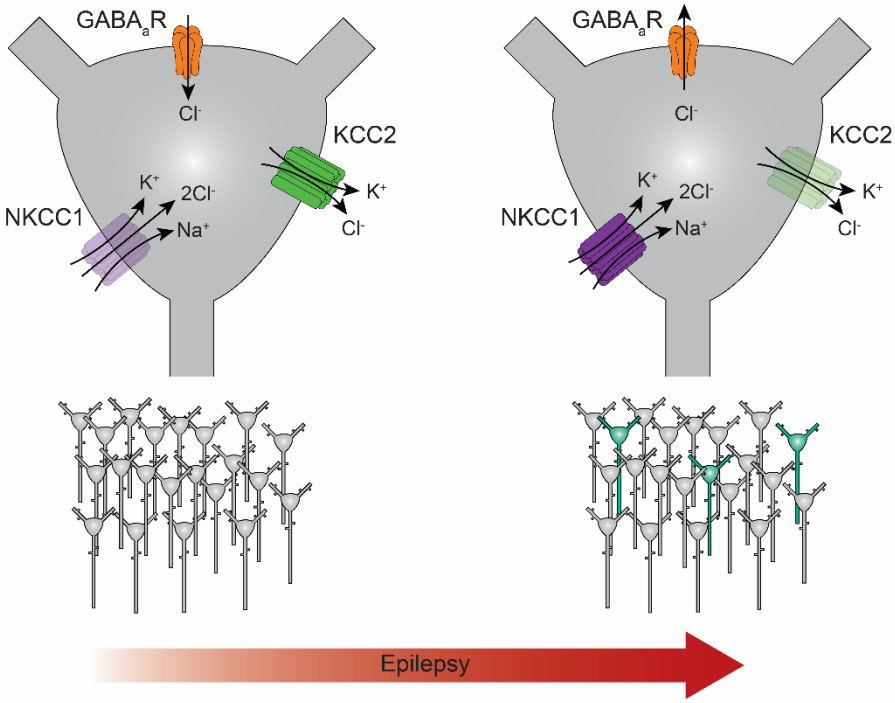

Figure 1.5: Changes in KCC2 expression in pyramidal neurons
Pyramidal neurons typically express high levels of KCC2, a chloride transporter which exports chloride ions. This results in a hyperpolarized reversal potential for $GABA_A$ receptors. A subset of pyramidal neurons decrease expression of KCC2 and begin to re-express NKCC1, leading to elevated levels of intracellular chloride and shifting the $GABA_A$ receptor reversal potential to a more depolarized value.

implanted microelectrodes showed that interneuron firing begins up to 10 seconds before seizure onset in TLE patients (Elahian et al., 2018). One possibility is that CA1 sclerosis in epileptic patients results in deafferentation of CA1 inputs onto the subiculum, causing pyramidal cells to revert to a more developmental-like state. If this is the case, changes in chloride transporter expression would be expected, especially in neurons in which GABAergic input was excitatory. This hypothesis was later tested, again in human tissues. Immunohistochemical and *in situ* hybridization experiments showed that KCC2 expression was absent from cells that were excited during interictal-like population bursts (Palma et al., 2006; Huberfeld et al, 2007). Furthermore, the NKCC1 antagonist bumetanide suppressed interictal activity. Direct injection of the highly selective KCC2 blocker VU0463271 (Delpire et al., 2012) into the dorsal hippocampus rapidly induced epileptiform discharges in mice. Additionally, hippocampal slices perfused with VU0643271 exacerbated epileptiform activity induced by low Mg^{2+} ACSF (Sivakumaran et al., 2015; Kelley et al., 2016). Together, these data point to a vital role of KCC2 expression in inter-ictal like activity. However, these experiments were done on the intact hippocampus or on hippocampal slices. In these cases, the drug could possibly defuse and affect neighboring regions, making region-specific interpretations difficult and not fully recapitulating the subiculum-specific changes. To date, no experiments have been carried out to determine if the subiculum alone can generate inter-ictal like activity if KCC2 activity is diminished only in this region after the subiculum is isolated from extra-subicular inputs.

The role of PV+ interneurons in TLE

The evidence implicating depolarizing GABA in TLE highlights the potential role that GABAergic interneurons might have in the disease. There are many ways to classify inhibitory interneurons,

and a common qualifier for classification is whether they tend to form synapses along sites near and on the soma or further away on distal dendrites. The location of the inhibitory synapse strongly influences the properties of the inhibition. Inhibitory synapses located close to the soma and action potential initiation site can powerfully control action potential firing, and inhibitory synapses located near excitatory synapses on distal dendrites can silence nearby synapses. Parvalbumin expressing interneurons are the classical example of a perisomatic targeting interneuron. These interneurons express the calcium binding protein parvalbumin and typically target the soma and proximal dendrites (PV+ basket cell) or the axon initial segments of pyramidal cells (PV+ axo-axonic cells). PV+ interneurons form powerful feed-forward microcircuits, acting to sharpen the temporal firing of neurons.

The role that PV+ interneurons play in epilepsy is unclear. One prevailing idea is that PV+ interneuron activation is anti-epileptic. Optogenetic activation of PV+ interneurons in a kainic acid model of TLE shortened the duration of seizures and improved spatial memory (Krook-Magnuson et al., 2013; Kim et al., 2020). Other studies have suggested that PV+ interneuron firing gates seizure propagation to extra-hippocampal regions, and the gating breaks down after PV+ interneurons are driven into depolarization block (Cammarota et al., 2013). Indeed, a number of epilepsy models are characterized by intense PV+ interneuron activation prior to the beginning of a seizure (Miri et al., 2018). However, optogenetic activation of entorhinal cortex PV+ interneurons in the 4-AP model enhanced epileptiform activity *in vitro,* and activation of PV+ interneurons in the epileptic focus failed to stop the spread of epileptiform activity in a focal model of epilepsy (Yekhlef et al., 2015; Sessolo et al., 2015). Fewer studies have focused specifically on PV+ interneurons in the subiculum. Recently, a similar optogenetic approach was used to evaluate how activation of subicular PV+ interneurons impacted secondary generalized seizures in a

kindling epilepsy model *in vivo* (Wang et al., 2017). Repeated optogenetic activation of PV+ interneurons slowed the acquisition of secondary generalized seizures but exacerbated their expression after the seizures were established. In contrast, activation of somatostatin (SST) expressing interneurons, a distinct interneuron group that tends to target more distal dendritic compartments, both slowed acquisition of seizures and had an anti-epileptic effect. To date, no studies have examined what impact subicular PV+ interneurons might have in a subicular network where KCC2 is pharmacologically inhibited. Such an experiment would parallel the subiculum specific decreases seen in patients with TLE.

Overview of thesis chapters

In summary, the subiculum is a vital component of the hippocampal formation, and recent work has implicated the subiculum in generating network activity that has been linked to seizures. Despite this important link, there has not been a quantitative assessment of the subicular network connections that contribute to the generation of this activity or the physiological processes that might precipitate its onset. Broadly, my thesis work has been dedicated to understanding the role of synaptic connections between excitatory cells in the subiculum in epilepsy and how certain epileptogenic changes might impact how these microcircuits function. Chapter 2 of my thesis focuses on examining the pattern of connectivity between the homogenous excitatory neurons of the subiculum using quantitative methods and how these local excitatory connections are sufficient to generate epileptiform like activity when GABA signaling is compromised (Fiske et al., 2020). Chapter 3 of my thesis examines the role that subicular PV+ interneurons play in a KCC2 down-regulation model of epileptogenesis (*In preparation*, Anstötz et al., 2021). Chapter 4 includes a general discussion of important findings from my work.

Chapter 2. The intrinsic cell type-specific excitatory connectivity of the mouse subiculum is sufficient to generate synchronous epileptiform activity

Adapted from: Fiske MP, Anstötz M, Welty LJ, Maccaferri G (2020). J Physiol 598:1965-1985.

Introduction

Neuronal diversity is a key determinant of the functional specificity of brain regions and networks (Kandel et al., 2012). In particular, the spatiotemporal integration of the activity of different subclasses of cortical neurons (Pelkey et al., 2017; Cembrowski and Spruston, 2019) expressing cell type-specific intrinsic conductances (Hille, 2001) and synaptically connected according to precise architectural rules (Somogyi et al., 1998; Klausberger and Somogyi, 2008) produces the complex computations that are required by sensory, motor, and cognitive physiological processes (Kandel et al., 2012). In addition, in the epileptic brain, the specificity of neuronal circuits is an important determinant of the regional vulnerability to ictal and interictal events.

Neurophysiological studies at the microscopic level have underscored three main factors that appear to be mechanistically related to the overall susceptibility of a particular network to epileptiform activity. The first factor is the presence of a substantial proportion of intrinsically bursting cells in the circuit (Traub and Miles, 1991) as found, for example, in the CA3 subfield (Wong and Prince, 1978; Masukawa et al., 1982; Bilkey and Schwartzkroin, 1990) and in the subiculum (Mason, 1993; Mattia et al., 1993; Taube, 1993; Behr et al., 1996; Greene and Totterdell, 1997; Staff et al., 2000; Menendez de la Prida, 2003; Menendez de la Prida et al., 2003; Jarsky et al., 2008; Kim and Spruston, 2012; Panuccio et al., 2012; Böhm et al., 2015; Cembrowski et al., 2018) of the hippocampal formation. Both networks are commonly involved in sustaining pathological discharges in human patients (Cohen et al., 2002; Wozny et al., 2005; Huberfeld et

al., 2007,2011; Alvarado-Rojas et al., 2015; Wang et al., 2017) and animal models (Fujita et al., 2014; Toyoda et al., 2015) of temporal lobe epilepsy (TLE). Although burst firing is necessary for a variety of physiological signaling states (Cooper et al., 2005; Simonnet and Brecht, 2019), trains of spikes at high frequency increase the reliability of excitatory synaptic connections (Lisman, 1997) and may trigger plasticity in positive feedback loops (Bains et al., 1999). Thus, the interplay of burst firing with synaptic facilitation may potentially lower the threshold for runaway excitation and generate pathological firing.

The second factor involves the degree of local connectivity and anatomical synaptic divergence/convergence of excitatory neurons. For example, in the hippocampus, epileptiform bursts originated by the branches of the CA3 pyramidal cell local axons may become sufficient to recruit the entire population of the subfield and then project interictal spikes to downstream regions (Traub and Miles, 1991).

Lastly, the efficacy of GABAergic inhibition has long been recognized to play a fundamental role in preventing epileptiform population activity. In fact, blockade of GABA receptors is an efficient and reliable pharmacological manipulation that induces epileptiform activity in susceptible networks both in vitro (Schwartzkroin and Prince, 1978; Wong and Traub, 1983; Miles and Wong, 1983) and in vivo (reviewed by Fisher, 1989).

The critical importance of the interaction among these three factors was elegantly shown by Miles and Wong (1983) with a direct experiment performed in pharmacologically disinhibited CA3 hippocampal slices. Under these conditions, a current-evoked burst of action potentials produced in an individual neuron generated fully synchronized population discharges.

Surprisingly, despite its involvement in the generation of epileptiform activity and in contrast to the wealth of information available on the synaptic architecture of the CA3 subfield (Traub and

Miles, 1991, Guzman et al., 2016), to our knowledge, only a single study has directly examined the local functional connectivity of subicular cells (Böhm et al, 2015).

Here, we have taken advantage of simultaneous double and triple patch-clamp recordings and anatomical reconstructions to examine the connectivity between subicular pyramidal cells classified by objective multivariate methods. Additionally, we have tested whether these connections are sufficient to lead to the emergence of synchronized population activity in pharmacologically disinhibited slices.

In this chapter, I address two important questions regarding the subiculum's involvement in generating activity linked to epilepsy. Are the pyramidal neurons of the subiculum, classified using objective, quantitative methods, connected in a cell-type specific manner? And, are these local excitatory connections sufficient to lead to the emergence of synchronized population activity in pharmacologically disinhibited slices? We find that the pyramidal neurons in the subiculum, when classified using PCA and Gaussian mixture modeling, belong to two separate groups. These two groups are synaptically connected with a high degree of connectivity and are connected in a non-random pattern. Anatomically, these connections are biased towards forming synapses on the basal dendrites of post-synaptic neurons. Under conditions where extra subicular inputs are physically severed, synchronous epileptiform events emerge when GABA signaling has been blocked. These results fit well with suggestions that excitatory events in the subiculum might underlie the pre-ictal discharges that govern interictal to ictal transitions.

Materials and methods

Ethical approval

All animal procedures conducted in this study complied with the guidelines set forth by the Institutional Animal Care and Use Committee of Northwestern University, the National Institutes of Health, and conform to the principles and regulations as described in the Editorial by Grundy (2015). The investigators understand the ethical principles under which the Journal of Physiology operates and that their work complies with this animal ethics checklist.

Animals

Male and female wild-type C57BL/6J animals (stock number: 000664; RRID: IMSR_JAX:000664, Jackson Laboratory, Bar Harbor, ME) between the age of P14-P21 were used for experiments. Animals were housed on a 14/10 light/dark schedule with *ad libitum* access to food and water.

Acute slice preparation

Mice were deeply anesthetized with isoflurane in an induction chamber with a separating platform to avoid direct contact between the animals and the anesthetic. After decapitation, the brain was carefully removed and glued to a specimen block in a chamber filled with cooled artificial cerebrospinal fluid (ACSF) with the following composition (in mM): 130 NaCl, 24 NaHCO3, 3.5 KCl, 1.25 NaH2PO4, 1 CaCl2, 2 MgSO4, 10 glucose, saturated with 95% O2, 5% CO2 at pH = 7.4. Transverse sections (400 µm) of an entire brain hemisphere containing the hippocampal formation were cut using a vibrating microtome (Leica VT 1200 S, Leica Biosystems). Slices recovered at 30-32°C for at least 30 min and were then stored at room temperature until use.

Subicular mini slices were prepared from regular slices by severing the connections between the subiculum and CA1 hippocampal subfield/entorhinal cortex. Cuts were performed at locations with clear scatter of pyramidal cell bodies and with unambiguous widening of the pyramidal cell layer.

Electrophysiological recording and analysis

Slices/mini slices were transferred to a recording chamber positioned under a direct microscope (Scientifica) equipped with oblique illumination optics (Olympus) and an infrared camera system (VX-45, TILL Photonics). Cells were visualized using a 60x infrared water-immersion objective. Slices/mini slices were superfused with preheated ACSF (31-33°C, TC-324B, Warner Instruments) with the following composition (in mM): 130 NaCl, 24 NaHCO3, 3.5 KCl, 1.25 NaH2PO4, 2 CaCl2, 1 MgCl2, 10 glucose, saturated with 95% O2, 5% CO2 at pH 7.4.

Pipettes were pulled from thin borosilicate capillaries (Prism FLG15, Dagan Corporation, Minneapolis, MN, USA) with a resistance of 3-5 MΩ when filled with an internal solution containing the following (in mm): 115 K-methylsulfate, 10 KCl, 5 creatine phosphate, 5000 units creatine kinase, 4 ATP-Mg, 0.3 GTP-Na3, 16 KHCO3, 0.25% biocytin equilibrated with 95% O2–5% CO2 at pH 7.3. Recordings were performed using a Multiclamp 700 amplifier (Molecular Devices). Series resistances were balanced via a bridge circuit. Signals were filtered at 3 KHz and digitized at a minimum of 20 KHz using a Digidata 1550A and the Clampex 9 program suite (Molecular Devices).

Paired recordings and connectivity

Simultaneous double and triple whole-cell current clamp recordings from pyramidal neurons in the subiculum were performed to assess functional connectivity or epileptiform activity. Holding current was injected to maintain the cells close to their resting potential at ~-65 mV. Each recorded neuron was stimulated in an alternating fashion to trigger single action potentials at low frequency (0.1 Hz) using a 1 ms supra-threshold current injection. A functional connection was identified based on the presence of a short latency post-synaptic unitary excitatory postsynaptic potential (uEPSP) in the other cell(s) of the pair/triple recording, following the action potential in the stimulated neuron. For each connection identified as described (n=63), several traces (n=30) were collected, averaged, and the resulting uEPSPs measured and analyzed. Amplitude, half-width, 20-80% rise time, were estimated using the Clampfit 9 program (Molecular Devices). Putative failures were identified visually. When single spikes at low frequency in the putative presynaptic neuron did not reveal uEPSPs, we performed spike triggered averaging of the action potentials generated by the long current pulses (1 sec) used to define their firing patterns and other electrophysiological properties of the recorded cells. In a minority of cases (32 out of 1787), this analysis revealed uEPSPs that were not unequivocally apparent by single spikes at low frequency. These results were considered for the study of connectivity, but the underlying uEPSPs were neither quantified nor included in the analysis of uEPSP properties. In a few cases, as indicated in the text, voltage-clamp recordings were made in cell-attached configuration to evaluate epileptiform activity, and the command voltage was -60 mV.

Anatomical recovery of biocytin-filled pairs

Slices with filled neuron pairs were fixed for 24 hours in 4% paraformaldehyde solution in 0.1 M PB at 4°C. Endogenous peroxidase activity was quenched using 3% H_2O_2 solution for 20 mins.

Slices were then incubated overnight at 4°C in an avidin-biotinylated-HRP complex (VECTASTAIN ABC Elite Kit, Vector Laboratories, Burlington, ON, Canada), permeabilized with 0.1% Triton X-100 in 0.1 M PB, and visualized by a peroxidase reaction using 3,3'-diaminobenzidine tetrahydrochloride as a chromogen. The labeling was intensified with 0.0012% $NiNH_4SO_4$ and 0.0016% $CoCl_2$. Slices were then post-fixed with 0.1% OsO_4 in 0.1 M PB for 1-2 min, mounted on slides and coverslipped with Mowiol.

Filled connected neurons were reconstructed in 3D using a Neurolucida-based station and software (MBF Bioscience, Williston, VT, USA). Putative synapses were identified by light microscopy as locations at which a pre-synaptic axon and a post-synaptic dendrite were in close apposition in the same focal plane with an enlargement (bouton) of the pre-synaptic side. The synaptic distance from the soma was calculated as the average of all the identified putative contact sites. Only neurites with no obvious truncation were used for subsequent analysis.

Drugs

Gabazine (SR 95531 hydrobromide) was purchased from Tocris, prepared as a stock solution in water, and used in experiments at 12.5 µM. CGP55845 was purchased from Tocris, prepared as a stock solution in DMSO, and used at 5 µM. DMSO (0.005%) was also included in control solutions when experiments involved the use of CGP55845.

Experimental design and statistical treatment of the data

Separation of neurons in subpopulations (type 1 and type 2) based on their electrophysiological properties

For classification purposes, neurons were studied by injecting long (1 sec) current pulses in the hyperpolarizing and depolarizing direction from a membrane potential held close to rest (~-65

mV). Both the peak and steady state voltage responses to hyperpolarizing current steps (-200 to -25, 25 pA steps) were measured and linearly fit to estimate values of membrane input resistance at these two time points. Additional electrophysiological parameters were also quantified in the responses to a current injection level equal to the first intensity able to trigger firing, increased by 50 pA. We counted the total number of spikes produced, and studied several parameters for the first two spikes of the response. In particular, we measured: spike threshold (reached when membrane potential dV/dt exceeds 10 V/s, Fricker et al., 1999), amplitude (difference between threshold and action potential peak), half width, time of peak (from the beginning of the current pulse), amplitude of peak afterdepolarization/afterhyperpolarization (difference between threshold and the maximal positive/negative voltage following the spike), and afterdepolarization/afterhyperpolarization latency from the preceding spike. These 15 parameters were subjected to principal component analysis (PCA, Joliffe, 1986) using OriginPro 2019b (Origin Lab, Northampton, MA, USA). We further considered only the first three extracted principal components, which accounted for 32% (PC1), 26% (PC2) and 12% (PC3) of total data variance. Euclidian distances (Ed) between individual data points were calculated as $Ed = \sqrt{[(\Delta PC1)^2 + (\Delta PC2)^2 + (\Delta PC3)^2]}$. OriginPro 2019b was also used to fit Gaussian mixture models (GMM, Hartigan, 1975) to the three principal components, and separate the recorded neurons in subpopulations based on Baeysian Information Criterion analysis (BIC, Schwartz, 1978).

Sholl analysis

Radial segments of 50µm intervals were centered to the soma of the analyzed cell. The total length of every neuronal branch (axon, basal dendrite, and apical dendrite) within each segment was calculated for every measured neuron using a custom script in VisualBasic.

Anatomical density plots of pairs

Reconstructed pairs were merged and aligned to the apical dendrite of the individual post-synaptic neuron. For the subsequent analysis only the post-synaptic dendrites and the pre-synaptic axons were used. The combined reconstructed pairs were placed in a Cartesian grid and the average length of each neuronal segment within grid-boxes of 25 µm by 25 µm was calculated, yielding a raw density matrix. To obtain the axo-dendritic overlap, the axonal/pre-synaptic matrix was multiplied by the dendritic/post-synaptic matrix and then normalized by the sum of all values. The matrices were then transferred to OriginPro 2019b (Origin Lab, Northampton, MA, USA) to create a contour plot.

Network activity of subicular mini slices

Baseline activity was recorded in simultaneous double and triple recordings for 3 minutes in control solutions (DMSO, 0.005%) before the application of gabazine and CGP55845 for at least 15 minutes. Synchronous discharges were quantified by measuring their area (from beginning to return to initial resting potential), frequency of firing, number of spikes and overall duration (time between first and last spike of the discharge) using Clampfit.

In case of homotypic pairs, Δ latency values were calculated by randomly assigning one cell of the pair as the reference neuron. In the case of heterotypic pairs, type 1 pyramidal cells were always considered as the reference neuron (i.e. positive Δ latency values indicate initial spikes occurring earlier in a type 2 cell compared to a type 1 neuron).

Modeling the impact of misclassification on connection probabilities

We estimated 95% confidence intervals of the estimated connection probabilities for each pairing, taking misclassification into consideration, using the approach described below. We denote the misclassification probability as α. Our computations assume that misclassification is independent of the presence of a functional connection in the tested pairs.

To begin, we define the following quantities:

N_{11} = Number of observed type 1 to type 1 pairs

p_{11} = Proportion of functional connections in observed type 1 to type 1 pairs

N_{12} = Number of observed type 1 to type 2 pairs

p_{12} = Proportion of functional connections in observed type 1 to type 2 pairs

N_{21} = Number of observed type 2 to type 1 pairs

p_{21} = Proportion of functional connections in observed type 2 to type 1 pairs

N_{22} = Number of observed type 2 to type 2 pairs

p_{22} = Proportion of functional connections in observed type 2 to type 2 pairs

The ***observed*** pair subtypes are defined by our original multivariate analysis applied to whole-cell recording data and therefore may include experimental misclassifications (run-down, see Result section).

We can treat $\hat{p}_{11}$ a binomial proportion that is approximately normally distributed, namely $\hat{p}_{11} \sim N(p_{11}, \sqrt{p_{11}(1 - p_{11})/N_{11}})$. Using this normal approximation to the binomial requires that $p_{11}N_{11} \geq 5$ and $(1 - p_{11})N_{11} \geq 5$, which is the case for our observed data. We treat $\hat{p}_{11}, \hat{p}_{12}$, and $\hat{p}_{22}$ similarly. (Of note, the data for the type 1 to type 1, type 1 to type 2 and type 2

to type 2 conditions also satisfy the more stringent condition that these quantities be greater than or equal to 9 for the normal approximation to hold).

For notational convenience, we define $\sigma_{11}\ldots\ \sigma_{22}$ as the corresponding standard deviations:

$\sigma_{11} = \sqrt{p_{11}(1 - p_{11})/ N_{11}}$

$\sigma_{12} = \sqrt{p_{12}(1 - p_{12})/N_{12}}$

$\sigma_{21} = \sqrt{p_{21}(1 - p_{21})/N_{21}}$

$\sigma_{22} = \sqrt{p_{22}(1 - p_{22})/ N_{22}}$

Now we let M_{11} = Number of **actual** type 1 to type 1 pairs (without misclassification), and define M_{12}, M_{21}, and M_{22} analogously. Similarly, we let q_{11} = proportion of functional connections in **actual** type 1 to type 1 pairs, and we define q_{12}, q_{21}, and q_{22} analogously.

Then using E to denote the expected value, we have

$E(M_{11}) = (1-\alpha)^2 N_{11}$

$E(M_{12}) = \alpha(1-\alpha)N_{11} + (1-\alpha)N_{12}$

$E(M_{21}) = \alpha(1-\alpha)N_{11} + (1-\alpha)N_{21}$

$E(M_{22}) = \alpha^2 N_{11} + \alpha N_{12} + \alpha N_{21} + N_{22}$

It follows that each of the q's can be expressed as a weighted sum of the p's:

$q_{11} = \frac{(1-\alpha)^2 N_{11} \cdot p_{11}}{(1-\alpha)^2 N_{11}} = p_{11}$

$q_{12} = \frac{\alpha(1-\alpha)N_{11}}{\alpha(1-\alpha)N_{11}+(1-\alpha)N_{12}} \cdot p_{11} + \frac{(1-\alpha)N_{12}}{\alpha(1-\alpha)N_{11}+(1-\alpha)N_{12}} \cdot p_{12}$

$$q_{21} = \frac{\alpha(1-\alpha)N_{11}}{\alpha(1-\alpha)N_{11} + (1-\alpha)N_{21}} \cdot p_{11} + \frac{(1-\alpha)N_{21}}{\alpha(1-\alpha)N_{11} + (1-\alpha)N_{21}} \cdot p_{21}$$

$$q_2 = \frac{\alpha^2 N_{11}}{\alpha^2 N_{11} + \alpha N_{12} + \alpha N_{21} + N_{22}} \cdot p_{11} + \frac{\alpha N_{12}}{\alpha^2 N_{11} + \alpha N_{12} + \alpha N_{21} + N_{22}} \cdot p_{12}$$
$$+ \frac{\alpha N_{21}}{\alpha^2 N_{11} + \alpha N_{12} + \alpha N_{21} + N_{22}} \cdot p_{21} + \frac{N_{22}}{\alpha^2 N_{11} + \alpha N_{12} + \alpha N_{21} + N_{22}} \cdot p_{22}$$

Because the q's are sums of independent normal random variables, they are also normally distributed as follows:

$\hat{q}_{11} \sim N(p_{11}, \sigma_{11})$

$\hat{q}_{12} \sim N(w_{12}^a \cdot p_{11} + w_{12}^b \cdot p_{12}, \sqrt{{w_{12}^a}^2 \cdot \sigma_{11}^2 + {w_{12}^b}^2 \cdot \sigma_{12}^2})$

$\hat{q}_{21} \sim N(w_{21}^a \cdot p_{11} + w_{21}^b \cdot p_{21}, \sqrt{{w_{21}^a}^2 \cdot \sigma_{11}^2 + {w_{21}^b}^2 \cdot \sigma_{21}^2})$

$\hat{q}_{22} \sim N((w_{22}^a)^2 \cdot p_{11} + (w_{22}^b)^2 \cdot p_{12} + (w_{22}^c)^2 \cdot p_{21} + (w_{22}^d)^2 \cdot p_{22},$

$\sqrt{{w_{22}^a}^2 \cdot \sigma_{11}^2 + {w_{22}^b}^2 \cdot \sigma_{12}^2 + {w_{22}^c}^2 \cdot \sigma_{21}^2 + {w_{22}^d}^2 \cdot \sigma_{22}^2}$

Where the w's are:

$$w_{12}^a = \frac{\alpha(1-\alpha)N_{11}}{\alpha(1-\alpha)N_{11} + (1-\alpha)N_{12}}$$

$$w_{12}^b = \frac{(1-\alpha)N_{12}}{\alpha(1-\alpha)N_{11} + (1-\alpha)N_{12}}$$

$$w_{21}^a = \frac{\alpha(1-\alpha)N_{11}}{\alpha(1-\alpha)N_{11} + (1-\alpha)N_{21}}$$

$$w_{21}^{b} = \frac{(1-\alpha)N_{21}}{\alpha(1-\alpha)N_{11} + (1-\alpha)N_{21}}$$

and

$w_{22}^{a} = \frac{\alpha^2 N_{11}}{d}$, $w_{22}^{b} = \frac{\alpha N_{12}}{d}$, $w_{22}^{c} = \frac{\alpha N_{21}}{d}$, and $w_{22}^{d} = \frac{N_{22}}{d}$

with $d = \alpha^2 N_{11} + \alpha N_{12} + \alpha N_{21} + N_{22}$.

The 95% confidence intervals for $\hat{q}_{11}, \ldots \hat{q}_{22}$ were generated from these normal distributions.

Data presentation and statistical tests

Unless otherwise indicated in the legend, data are presented in the manuscript as mean (SD). Box charts indicate the median as a middle line, lower and upper quartiles as upper and lower box borders and minimum and maximum as whiskers. Statistical tests were used to estimate the probability of the null hypothesis, and p values (rounded to 2 decimal places) are directly indicated. Tests used are abbreviated in the manuscript as follows: Mann-Whitney test: M-W, two way ranked ANOVA: 2-r-ANOVA, and chi square test: χ^2.

Results

As mentioned above, several studies have provided strong and converging evidence for functional diversity in subicular pyramidal cells by revealing the existence of neurons responding to current injections with either regular- or bursting trains of action potentials (Mason, 1993; Mattia et al., 1993; Taube, 1993; Behr et al., 1996; Greene and Totterdell, 1997; Staff et al., 2000; Menendez de la Prida, 2003; Menendez de la Prida et al., 2003; Jarsky and Spruston, 2008; Kim and Spruston, 2012; Panuccio et al., 2012; Böhm et al., 2015; Cembrowski et al., 2018). However, the separation of subicular cells into these two functional classes based on the examination of their firing pattern in response to current pulses does present technical ambiguities, as the definition of burst itself has not been univocal in the literature.

For example, the number of spikes required in the recorded response to be defined as a burst has ranged from 2-4 (Mason, 1993), 3-5 (Taube, 1993), 2-3 (Behr et al., 1996; Menendez de la Prida, 2003; Menendez de la Prida et al., 2003; Kim and Spruston, 2012), 2 or more (Staff et al., 2000), to 3 or more (Greene and Totterdell, 1997; Panuccio et al., 2012; Böhm et al., 2015). Similarly, the minimal spike frequency necessary to define a burst has been subjected to variable requirements (>200 Hz: Staff et al., 2000; >100 Hz: Kim and Spruston, 2012 and Graves et al., 2012, >125 Hz: Böhm et al., 2015). Lastly, the intensity and duration of the current step injected into cells has also been quite variable across studies, with the use of different parameters potentially affecting the resulting classification (as shown by Cooper et al., 2003).

Furthermore, the existence of subpopulations within the two main groups of regular-firing and bursting neurons has also been proposed. For example, regular firing cells displaying different accommodation properties have been described (Menendez de la Prida et al., 2003), as well as the

presence of “weak” and “strong” bursting neurons (depending on the number of bursts generated during a 1 second-long current pulse: Staff et al., 2000).

Thus, biological diversity, coupled to the use of non-uniform and potentially subjective criteria for cell classification, may make the comparison of results obtained in different studies inherently problematic.

More recently, the use of multivariate methods that take into consideration multiple electrophysiological membrane properties have reinforced the idea that two separate groups of subicular pyramidal cells with regular and bursting firing patterns can be objectively dissected and identified (Graves et al., 2012).

To our knowledge, only a single study has examined the detailed cell type-specific connectivity between functionally distinct types of subicular neurons (Böhm et al., 2015). Therefore, we decided to re-examine this issue both functionally and anatomically in subicular pyramidal cells classified by the combined use of principal component analysis (PCA) and Gaussian mixture models (GMM)- Bayesian information criterion (BIC). Figures 2.1A and 2.1B show the results from the PCA of 15 electrophysiological parameters measured in n=70 double and n=285 triple simultaneous recordings (total n=995 cells, for details please see the Methods section and the Figure legend). Application of GMM-BIC analysis suggested the presence of two groups of functionally diverse cells, which we termed “type 1” and “type 2” (Figures 2.1B, 2.1C, and 2.1D). This result matches well with the firing pattern of the cells. As shown in Figure 2.1C, the overall distribution of the initial firing frequency of the studied cells was clearly multimodal, with type 1 and type 2 cells associated with the lower and higher initial frequency peak, respectively (type 1: 16 (SD 22) Hz, n=486 vs type 2: 169 (SD 34) Hz, n=509). Figure 2.1D directly shows the similarity among cells belonging to the same group and the differences between the two

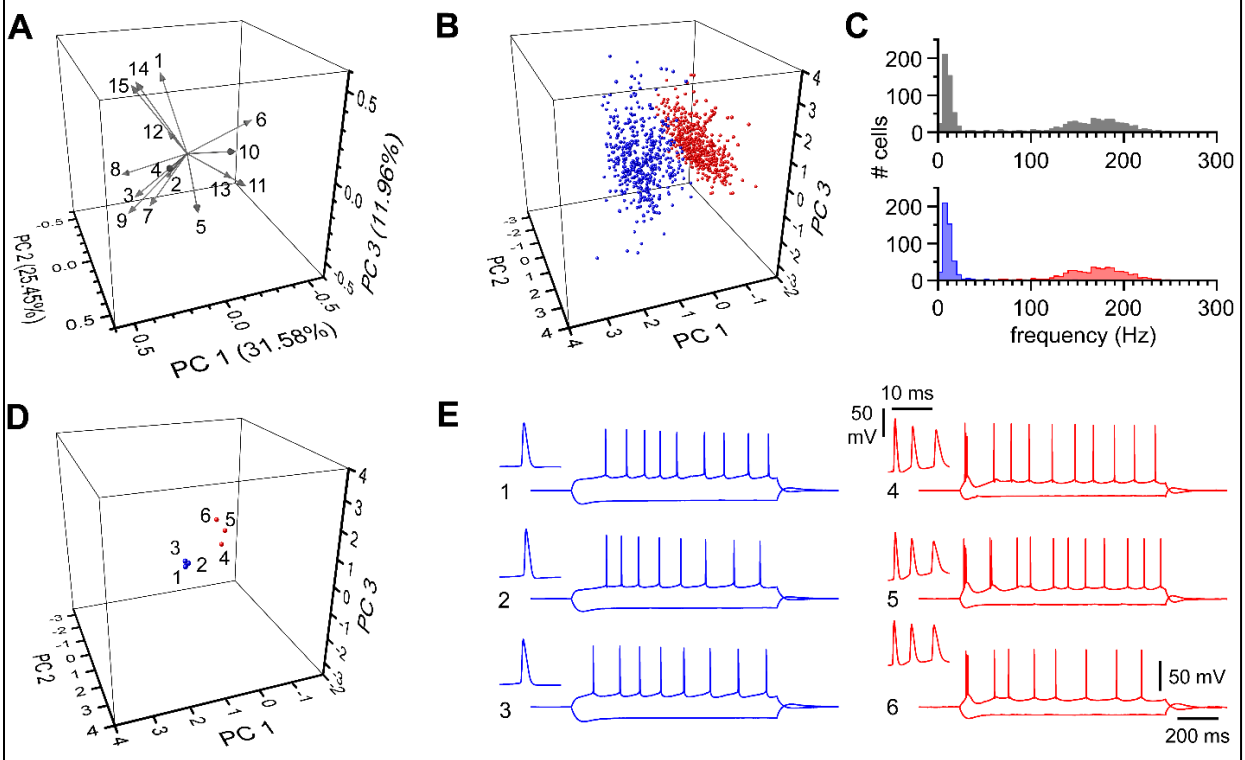

Figure 2.1: Principal component and Gaussian mixture models analysis of functional diversity in subicular pyramidal cells

A) 3D loading plot for the different variables measured in response to a depolarizing and hyperpolarizing response (see Methods for details). Number of spikes (1), amplitude of first (2) and second spike (3), time of the first (4) and second (5) spike, half-width of the first (6) and second spike (7), threshold voltage of the first (8) and second (9) spike, amplitude of the afterpotential following the first (10) and second (11) spike, latency from spike peak of the afterpotential following the first (12) and second (13) spike, membrane input resistance at peak (14) and steady-state of the hyperpolarizing (15) response.

B) Summary scatterplot of the sample of 995 recorded cells represented in the 3D principal component space. Colours distinguish type 1 from type 2 cells (blue and red, respectively), as determined by BIC.

C) Summary plot of the frequency of the first two action potentials measured in depolarizing responses. Top and bottom graphs show the overall distribution before (grey) and after the distinction in type 1 (blue) and type 2 (red) neurons. Note the bimodal shape of the plot and that type 1 cells are associated with the lower frequency peak compared to type 2 cells.

D) Selected examples of type 1 (blue) and type 2 (red) neurons in the 3D space given by the PCA.

E) Actual recordings showing the responses to depolarizing and hyperpolarizing responses. Note the regular firing and bursting phenotype of type 1 (blue) and type 2 (red) cells, respectively. Insets show the initial spikes at higher temporal resolution.

classes. These responses are also very similar to what has been previously described for regular firing (type 1) and intrinsically bursting (type 2) subicular pyramidal neurons.

In addition to recording their firing pattern and membrane properties, the neurons described in Figure 2.1 were tested for functional synaptic connectivity as shown in Figure 2.2. Both homotypic (type 1 to type 1 or type 2 to type 2, Figures 2.1A and 2.1B) and heterotypic pairs (type 1 to type 2, Figures 2.2C and 2.2D and type 2 to type 1, Figures 2.2E and 2.2F) of neurons were tested. Unitary excitatory postsynaptic events (uEPSPs) were observed in ~5% of the cases (95/1850), which compares well to the estimate of ~4% reported by Böhm et al. (2015). This value appears higher than what has been reported for the local excitatory connectivity of other regions of the hippocampal formation (CA1: ~1%, Deuchars and Thomson, 1996, CA3 ~2%: Miles and Wong, 1986 and ~1%: Guzman et al., 2016) and may underlie the vulnerability of the subicular network to epileptiform activity.

Within each subgroup (homotypic or heterotypic) of connections tested, the similarity between the cells of the pair did not seem to differ in non-connected vs. connected pairs. The Euclidean distances between homotypic pairs of non-connected and connected type 1 cells were 1.55 (SD 0.83) a.u (n=597 pairs) and 1.37 (SD 0.74) a.u. (n=29 pairs) respectively (p=0.26, M-W). Similar values were also found between homotypic non-connected and connected type-2 cells [1.42 (SD 0.81) a.u, n=618 pairs and 1.54 (SD 0.84) a.u, n=34 pairs respectively, p=0.44, M-W]. In the cases of heterotypic pairs (type 1 to type 2), the distance was 2.40 (SD 0.82) a.u in non-connected pairs (n=261) and 2.18 (SD 0.76) a.u in connected pairs (n=25), respectively (p=0.20, M-W). Lastly, in type 2 to type 1 pairs, distance was 2.39 (SD 0.82) a.u. in non-connected (n=279) vs. 2.00 (SD 0.57) a.u. in connected pairs (n=7, p=0.24, M-W). The most parsimonious explanation of these results is that subicular pyramidal neurons are not homogenous, but belong to at least two

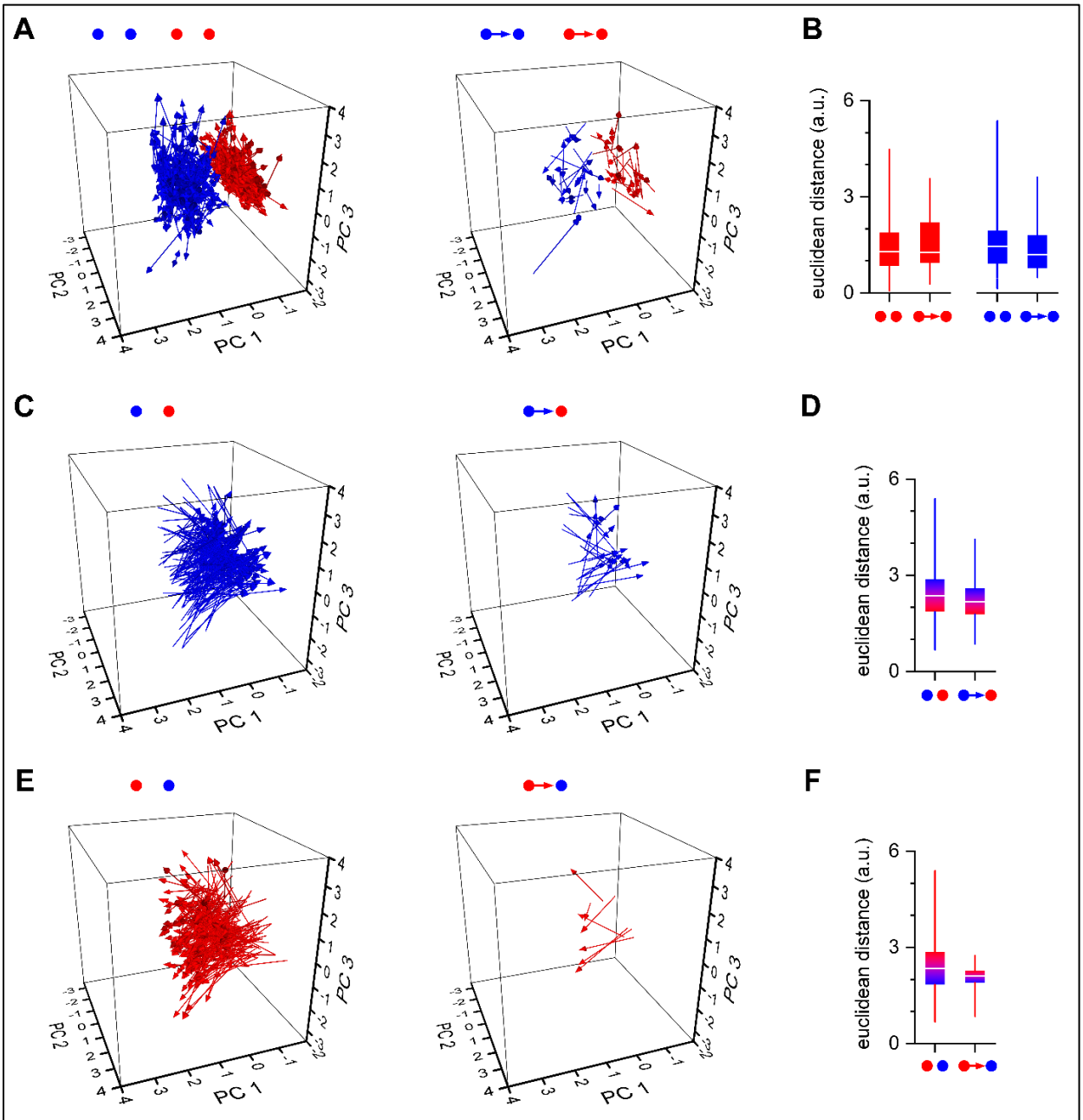

Figure 2.2: Principal component analysis of the connectivity between homotypic and heterotypic pairs of cells

A) 3D summary plot for type 1 (blue) and type 2 (red) homotypic pairs. Arrows indicate the direction of the connection tested from presynaptic to postsynaptic neurons. Left: unconnected neurons; right: connected pairs.

B) Boxplots comparing the Euclidean distances for unconnected (circles) and connected (circles and arrow) neurons in type 1 (blue) and type 2 (red) homotypic pairs.

C-F) similar plots for heterotypic type 1 to type 2 (blue vectors and bicolour boxplots with blue at the top and red at the bottom) and type 2 to type 1 connections (red vectors and bicolour boxplots with red at the top and blue at the bottom).

distinct functional groups (as suggested by BIC, see Methods) or, alternatively, that subclasses within the two main groups do not play a major role in determining their synaptic connectivity.

In order to corroborate this interpretation and our suggestion that PCA and GMM can accurately distinguish the two different classes of pyramidal neurons, we decided to compare their anatomical properties in a sample of cells that were filled with biocytin during whole-cell recording and then digitally reconstructed (Figure 2.3A and 2.3B). As shown in Figures 2.3C and 2.3D, a remarkable similarity was found in most, but not in all membrane domains. No differences were revealed by either Sholl analysis for either basal dendrites ($p=0.61$, $n=19$ and 29 type 1 and type 2 neurons, respectively) or axons ($p=0.10$, $n=18$ and 24 type 1 and type 2 neurons, respectively). However, a significant difference was found when the apical dendrites were compared ($p=0.01$, $n=21$ and 29 type 1 and type 2 neurons, respectively 2-r-ANOVA). Consistently, measurements of total length for basal dendrites and axons were not different in type 1 vs type 2 cells [type 1 basal dendrites: 2590 (SD 904) µm ,$n=19$ and type 1 axons: 2415 (SD 1148) µm, $n=18$, compared to type 2 basal dendrites: 2811 (SD 1516) µm ,$n=29$ and type 2 axons: 3022 (SD 1787) µm, $n=22$, $p=0.35$ and $p=0.39$, respectively]. In contrast, the estimated values for the total length of apical dendrites were higher in type 1 [5574 (SD 1059) µm, $n=21$] compared to type 2 neurons [4579 (SD 1599) µm, $n=29$, $p=0.01$]. This result extends our previous interpretation that type 1 and type 2 cells revealed by PCA and GMM-BIC analysis represent, in fact, two distinct subpopulations of pyramidal cells both functionally and structurally.

Next, we measured the properties of uEPSPs triggered by a single action potential at low frequency (0.1 Hz) in homotypic and heterotypic connections. As shown in Figures 2.4A, 2.4B, 2.4C, 4D, 2.4E and 2.4F a large degree of functional variability was present, even within the same group of connections. Homotypic type 1 connections (Figures 2.4A and 2.4B) generated uEPSPs

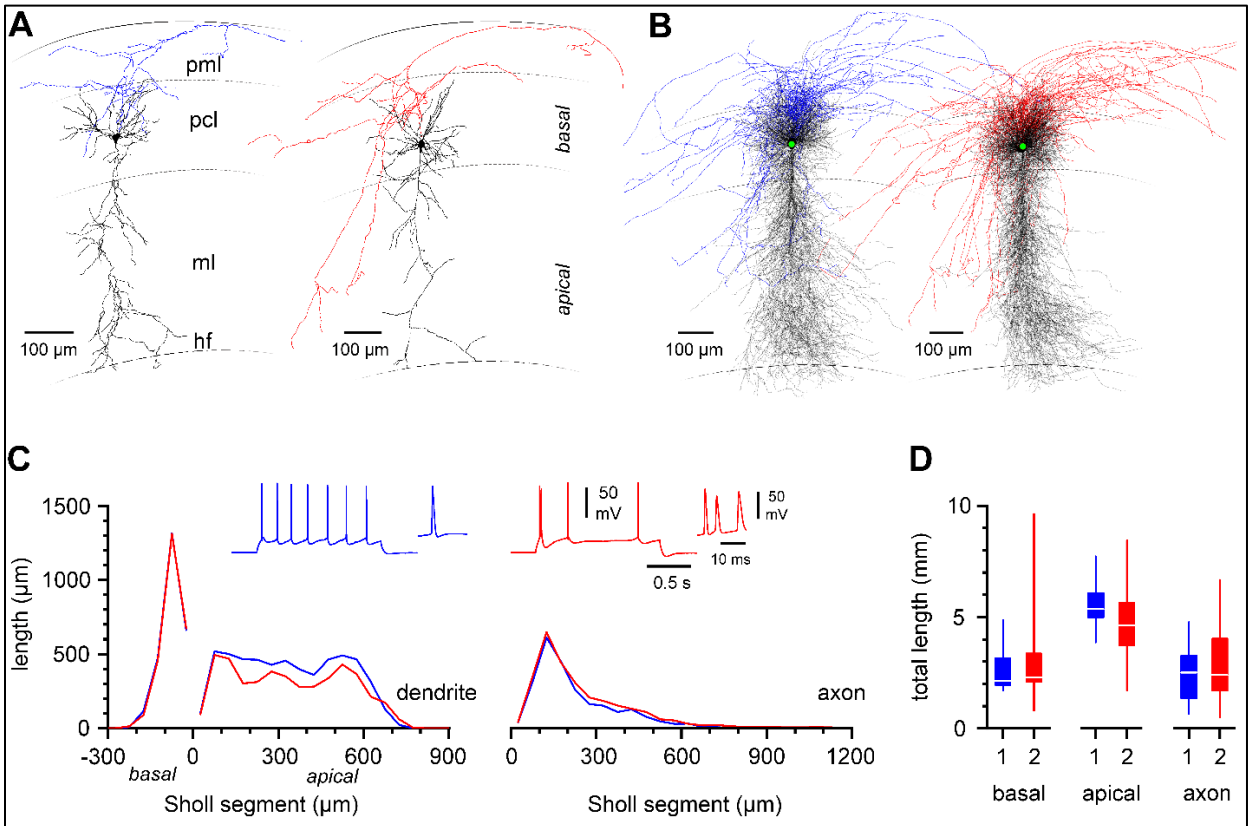

Figure 2.3: Anatomical properties of type 1 and type 2 pyramidal neurons
A) Individual examples of reconstructions of a type 1 (left) and type 2 (right) subicular cell. Soma and dendritesare in black, the axon is either in blue (type 1 cell) or in red (type 2 cell). Pml: polymorphic layer, pcl: pyramidal cell layer, ml: molecular layer, hf: hippocampal fissure.
B) Superimposition of all the reconstructed neurons separated according to their subclass (type 1: left; type 2: right).
C) left: Sholl analysis comparing the properties of basal (negative Sholl segment values) vs. apical (positive Sholl segment values) dendrites in type 1 (blue) and type 2(red) neurons. Right: summary plot of the same type of analysis for the axon of the reconstructed cells. Note the selective difference in the apical dendritic arborization and the similarity of basal dendrites and axons. The insets show examples of depolarizing responses in type 1 (blue) and type 2 (red) neurons with magnifications of the initial action potentials.
D) Summary plots of the dendritic lengths for the three membrane compartments (basal, apical dendrites and axon) for the two different cell groups (type 1: blue; type 2: red).

with failure rates of 42 (SD 21)%, amplitudes of 0.53(SD 0.39) mV, and risetimes and half widths of 2.3(SD 1.1) ms and 23.6(SD 6.4) ms, respectively (n=20 uEPSPs). Similar values were observed in the case of uEPSPs recorded between pairs of type 2 cells (Figures 2.4C and 2.4D: failure rates: 39 (SD 25) %, amplitudes: 0.53 (SD 0.37) mV, risetimes: 2.5 (SD 0.9) ms and half widths: 21.5 (SD 5.1) ms, n=22 uEPSPs). Heterotypic connections between type 1 and type 2 neurons were also identified (Figures 2.4E and 2.4F) and their parameters were similar to what was estimated in homotypic uEPSPs (failure rate: 41 (SD 26) % amplitude: 0.56 (SD 0.78) mV, risetimes: 2.6 (SD 0.6) ms and half widths: 21.9 (SD 6.0) ms, n=18).

In contrast, heterotypic uEPSPs between type 2 and type 1 cells could be measured only in 3 connections, revealed by low frequency single spikes [Figure 2.5A, failure rate: 13 (SD 10) %, amplitude: 0.57 (SD 0.37) mV, risetime: 2.9 (SD 0.9) ms and half width: 28.1 (SD 9.9) ms]. However, some paired recordings from apparently synaptically unconnected type 2 to type 1 neurons revealed very small amplitude uEPSPs when spike-triggered averaging was performed on the traces recorded during the current steps injected to determine firing patterns (Figure 2.5B). This suggests the possibility that these connections may be easily missed because of their small amplitude and/or because of their frequency dependence. Unitary EPSPs from these connections could not be accurately measured and therefore their properties were not further analyzed.

When we considered the overall probability of finding functional connections (revealed either by single spikes as in Figure 4 or by firing pattern steps as in Figure 2.5B), we observed a cell type-specific-dependent organization (Fig 2.5C, $p=0.01$, χ^2). In particular, we estimated the following probabilities for the various types of connections: type 1 homotypic 4.6% (626 tested), type 2 homotypic 5.2% (652 tested), type 1 to type 2 heterotypic 8.7% (286 tested), and type 2 to type 1 2.4% (286 tested).

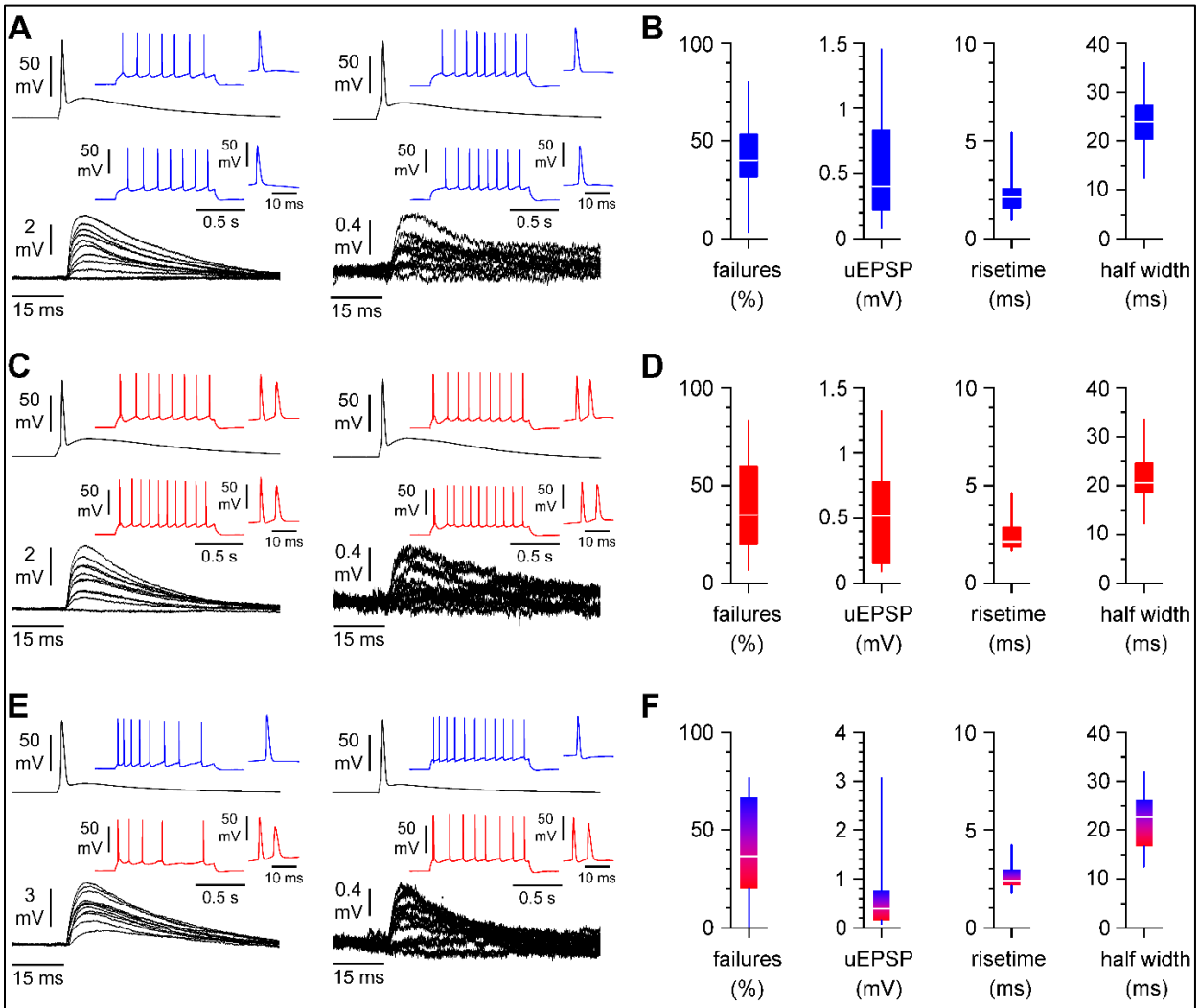

Figure 2.4: Properties of uEPSPs generated by low frequency spikes (0.1 Hz, see Methods for details) in the most commonly encountered connections in subicular local circuits.
A) Homotypic type 1 to type 1 cell connection. Examples of a strong (left) and weak (right) uEPSP. The presynaptic action potential (average of 12 spikes) and postsynaptic responses (12 superimposed traces) are shown in the top and bottom panels, respectively. The insets show the response to depolarizing current injections (blue) used for the classification of the cells, with the initial action potential enlarged in the sub-insets.
B) Summary plots of the failure rate, peak amplitude, 20-80% risetime, and half width of the population uEPSPs.
C), **D)** and **E)**, **F)** Same organization as **A)**, **B)** for uEPSPs recorded between homotypic type 2 and heterotypic type 1 to type 2 connections, respectively.

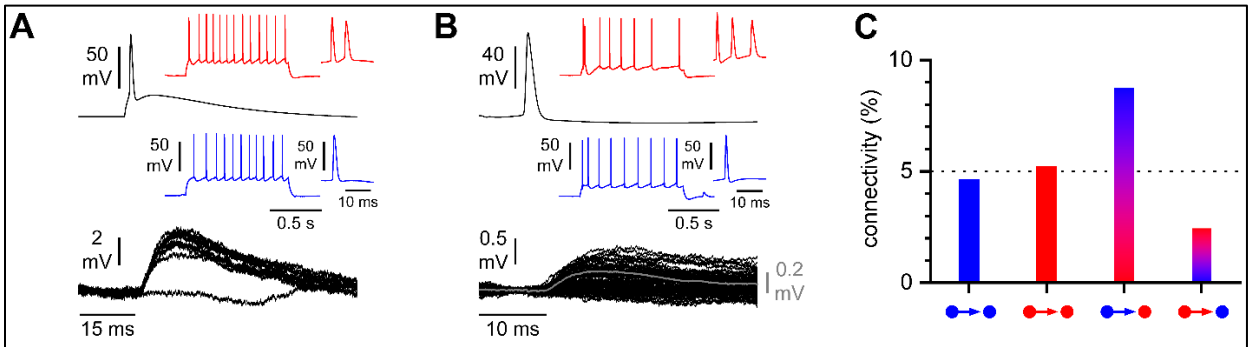

Figure 2.5: Properties of uEPSPs of the rarest connection between type 2 and type 1 cells and overall cell type-specificity of local subicular excitatory circuits.

A) Example of a uEPSP generated by generated by low frequency spikes (0.1 Hz, see Methods for details) recorded between a presynaptic type 2 cell and a postsynaptic type 1 cell. The presynaptic action potential (average of 12 spikes) and postsynaptic responses (12 superimposed traces) are shown in the top and bottom panels, respectively. The insets show the response to depolarizing current injections (red, presynaptic cell and blue, postsynaptic neurons) used for the classification of the cells, with the initial action potential enlarged in the sub-insets.

B) Example of a heterotypic type 2 to type 1 connection revealed by spike-triggered averaging of the action potentials generated by the depolarizing currents used for classification of the cells (see insets and sub-insets with the same color code as in **A**). Top panel: average of presynaptic spikes (n=77). Lower panels: several individual traces (n=77) superimposed (black) and their average (grey).

C) Summary plot of the connectivity probability between different types of cells (blue, type 1 cells and red type 2 cells). Notice the asymmetry in the connectivity between heterosynaptic pairs.

Assuming that type 1 and type 2 cells can be translated into regular firing and bursting neurons, then our results would appear very similar to what was reported by Böhm et al. (2015). The only difference is that we suggest the existence of heterotypic connectivity in both directions, whereas the aforementioned study reported exclusively a strict unidirectional heterotypic connectivity from regular spiking to bursting cells, with no uEPSPs generated by bursting cells onto regular firing neurons.

As whole-cell recordings are susceptible to run-down, which could affect intrinsic properties and the resulting classification as type 1 vs. type 2 neurons, we decided to measure with a combined experimental/modelling approach its potential effect on our connectivity estimates. First, we recorded membrane properties and responses to depolarizing current injections from an additional sample of cell (n=112) immediately after breakthrough and after 10 minutes, which is the maximum length of our physiological experiments. As shown in Figure 2.6A, these neurons were then classified as type 1 or type 2 cells using the same methods described for the pairs tested for connectivity. Although most cells maintained their classification, a small percentage (7.9%) showed a time-dependent loss of its initial type 2 phenotype (Figure 2.6B). This is probably explained by the run-down of the calcium currents underlying bursting (Jung et al., 2001). In contrast, no cell that was initially classified as type 1 transitioned to the type 2 phenotype. We then built a mathematical model (see Methods for details) that allowed us to estimate the confidence intervals of the connectivity for various misclassification rates (Figure 2.6C: experimentally determined α=7.9% and Figure 2.6D from 5% to 35%). As indicated in Figures 2.6C and 2.6D, misclassification (even at high rates) would not completely eliminate the presence of type 2 to type 1 connections, therefore indicating that our observation is unlikely to be due to a run-down artefact, but a real biological phenomenon.

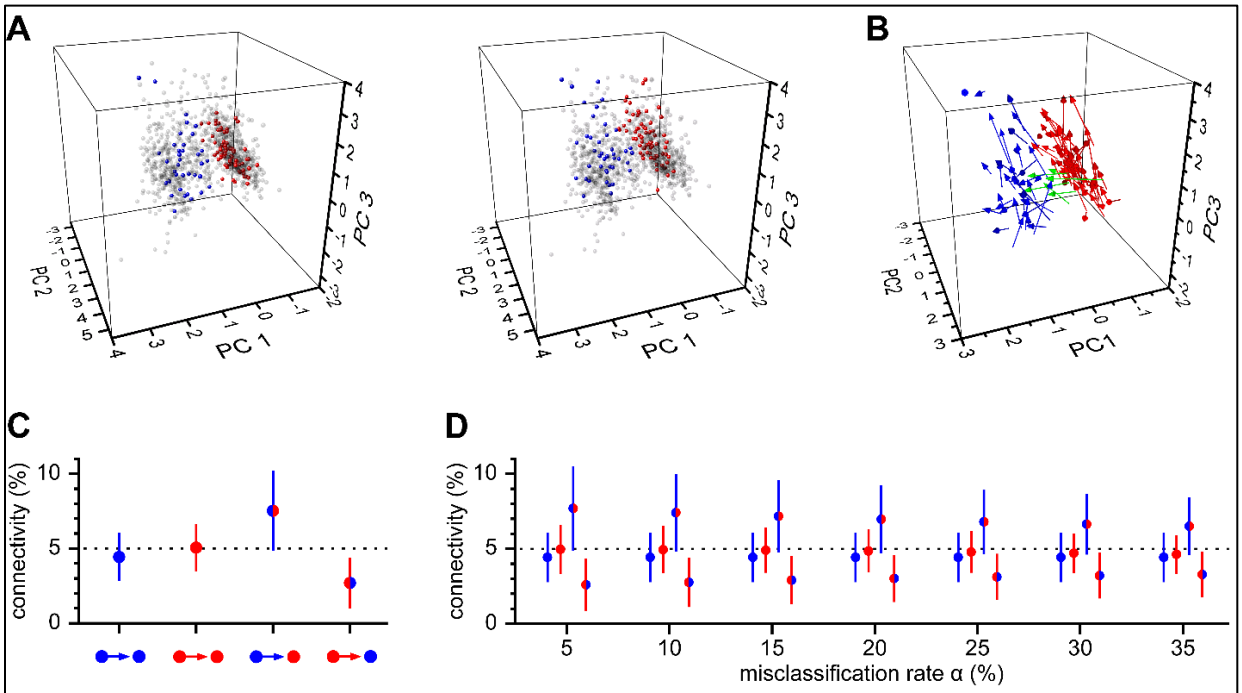

Figure 2.6: Effect of prolonged recording on membrane properties and cellular classification.
A) Left panel: a sample of subicular cells (n=112) recorded immediately after breakthrough and classified as type 1 (blue) or type 2 cell (red) added to the cells used to test for connectivity in Figure 1 (grey, n=995). Right panel: same analysis performed after 10 minutes of recording.
B) The shift of the position of the cells shown in the left and right panels of
A) is indicated by vectors. Blue and red vectors indicate type 1 and type 2 cells maintaining their phenotype, whereas green vectors indicate type 2 cells acquiring type 1 phenotype (n=6 out of 76). Notice that no type 1 neuron transitioned to a type 2 phenotype.
C) Cell type-specific connectivity after correction using the experimentally determined misclassification rate of 7.9%. Circles and bars indicate the estimated connectivity probability and its 95% confidence interval.
D) Plot of the cell type-specific connectivity and 95% confidence intervals after correction for different misclassification rates (5%, 10%, 15%, 20%, 25%, 30% and 35%). Notice that type 2 to type 1 connections persist even at the highest values of misclassification rate.

From a structural point of view, the location of synaptic contacts established by the different subgroups of subicular pyramidal cells is currently unknown. In the hippocampal formation, there are substantial differences between the CA3 and CA1 subfield with connections both on apical and basal dendrites in CA3 (Guzman et al., 2016; Ishizuka et al., 1990), but only on basal dendrites in CA1 (Deuchars and Thomson, 1996; Esclapez et al., 1999). Figure 2.7A, 2.7B and 2.8A and 2.8B show examples of reconstructions obtained from synaptically connected homotypic and heterotypic pairs. We examined areas of overlap between axonal branches of the presynaptic cell and the dendritic arborization of the postsynaptic neuron with the aim of identifying putative synaptic sites. Figures 2.9A, 2.9B and 2.9C show summary plots of all the identified putative contact sites and of the relative position of all presynaptic neurons of the connected pairs to their postsynaptic targets.

The number of putative contact sites found in n=5 homotypic type 1 pairs was 3.0 (SD 2.0), and the vast majority (87%) appeared located on postsynaptic basal dendrites with an overall mean distance of 120 (SD 39) µm from the soma. Similarly, we identified 2.1 (SD 1.1) close appositions in homotypic type 2 connections, located, for the most part, on basal dendrites (84%, mean distance from the soma 97 (SD 40) µm, n=12 pairs). In the case of heterotypic pairs we found 2.2 (SD 1.2) close appositions in type 1 to type 2 connections and 1.0 (SD 0.0) in type 2 to type 1 pairs, with, in both cases, a predominant preference for the basal dendrites of the postsynaptic cell (90% and 100%, respectively). The average distances from the soma were 132 (SD 73) µm and 103 (SD 31) µm, (n=10 and n=3, respectively).

It is also interesting to note, as shown in Figure 2.9C, that presynaptic neurons of connected pairs were located in the more superficial (i.e. closer to the fissure) and proximal (i.e. more towards

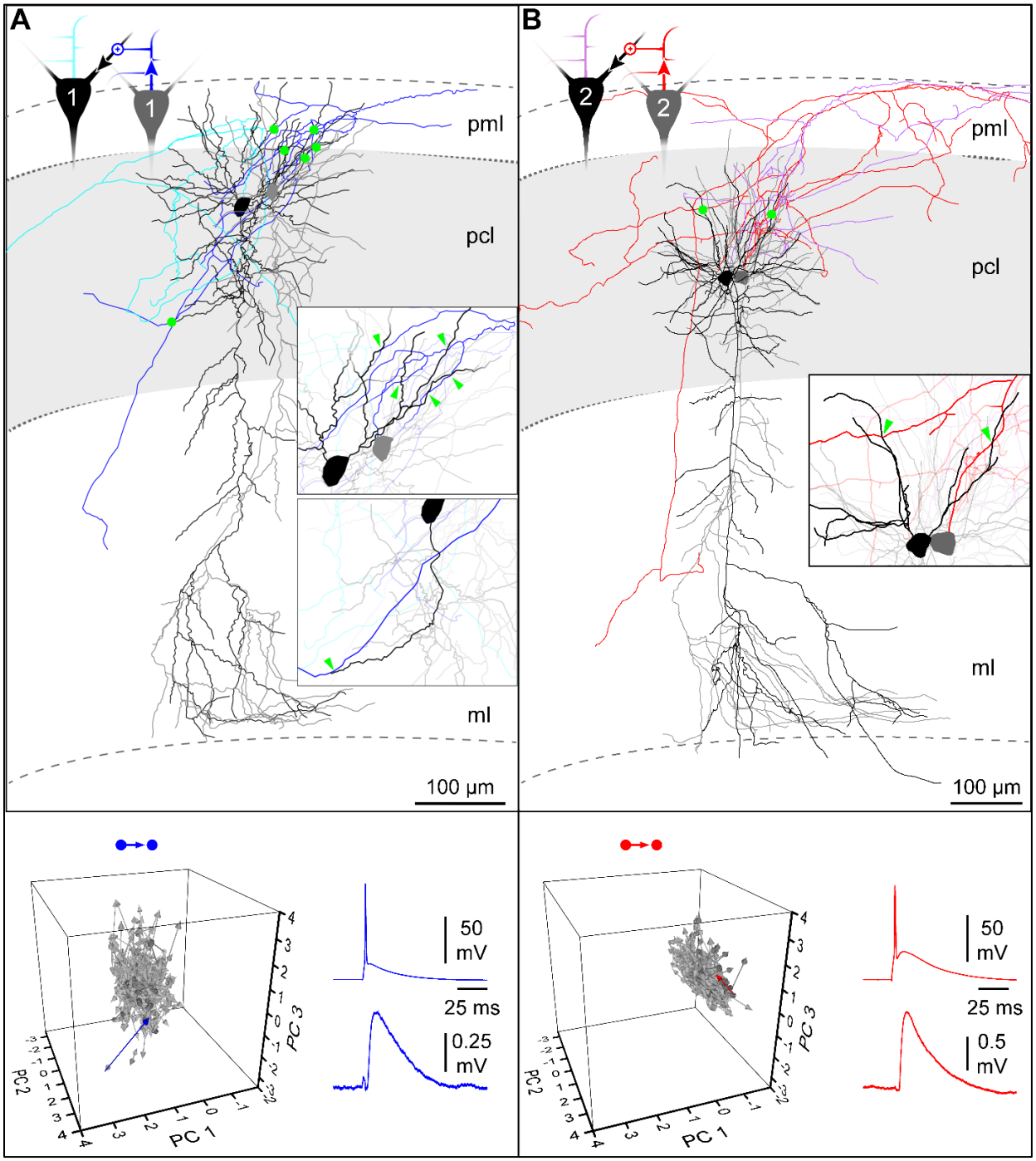
A
1
1
pml
pcl
ml
100 µm
B
2
2
pml
pcl
ml
100 µm
PC 1
PC 2
PC 3
50 mV
25 ms
0.25 mV
PC 1
PC 2
PC 3
50 mV
25 ms
0.5 mV

Figure 2.7: Anatomical properties of homotypic connections.
A) Upper boxed panel: anatomical reconstruction of a type 1 to type 1 connected pair with putative contact sites (green arrowheads). The dendrites of the presynaptic neuron are in light gray and the axon in blue. The postsynaptic neuron is represented with black dendrites and light blue axon. The cartoon in the inset (left upper corner) indicates the relative position of the two cells and the arrow in the axon the direction of the connectivity. The boxed insets to the right show the location of the putative contact sites. Lower panel, left: 3D representation, in the multimedial space of the connection between the reconstructed pair in the upper
panel (blue vector). Gray vectors represent all the homotypic type 1 pairs tested. Right: presynaptic action potential and uEPSP between the reconstructed cells (average of 30 traces).
B) Identical organization as in **A)**, but for a type 2 homotypic connection. Axons are in bright and pale red for the presynaptic and postsynaptic neuron, respectively.

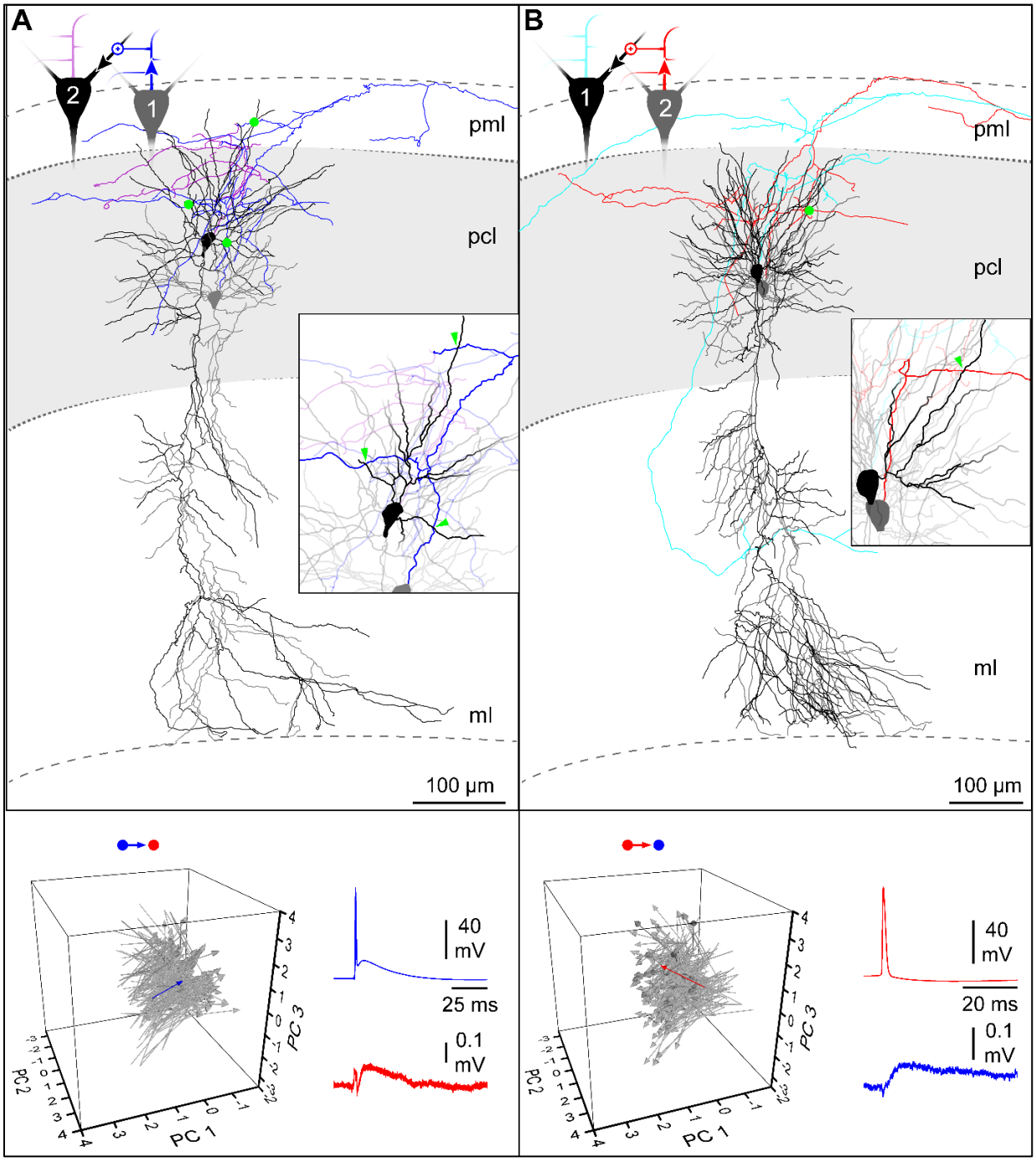
A
B
2
1
pml
pcl
ml
100 µm
40
mV
25 ms
0.1
mV
20 ms
PC 1
PC 2
PC 3

Figure 2.8: Anatomical properties of heterotypic connections
A) Upper boxed panel: anatomical reconstruction of a type 1 to type 2 connected pair with putative contact sites (green arrowheads). The dendrites of the presynaptic neuron are in light gray and the axon in blue. The postsynaptic neuron is represented with black dendrites and pale red axon. The cartoon in the inset (left upper corner) indicates the relative position of the two cells and the arrow in the axon the direction of the connectivity. The boxed inset to the right show the location of the putative contact sites. Lower panel, left: 3D representation, in the multimedial space of the connection between the reconstructed pair in the upper panel (blue vector). Gray vectors represent all the heterotypic type 1 to type 2 pairs tested. Right: presynaptic action potential and uEPSP between the reconstructed cells (average of 30 traces).
B) Identical organization as in **A)**, but for a type 2 to type 1 heterotypic connection. Axons are in bright red and light blue for the presynaptic and postsynaptic neuron, respectively.

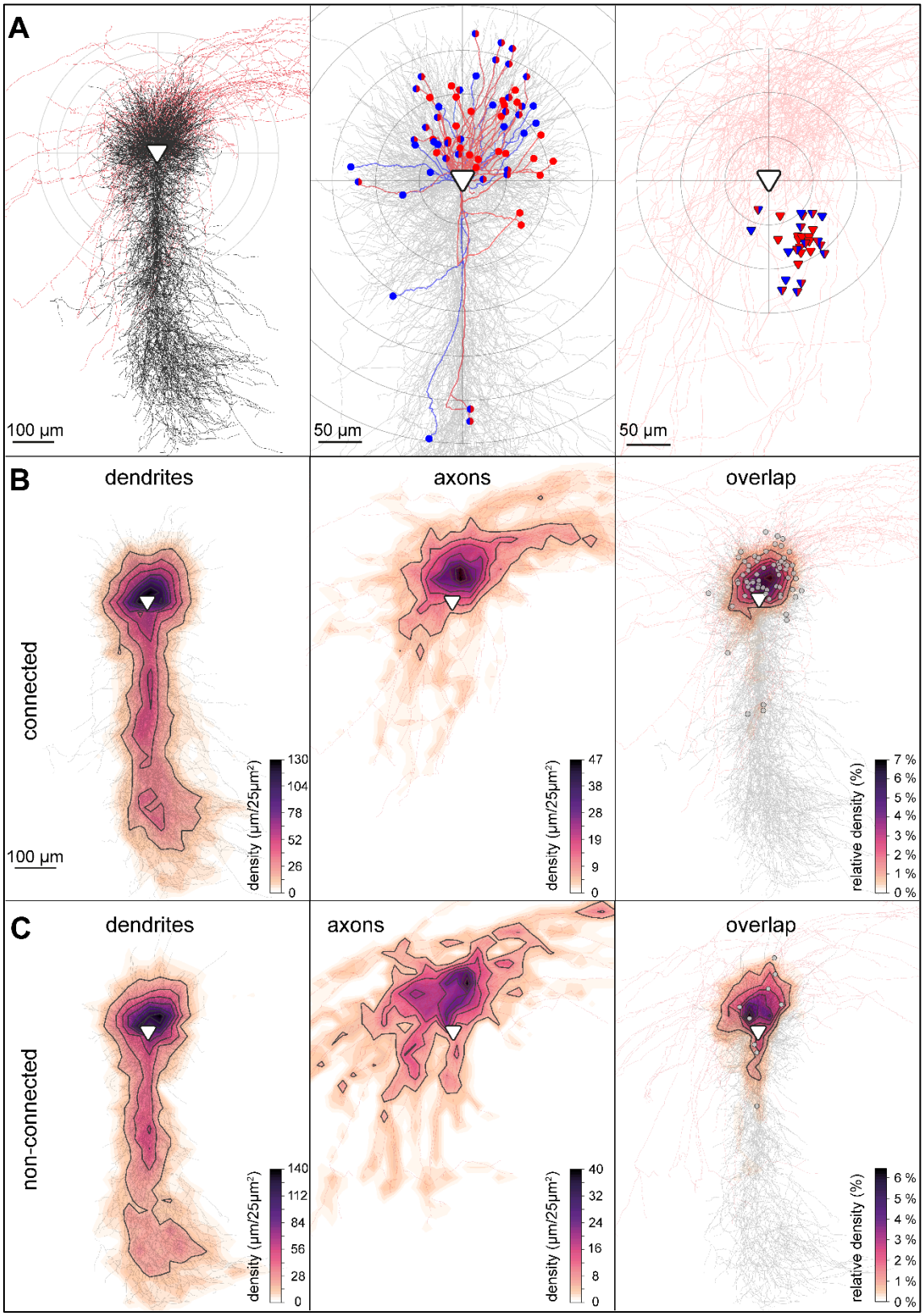
A
100 µm
50 µm
50 µm
B
dendrites
axons
overlap
connected
100 µm
density (µm/25µm²)
130
104
78
52
26
0
density (µm/25µm²)
47
38
28
19
9
0
relative density (%)
7 %
6 %
5 %
4 %
3 %
2 %
1 %
0 %
C
dendrites
axons
overlap
non-connected
density (µm/25µm²)
140
112
84
56
28
0
density (µm/25µm²)
40
32
24
16
8
0
relative density (%)
6 %
5 %
4 %
3 %
2 %
1 %
0 %

Figure 2.9: Biometric properties of connected pyramidal neurons and putative synapses.
A) Left: superimposed images of pre-synaptic axons (red) and post-synaptic dendrites (black) from all reconstructed pairs (n=30); all cells aligned to the post-synaptic soma (white triangle). Middle: light-microscopically identified putative synapses and connected post-synaptic dendritic segments (type 1: blue, type 2: red). The type of synaptic pair is coded by the filled circles (homotypic type 1 connections: blue circles, homotypic type 2 connections: red circles, heterotypic type 1 to type 2 connections: blue-red circles, heterotypic type2 to type 1 connections: red-blue circles). Right: location of pre-synaptic somata (triangles – same color code as in the previous panel) relative to the postsynaptic cell (white triangle).
B) Density plot of post-synaptic dendrites (left: dendrites) and pre-synaptic axons (middle: axons) of functionally connected pairs. Right: calculated axo-dendritic overlap with putative synapses indicated by the grey dots (overlap).
C) Same analysis as in **B)** but performed on non-connected pairs. Notice the lower number of points of background close appositions.

CA1) quadrant relative to their targets ($p<0.01$, χ^2), suggesting a preferential directional bias in the flow of local excitatory connectivity.

We decided to evaluate the degree of reliability for our estimation of putative contact sites (Figure 2.9). First, we calculated density maps for the presynaptic axonal cloud and postsynaptic dendritic tree of functionally connected pairs, and from them obtained a quantitative estimation of their degree of overlap. As shown in Figure 2.9, and as expected, close appositions between the pre- and postsynaptic structures of connected cells were concentrated in the areas of stronger overlap. In total, from 30 functionally connected pairs, we identified 67 putative contact sites for an average of 2.2 putative contacts per functional connection. However, when the same analysis was performed from pairs with no functional evidence of synaptic connections, the number of putative contact sites per cell pair was 0.6, suggesting that ~73% of the putative contact sites were actual synapses and only 27% were false positive results.

Next, we applied another test of our approach based on the knowledge that the spatial location of synaptic contacts has important physiological implications. For example, the cable properties of dendrites (Rall, 1977) may filter events and impact both amplitudes and kinetics of postsynaptic potentials propagating to the soma (Spruston et al., 1994). As shown in Figure 2.10, this was likely the case under our experimental conditions, as a significant correlation between amplitude and risetime of all the uEPSPs recorded was present ($r=-0.29$, $p=0.02$, $n=63$ uEPSPs). Therefore, we reasoned that if our estimated somatic distance of putative contact sites was (even partially) correct, then we would expect to observe a correlation with the measured risetimes of the uEPSPs. As shown in Figure 2.10, this expectation was verified and a significant correlation was found ($r=0.66$, $p=0.00$, $n=22$ uEPSPs), further corroborating the validity of our approach.

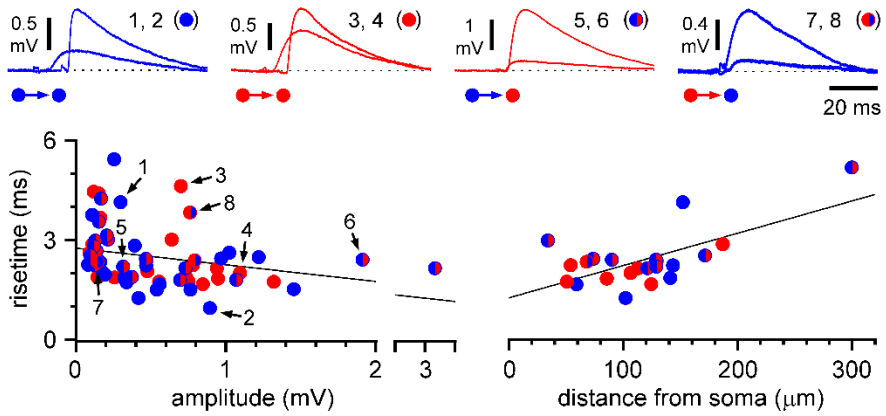

Figure 2.10: Correlation between amplitude and putative synapse location with uEPSP risetime. Left: summary plot showing the correlation between peak of uEPSP and its risetime. Homotypic type 1 connections: blue circles, homotypic type 2 connections: red circles, heterotypic type 1 to type 2 connections: blue-red circles, heterotypic type2 to type 1 connections: red-blue circles. Right: population graph of the correlation between uEPSP risetime and location of putative contact sites. The inset show specific uEPSPs (as indicated by the numbers and arrows) from the different groups of connections (according to the schematics shown by circles and arrows, blue: type 1 neuron and red type 2 cells). Differences in amplitude and kinetics have been highlighted by superimposing pairs of uEPSPs aligned onto their peaks.

So far, our results suggest the existence of a high degree of excitatory local circuit connectivity mostly mediated by synapses on the basal dendrites of pyramidal cells. As discussed above, the subiculum appears to have the highest level of local excitatory interconnectivity compared to other regions of the hippocampal formation. Thus, we decided to directly test whether this can be translated in a propensity for both hyper-synchronicity and hyper-excitability under conditions of impaired GABAergic neurotransmission.

We prepared subicular slices surgically isolated from its main afferents, i.e. the CA1 hippocampus and adjacent cortical areas. (Figure 2.11A). Under these experimental conditions, recorded subicular cells did not show any type of supra-threshold synchronization (n=6 slices, Figure 2.11B). In contrast, when antagonists of $GABA_A$ and $GABA_B$ receptors (gabazine, 12.5 μM and CGP55845, 5 μM) were applied, large synchronous epileptiform events appeared in n=11 out of 13 slices (Figures 2.11C, 2.11D, and 2.11E, p=0.00, χ^2). These events were quite variable and

produced 28 (SD 23) spikes at a frequency of 58.9 (SD 40.1) Hz (n=24 cells recorded in whole-cell mode and 3 in cell-attached configuration from 11 slices). Their duration was 735 (SD 697) ms and their overall strengths, quantified as the integral of membrane voltage in time was 20.1 (SD 14.7) V*ms (n=24, in the 3 cells recorded in cell attached configuration these measurements could not be made). Thus, under reduced conditions as in a mini-slice, subicular local excitatory circuits appear to be sufficient to integrate intrinsic excitability and produce population discharges. In order to further explore the potential differential contribution of type 1 and type 2 pyramidal cells to these hyper-synchronous events, we carried out similar experiments preceded by current step injections before the addition of gabazine so that the recorded pyramidal cells could be classified as type 1 or type 2 (Figures 2.12A, 2.12B, 2.12C, 2.12D, 2.12E, 2.12E, 2.12F and 2.13A and 13B). We analyzed the population events (Figures 2.12B, 2.12D and 2.12F) according to the pyramidal cell subtype (Figures 2.12A, 2.12C, and 2.12E), as determined by PCA GMM-BIC analysis (Figure 2.13A). No differences were noticed (Figure 2.13B) either in their overall strength [16.1 (SD 12.4) V*ms vs. 18.0 (SD 14.6) V*ms for type 1 (n=22) and type 2 (n=38) cells, respectively, p=0.54] or duration [909 (SD 620) ms vs. 862 (SD 592) ms for type 1 (n=21, the presence of a cell generating single-spike events prevented the calculation of duration) and type 2 (n=38) cells, respectively, p=0.98].

In contrast, cell type-specificity was revealed (Figure 2.13B) in the number of action potentials produced [17 (SD 15) spikes vs. 26 (SD 19) spikes for type 1 (n=22) and type 2 (n=38) cells], and in their frequency [27.5 (SD 14.4) Hz vs. 47.7 (SD 38.4) Hz for type 1 (n=21, the presence of a cell generating single-spike events prevented the calculation of frequency) and type 2 (n=38) cells, respectively, p=0.00]. Lastly, when we compared (within pairs of simultaneously recorded neurons) the difference in timing between the first spikes of the population event, we also

noticed cell type-specific differences. The first action potentials in type 2 neurons occurred within 1±4 ms (Δ latency, n=28 pairs), compared to 20±6 ms (n=5 pairs) and 10±7 ms (n=17 pairs) for type 1 and type 1/type 2 double recordings (p=0.03).

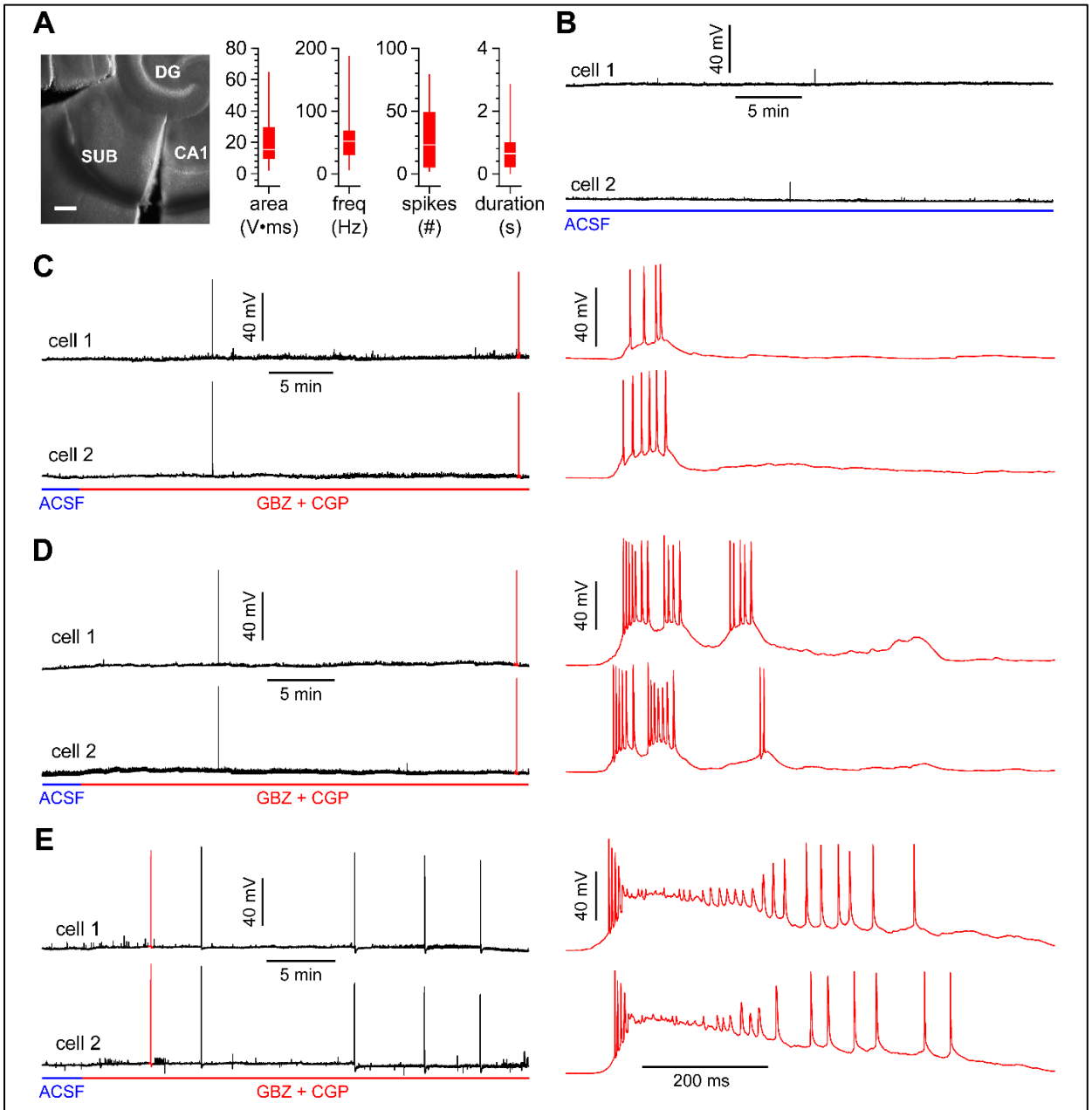

Figure 2.11. Epileptiform activity sustained by local excitatory circuits in subicular mini slices.
A) Left: micrograph of a subicular mini slice. Notice the surgical cuts isolating the subiculum both from the hippocampal CA1 subfield and the adjacent cortex. Right: summary plots of the properties of supra-threshold synchronous events recorded in six double and five triple recordings from n=11 slices exposed to gabazine (12.5 µM) and CGP55845 (5 µM).
B) Example of a control experiment showing the lack of supra-threshold epileptiform activity in mini slices exposed to drug-free ACSF. Simultaneous recording from two subicular pyramidal neurons (cell 1 and cell2).
C-E) Left: examples of synchronous epileptiform discharges in slices exposed to blockers of GABA receptors. The discharges highlighted in red are shown at expanded time scale to the right.

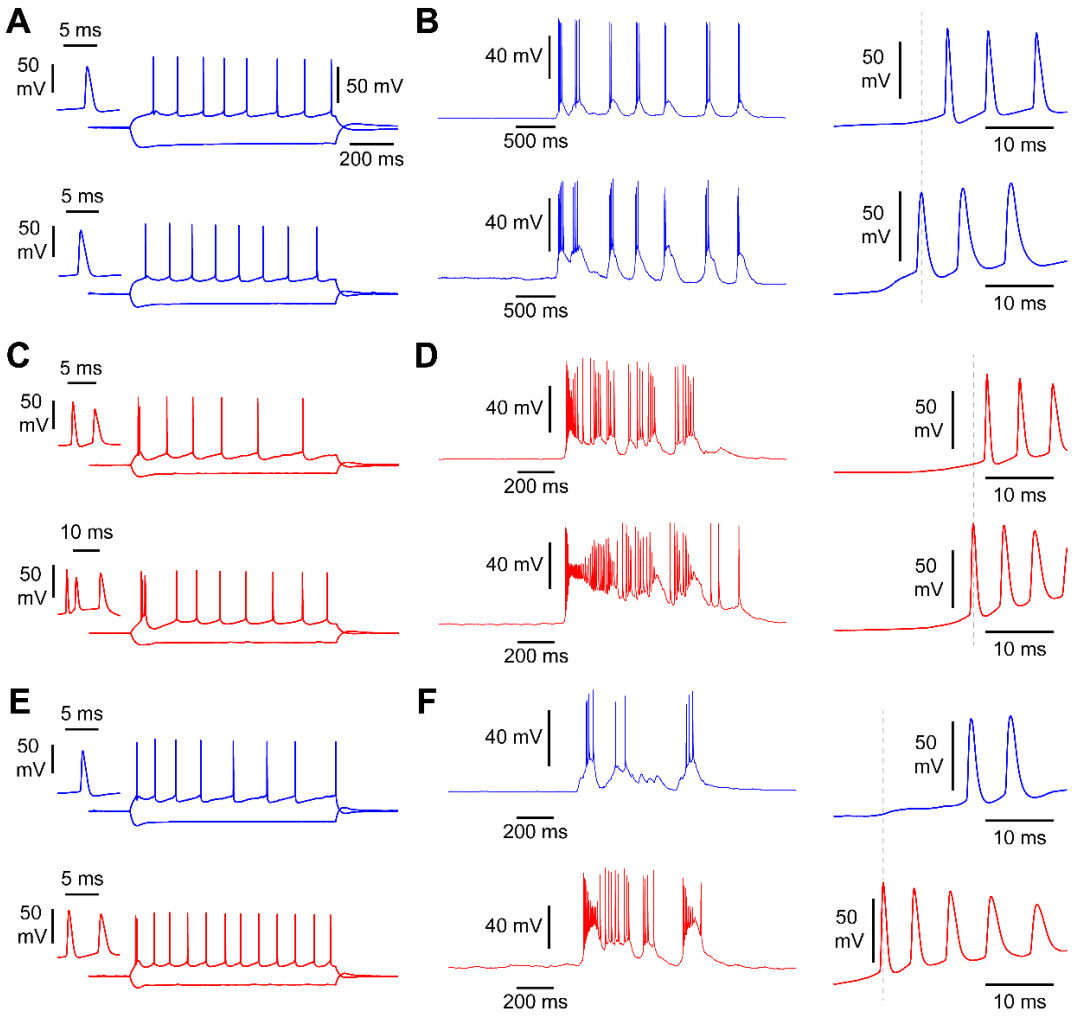

Figure 2.12. Spike timing of epileptiform activity in type 1 and type 2 subicular cell recorded in mini slices. Examples from different combinations in simultaneous recordings.
A) Membrane properties and firing patterns of a homotypic type 1 cell pair following current injection (blue traces). Insets show the first action potential generated by the positive current step.
B) Same pair as in **A)** in the presence of gabazine (12.5 µM) and CGP55845 (5 µM). Left panel: overall view of a synchronized event. Right panel: temporally expanded view of the initial firing. Notice the time difference between the first spikes in the two cells. Vertical black dotted line indicates the peak of the action potential of the earliest firing cell of the pair for reference.
C-F) Identical to **A)** and **B)** in a homotypic type 2 cell pair (red traces) and in heterotypic type 1/type 2 pair (blue and red traces, respectively). Notice the reduced number of action potentials in the type 1 compared to the type 2 cell in the mixed pair.

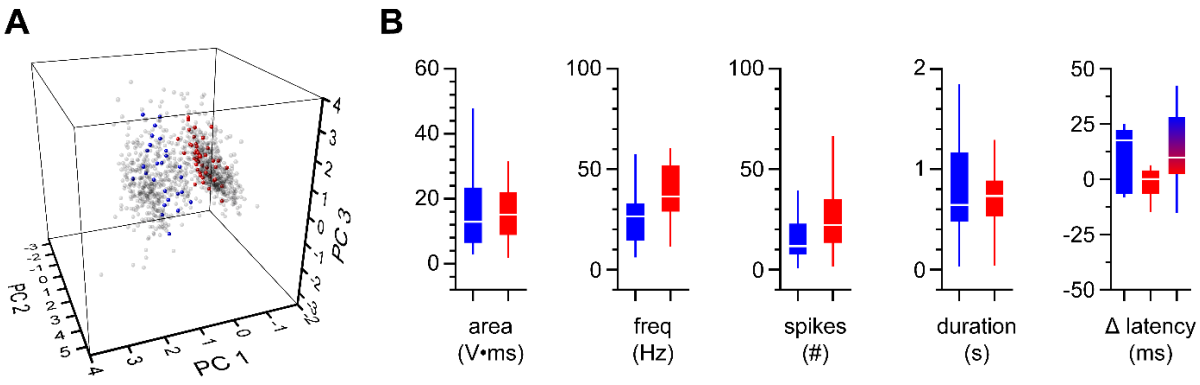

Figure 2.13: Cell type-specific properties of epileptiform activity in disinhibited subicular mini slices.

A) Subicular cells (n=60) classified at the beginning of the experiment as type 1 (blue) or type 2 cell (red) with the cells used to test for connectivity in Figure 1 in the background (grey, n=995).

B) Summary plots for different parameters of the epileptiform events (from left to right: area, spike frequency, number of spikes, event duration and time difference between the first spikes of events in double simultaneous recordings). The values for type 1 and type 2 cells are shown in blue and red respectively. Δ latency values measured in type1 and type 2 homotypic pairs are shown in blue and red, respectively. Mixed double recordings of type 1 and type 2 cells are shown by the blue-red box.

Discussion

A quantitative, objective approach to classification of pyramidal neurons

There is abundant evidence for a functional diversity in subicular pyramidal neurons. Several studies in a variety of animal models have shown subicular pyramidal neurons fall into different groups, as defined by their firing pattern in response to a current injection. Most commonly, they are classified as either burst-firing or regular-spiking, although some subclassification might also be possible. However, the methods used in past studies to classify subicular pyramidal neurons 1) have not been consistent and 2) rely on subjective classification criteria (see Introduction for specific classification criteria). In our work, we have attempted to remove as much subjectivity as possible, relying on PCA and GMM to objectively classify subicular pyramidal neurons into groups, type 1 and type 2. While the classification groups resulting from our analysis of n = 995 neurons strongly overlapped with the classically described burst-firing and regular-spiking groups, anatomical differences seen between reconstructed type 1 and type 2 neurons corroborates the validity of the approach.

To date, only a single study has addressed how the excitatory neurons in the subiculum are connected with each other. Indeed, our results match closely with this study with only small apparent differences. The Bohm et al study used a similar paired recording approach as we have, and the amplitude and kinetics of their connections match well with what we have observed. Their group saw both types of homotypic connections, but, unlike our work, they only saw one of the possible heterotypic connections (burst to regular). Several possible explanations exist for this relatively minor difference. Firstly, our classification methods were different. They used a more subjective classification criteria (at least 3 spikes, ISI of <8 ms) to group their cells in contrast to

our PCA and GMM approach. Therefore, it is possible that their classification might not have classified what we call type 2 neurons as bursting cells, and a connection between what appeared to them to be a regular spiking neuron to a regular spiking neuron might have actually been a bursting to a regular spiking neuron. They also did not include neurons in their analysis where the firing pattern was *not* easily discernible, while our classification methods were able to divide all of the cells of our sample population into separate groups based on BIC. Additionally, the strength of synaptic connections in the subiculum appears to be highly variable, ranging from several millivolts to a few hundred microvolts. This variability potentially reflects the impact of several physiological factors, such as the variable distances from the soma of the synapse at which the event originates, the current dynamic plastic state of the synapse and the probability of release at the synaptic site. A number of the type 2 to type 1 connections that we observed were only detectable through spike triggered averaging at high firing frequencies, and it is possible that their stimulation intensity was not high enough to detect these small amplitude connections.

It is also possible that misclassification of neurons could occur if the firing pattern of a burst-spiking neuron "runs-down" and starts to appear as a regular spiking neuron. Burst spiking is thought to be driven by a calcium tail current, generating an afterdepolarization that drives the neuron back to threshold and generates a burst. However, during prolonged recordings, the currents underlying this ADP could be diminished, potentially due to dialyzing out enzymes that maintain the phosphorylation dependent activity of the channel (Kostyuk et al., 1981). If this happened during our recordings, cells that our PCA and GMM approach classify as type 1 cells might actually be type 2 cells. Indeed, experimental testing of this hypothesis suggested that about 7.9% of type 2 cells might have been misclassified as type 1 cells. Interestingly, this paradoxically strengthens the notion that type 2 to type 1 heterotypic connections are not an artifact of run-down.

We modeled increasing percentage of misclassification and found that even as our misclassification rate increased, so too does the estimated connection probability of the heterotypic connection in question. The reason for this is, as misclassification increases, the estimated connection probability from type 1 to type 1 connections shifts as a consequence of some of these type 1 neurons being misclassified, paradoxically increasing the likelihood of finding a type 2 to type 1 connection. Our modeling suggests that the heterotypic type 2 to type 1 connection does exist and is not the result of neuronal misclassification.

Anatomical locations of local excitatory connectivity

A primary structural difference contrasting the subiculum with the hippocampus is the lack of defined pyramidal cell layers in the subiculum. While pyramidal cells in the CA subfields are geometrically aligned in distinct layers, pyramidal neurons in the subiculum are scattered, making predictions of where the synaptic contacts mediating these excitatory connections are located difficult. In CA3, for example, the axons of principal neurons ramify in both the stratum oriens and the radiatum, overlapping with the basal and apical dendrites of pyramidal cells in the respective layers (Ishizuka et al., 1990). Paired recordings of CA3 pyramidal neurons followed by complete reconstructions revealed that putative synaptic connections between excitatory neurons were located about equally on apical and basal dendrites (Guzman et al., 2016). Similar experiments on CA1 pyramidal neurons, where axons ramify mostly in the stratum oriens (Esclapez et al., 1999), revealed excitatory connections mediated by synaptic connections restricted to basal dendrites.

The non-aligned spatial distribution of pyramidal cells coupled with the large spread of their local axon hinders any prediction as to what dendritic compartment will be favored for

synaptic contact sites. Our data from functionally connected synaptic pairs suggest that pyramidal neurons in this area form synapses preferentially, but not exclusively, on basal dendrites. This arrangement appears to be intermediate between CA3 (equal basal and apical synapse distribution), and CA1 (exclusively basal distribution). Basal and apical dendrites are increasingly becoming recognized as having different properties that may underly complex signaling mechanisms. The domain-specific segregation of local inputs in the subiculum may reflect the physiological matching between specific presynaptic terminals and post-synaptic dendritic properties.

The role of excitatory circuits in epileptiform activity

Subicular neuronal circuits have been repeatedly implicated in the initiation of epileptiform activity in both human epileptic tissue (Cohen et al., 2002, Wozny et al., 2005, Huberfeld et al., 2007, Alvarado Rojas et al., 2015, Wang et al., 2017) and in animal models of TLE (Fujita et al., 2014, Toyoda et al., 2015). Inter-ictal activity has been shown to depend on the interplay of both glutamatergic and excitatory GABAergic signaling (Cohen et al., 2002). Pre-ictal activity, most often associated with the transition from inter-ictal to ictal states, was suggested to result from local glutamatergic signaling. Our studies have directly tested the hypothesis that subicular excitatory circuits are sufficient to generate synchronous epileptiform events in network states where inhibitory signaling is compromised. By physically cutting neighboring input regions, we have assured any recorded activity is resulting from neuronal connections within the subiculum. Our data show that pharmacologically suppressing GABAergic signaling is sufficient to induce synchronous epileptiform discharges in the isolated subiculum and that these events are mediated by the excitatory connections between pyramidal cells. Inhibitory circuits have been suggested to reduce the propensity for bursting in subicular pyramidal cells following antidromic stimulation.

Additionally, suppressing $GABA_A$ receptors influences the propensity of bursting cells. It is possible that pre-ictal events are locally generated in the subiculum, and when coupled to incoming extra subicular excitatory inputs (Benini and Avoli, 2005), can pre-dispose the network to explosive ictal discharges. Both burst-firing and regular spiking neurons project to the entorhinal cortex, and this positive feedback between the highly interconnected subiculum and entorhinal cortex might be required to generate full-blown ictal events. Additionally, as chapter 3 highlighted, excitatory activity in the subiculum might be amplified by the resulting depolarizing GABA signaling that has been observed in human TLE tissue (Cohen et al. 2002; Huberfeld et al. 2007, 2011; Wang et al. 2017).

An interesting finding from our work is that, although type 1 and type 2 pyramidal cells are recruited during these synchronous discharges in disinhibited subiculum slices, the timing of action potential occurrence during these events is different. Type 1 cells fire at lower frequencies and generate fewer temporally precise action potentials compared to type 2 cells. This has interesting implications for the timing of propagation of these events to their specific target regions. The proximal and distal subiculum generate outputs via distinct classes of neurons, but a lack of GABAergic inhibition, as has been suggested to occur during pre-dictal activity (Huberfeld et al. 2011), may result in a complex pattern of activity, leading to mixed population discharges mediated by subicular pyramidal cells. The cell type-specific synaptic output associated with these events would be predicted to be temporally with respect to the first action potential and shaped by different pre-synaptic spike numbers and frequencies. The resulting pathological signaling in the presence of GABAergic disinhibition would deviate significantly from what was reported by Bohm et al. (2015), where they saw bursting and regular spiking neurons participating differently (active vs silent) during network oscillations.

Chapter 3. Impaired KCC2 function triggers interictal-like activity driven by PV+ interneurons in the subiculum

Adapted from: Anstötz M*, Fiske MP*, Maccaferri G (2021). *In preparation*.

*Equal contributors

Introduction

Accumulating evidence suggests a critical role of subicular circuits (Lévesque and Avoli, 2002) in the initiation and propagation of interictal and ictal discharges in human patients(Cohen et al., 2002; Wozny et al., 2005; Huberfeld et al., 2007; Huberfeld et al., 2011; Alvarado-Rojas et al., 2015) and animal models(Fujita et al., 2014; Toyoda et al., 2015; Wang t al., 2017) of temporal lobe epilepsy (TLE).

In particular, the reduced expression of the KCC2 transporter in the subiculum (importantly, not in other regions of the surviving hippocampal formation (Hubferfeld et al., 2007; Palma et al., 2006; de Guzman et al., 2006) has been highlighted as a potential key epileptogenic step for the progression of the disease (Mules et al., 2012). Reduced KCC2 function is associated with the emergence of pathological network patterns, such as subicular-initiated interictal activity (Cohen et al., 2002; Buchin et al., 2016), interictal-ictal transitions (Huberfeld et al., 2011) and generalized convulsions (Wang et al., 2017).

So far, no study has directly examined whether reducing activity of KCC2 in subicular networks is, by itself, sufficient to trigger epileptiform activity or other epilepsy-related changes are necessary. This is an important point required to qualify subicular KCC2 down-regulation as a truly independent epileptogenic change. Although experiments using the selective KCC2 blocker

VU0463271 (Delpire et al., 2012) have highlighted the importance of KCC2 as a regulator of hyperpolarizing GABAergic signaling (Sivakumaran et al., 2015; Otsu et al., 2020), the ability of this drug to generate epileptic-like activity in vitro remains unclear. VU0463271 failed to originate epileptiform activity in naive slices (Sivakumaran et al., 2015; Kelley et al., 2016) despite being sufficient to alter it in tissue pre-exposed to a variety of convulsants (Sivakumaran et al., 2016; Kelley et al., 2016; Hamidi et al., 2015; Chen et al., 2019). Furthermore, interpretations of the aforementioned studies are also complicated because the effect of KCC2 blockade was not limited to the intrinsic subicular circuitry, as it would be required to mimic the subiculum-specific impairment of KCC2 function reported in epileptic tissue. Here, we have directly addressed this point by exposing isolated subicular slices of non-epileptic animals to VU0463271 and by studying the cellular mechanisms underlying the ensuing epileptiform activity.

In particular, we have focused on the role of a major class of GABAergic interneurons, PV-expressing fast spiking (PV^+) cells (Hu et al., 2014). We have quantified their morphofunctional characteristics, postsynaptic domain-specific connectivity and network roles during VU0463271-induced epileptiform discharges. We have found that pharmacological inhibition of KCC2 profoundly alters synaptic signaling of subicular PV^+ cells to the point that their activity becomes sufficient to initiate network bursts with physiological and pharmacological properties similar to what has been described for interictal events in human epileptic tissue. In contrast, reducing their firing decreases the frequency of the observed interictal-like discharges. Importantly, as we used slices from non-epileptic animals, no functional or structural epilepsy-related changes other than reduction of KCC2 function and PV^+ cell firing were required to produce interictal-like events. Thus, our results from a reduced animal model in vitro support the idea that the deafferentation-induced KCC2 down-regulation described in tissue from patients

suffering from TLE indeed has causal epileptogenic effects, which are mediated by altered PV^{+} cell signaling at critical perisomatic postsynaptic target domains.

Materials and methods

Ethical Approval

All experimental procedures used in this study were approved by the Institutional Animal Care and Use Committee of Northwestern University and complied with animal guidelines provided by the National Institutes of Health.

Animals

Mice were obtained from The Jackson Laboratory. In particular, the following strains were used: PV-cre (stock #008069), Thy1-cre (stock #006143), tdTomato^{flox} (stock #007909), ChR2(H134R)-EYFP (Stock #012569), ArchT-EGFP^{flox} (stock #021188), and GCaMP6s^{flox} (stock # 024106). Appropriate crossing of the aforementioned cre and floxed lines resulted in animals conditionally expressing tdTomato (PV-tdTomato), ChR2(H134R)-EYFP (PV-ChR2-EYFP), ArchT-EGFP (PV-ArchT-EGFP, and GCaMP6s (Thy1-GCaMP6s). Animals were housed on a 14/10 light/dark schedule with *ad libitum* access to food and water. Both male and female mice were used for the experiments.

Histology

PV-tdTomato (age P15-P60), PV-ChR2-EYFP (age P30), and PV-ArchT-EGFP (age P30) mice were anesthetized by intraperitoneal injection of Euthasol ® (calculated to yield a dose of pentobarbital of 300 mg/kg of bodyweight), and perfused with 0.9% NaCl saline followed by 4% paraformaldehyde (PFA) in 0.1M phosphate buffer (PB), pH 7.4. After perfusion, brains were extracted from the skull and transferred in fixative solution at 4°C for at least 24h. Transverse

hippocampal sections were cut serially at 50µm thickness on a Leica VT 1000 vibratome and collected free-floating in 0.01M Phosphate buffered Saline (PBS).

Immunohistochemistry

Slices were pre-incubated free-floating in a blocking solution containing 5% normal goat serum (NGS), 1% bovine serum albumin (BSA) and 0.2% Triton X-100 in PBS for 1h at room-temperature (RT). Afterwards, they were incubated free-floating in the same solution containing the primary antibodies (all 1:500, see below) at 4°C overnight. The primary antibodies used for the experiments of the main text were: mouse anti-NeuN (Abcam catalog #104224) and rabbit anti-KCC2 (Thermo Fisher Scientific Cat# PA5-78544, RRID: AB_2735976), mouse anti-Parvalbumin (Swant Cat# 235, RRID:AB_10000343). Please see Supplementary Methods for a list of the primary antibodies used for the experiments of Supplementary Figure 1. In the next step, slices were washed 3x15 min with fresh PBS and then incubated free-floating in a solution of 5% NGS, 1% BSA in PBS, containing secondary antibodies (all 1:500) at RT for 1 h. The secondary antibodies used for the experiments of the main text were (see Supplementary Methods for a list of the secondary antibodies used for the experiments of Supplementary Figure 1): Alexa Fluor 488 goat anti-mouse IgG (Thermo Fisher Scientific Cat# A-11001, RRID:AB_2534069), Alexa Fluor 488 goat anti-rabbit IgG (Thermo Fisher Scientific Cat# A-11034, RRID:AB_2576217), Alexa Fluor 568 goat anti-mouse IgG (Thermo Fisher Scientific Cat# A-11004, RRID:AB_2534072). Finally, slices were washed 3x15 min with fresh PBS with the second washing step containing DAPI (1:100 000, LifeTechnologies, #62249) and then mounted and coverslipped using Mowiol mounting medium.

Confocal Microscopy

Confocal microscopy image stacks were captured using a Nikon A1R confocal microscope. Multichannel fluorescence images were saved individually for analysis and merged together for co-localization studies using the ImageJ software suite.

Recovery of Biocytin-Filled Cells and Reconstructions

Biocytin-filled neurons were fixed in 4% PFA in 0.1M PB at 4°C for at least 24 h. Endogenous peroxidase activity was quenched with a 3% H_2O_2 solution for 15 min. Sections were incubated overnight at 4°C in avidin-biotinylated-HRP complex (Vectastain ABC Elite kit) with 0.1% Triton X-100 in PB, followed by a peroxidase reaction with DAB tetrahydrochloride as a chromogen. Cells were revealed by adding 0.025% H_2O_2, and the reaction was stopped when dendritic and axonal processes were clearly visible under light microscopy examination. After several washing steps in 0.1M PB, slices were postfixed with 0.1% OsO_4 in PB (1–2 min), and then mounted on slides with Mowiol (Hoechst AG, Frankfurt AM, Germany). Cells were reconstructed using a NEUROLUCIDA-based station and software.

Acute slice preparation

Mice (P21-P30) were deeply anesthetized with isoflurane in an induction chamber containing a separating platform to avoid direct contact between the animals and the anesthetic. After decapitation, the brain was carefully removed and glued to a specimen block in a chamber filled with cooled artificial cerebrospinal fluid (ACSF) with the following composition (in mM): 130 NaCl, 24 NaHCO3, 3.5 KCl, 1.25 NaH2PO4, 1 CaCl2, 2 MgSO4, 10 glucose, saturated with 95% O2, 5% CO2 at pH = 7.4. Transverse sections (400 µm) of an entire brain hemisphere containing

the hippocampal formation were cut using a vibrating microtome (Leica VT 1200 S, Leica Biosystems). Slices recovered at 30-32°C for at least 30 min and were then stored at room temperature until use. Subicular mini slices were prepared from regular slices by severing the connections between the subiculum and CA1 hippocampal subfield/entorhinal cortex as in Fiske et al.[24] Cuts were performed at locations with clear scatter of pyramidal cell bodies and with unambiguous widening of the pyramidal cell layer.

Electrophysiological recordings and analysis

General*:* Slices were transferred to a recording chamber positioned under a direct microscope (Scientifica) equipped with oblique illumination optics (Olympus) and an infrared camera system (VX-45, TILL Photonics). Cells were visualized using a 60x infrared water-immersion objective. Slices/mini slices were superfused with preheated ACSF (31-33°C, TC-324B, Warner Instruments) with the following composition (in mM): 130 NaCl, 24 NaHCO3, 3.5 KCl, 1.25 NaH2PO4, 2 CaCl2, 1 MgCl2, 10 glucose, saturated with 95% O2, 5% CO2 at pH 7.4.

Pipettes were pulled from thin borosilicate capillaries (Prism FLG15, Dagan Corporation, Minneapolis, MN, USA) with a resistance of 3-5 MΩ when filled with an internal solution containing the following for current clamp (in mm): 115 K-methylsulfate, 10 KCl, 5 creatine phosphate, 5000 units creatine kinase, 4 ATP-Mg, 0.3 GTP-Na3, 16 KHCO3, 0.25% biocytin equilibrated with 95% O2–5% CO2 at pH 7.3. Voltage clamp recordings were performed with an internal solution containing the following (in mm): 125 CH3CsO3S, 16 KHCO3, 4 ATP-Mg, 0.3 GTP-Na, 10 QX-314, 0.25% biocytin equilibrated with 95% O2–5% CO2 at pH 7.3 Recordings were performed using a Multiclamp 700 amplifier (Molecular Devices). Series resistances were balanced via a bridge circuit in current-clamp configuration and measured in voltage-clamp

recordings (17.4±8.5 MΩ, mean±SD, n=18). Signals were filtered at 3 KHz and digitized at a minimum of 20 KHz using a Digidata 1550A and the Clampex 10 program suite (Molecular Devices) was used for the analysis of membrane properties and action potentials.

Paired recordings: Simultaneous double and triple whole-cell recordings were performed with the postsynaptic pyramidal cell held in voltage clamp at +10 mV and the presynaptic PV^+ interneuron in current clamp. The interneuron was stimulated every 10 s with a 1 ms supra-threshold current injection to elicit a single action potential. Unitary inhibitory postsynaptic currents (uIPSCs) were identified by the presence of short-latency responses to the presynaptic action potential. For each connection identified (n=28), several uIPSCs (n=10) were collected and averaged, and the resulting average was measured and analyzed. Amplitude, half-width, and 20-80% rise time were estimated using the Clampfit 10 program (Molecular Devices). Latency was measured manually from the peak of the action potential in the interneuron to the onset of the uIPSC in the pyramidal neuron. Putative failures were identified visually.

Optogenetic stimulation*:* Control of cellular population expressing opsins [either ChR2(H134R)-EYFP or ArchT-EGFP] was achieved by exposing the slice to flashes of blue light of appropriate duration (either 1 ms or 15 s) generated by a collimated LED (460 nm, Prizmatix) attached to the epifluorescence port of the direct microscope. Light flashes were directed to the microscopic field via a mirror coupled to a 60× objective (1.0 numerical aperture).

Analysis of VU0463271-dependent epileptiform activity: These experiments were performed on surgically isolated subicular slices. For time course experiments, large amplitude events were selectively detected using the Strathclyde Electrophysiology Software (courtesy of Dr John Dempster, University of Strathclyde, Glasgow, UK), setting a threshold of 20X the standard deviation of a one-minute control period in the absence of the drug. All other VU0463271-related

experiments (without time course) were performed on slices showing spontaneous activity after pre-incubation in 10 µM VU0463271 at 30°C for at least 30 minutes. Electrical activity recorded in cell-attached or whole-cell configuration was measured using the Clampex 10 program suite (Molecular Devices).

Linear and non-linear fits*:* Linear and allometric fits were performed by Origin 2020b using the following equations: $y=a+b*x$ (linear) and $y=a*x^b$ (allometric).

Calcium Imaging and analysis

Images were acquired with a Scientifica Slice Scope equipped with an Olympus XLUMPlanF L N 20x/NA 1.0 lens. A collimated LED (460 nm, Prizmatix) used as an excitation source coupled to a GFP filter set (excitation band: 469 ± 17.5 nm; emission band: 525 ± 19.5 nm; dichroic reflection/transmission band 452–490 nm/505–800 nm; Thor labs). LED-generated flashes (50 ms duration) at 10 Hz were synchronized with the acquisition of emitted fluorescence by a Zyla sCMOS 4.2 camera (Andor). Data files were imported and analyzed using the µManager[25] and imageJ software packages. First, background and bleaching were corrected by subtracting a duplicate with a gaussian blur filter from the recording. Then, individual cells as regions of interests were outlined and their intensity over time measured. The intensity profile of each cell in a slice was normalized from 0 (minimal intensity) to 1 (maximal intensity). Peaks were detected and analyzed using the Peak Analyzer function of Origin 2020b. Cross Correlations were performed by comparing a cells intensity profile with the average intensity profile of all the cells of interest in the slice.

Morphological parameters (maximum cells distance, nearest neighbor distance and convex hull area) were analyzed using a custom Visual Basic (Microsoft) script. Probability maps of convex

hull contours were obtained by aligning them to their center of gravity and rotation. A 25 µm by 25 µm grid was used to measure different levels of enclosing probabilities and was displayed as a contour-plot.

Experimental design and statistical analysis

Data are presented in the text as mean±SD. Box plots in the illustrations show the median as middle dash, average as empty circle, lower and upper quartiles as upper and lower box borders, and minimum and maximum values as whiskers. Bands in time course plots figures are mean±SE. Statistical comparisons used two-sided non-parametric tests (two independent samples: Mann-Whitney; two paired samples: Wilcoxon signed rank; >2 groups paired samples, one-way repeated measures ANOVA on ranks with Bonferroni post-hoc adjustment). Significance was accepted at the level of $p < 0.05$. Probability values in the text are rounded to the third decimal place. Effect sizes are reported in the text as Cohen's d (d_{Cohen})[26] and were estimated following Lenhard and Lenhard.[27] Analysis was performed using the following software: Origin 2020 (OriginLabs), MS Excel (Microsoft), pClamp (Molecular Devices LLC) and the Strathclyde Electrophysiology Software (courtesy of Dr John Dempster, University of Strathclyde, UK). Blinding was not required as experiments were from a single group.

Drugs

VU0463271, gabazine, and NBQX were purchased from Tocris (Minneapolis, MN, USA). VU0463271 was prepared as a 10 mM stock solution in DMSO and used in experiments at 10 µm. Gabazine was prepared as a 25 mM stock solution in water and used in experiments at 12.5 µm. NBQX was prepared as a 100 mM stock solution in DMSO and used in experiments at 20 µm.

Aliquots were stored at -20°C prior to use. DMSO (0.1%) was also included in control solutions when experiments involved VU0463271.

Data Availability

Source data are contained in the main text and supplementary material and are available from the authors upon reasonable request.

Results

In order to mimic the effect of a subiculum-specific reduced function of the KCC2 transporter, we applied the selective blocker VU0463271 (10 μM) to slices with the subiculum surgically isolated from its hippocampal and cortical afferents, as previously described (Fiske et al., 2020). We recorded from simultaneous triplets (n=11) and pairs (n=1) of subicular pyramidal neurons (total=35 neurons) under whole-cell conditions. As shown in Figure 3.1, drug-treated slices slowly developed spontaneous network-driven, large-amplitude (threshold > 20x SD of baseline) synaptic events, which were not observed in tissue not exposed to the blocker (n=4 pairs and 8 triple recordings for a total of 32 cells).

The frequency of the events detected during the first five minutes following VU0463271 application [0.0±01 events/min (mean±SD)] was not different from to the one measured during the same time window in control slices [0.0±0.1 events/min (mean±SD), p=0.90, U=566, Z=0.12272, d_{Cohen}=0.03, Mann-Whitney test, two-sided]. In contrast, when we compared values at a later time (five minute period following thirty minutes of drug application) we found a clear significant difference [3.2±3.6 events/min (mean±SD) in treated tissue vs. 0.1±0.1 (mean±SD) events/min in control slices, p<0.001, U=220, Z=-4.46001, d_{Cohen}=1.3, Mann-Whitney test, two-sided).

Although this indicates that reduced KCC2 activity in the isolated subiculum is sufficient to trigger hyper-synchronization, most of these large-amplitude events remained subthreshold. We interpreted this apparently puzzling observation as the consequence of our recording conditions (whole-cell configuration), based on low-chloride containing pipettes (10 mM, see Material and Methods for details). We reasoned that the large volume of intracellular solution contained in the patch electrode would easily dialyze the cytoplasm of the recorded neuron. Therefore, despite the

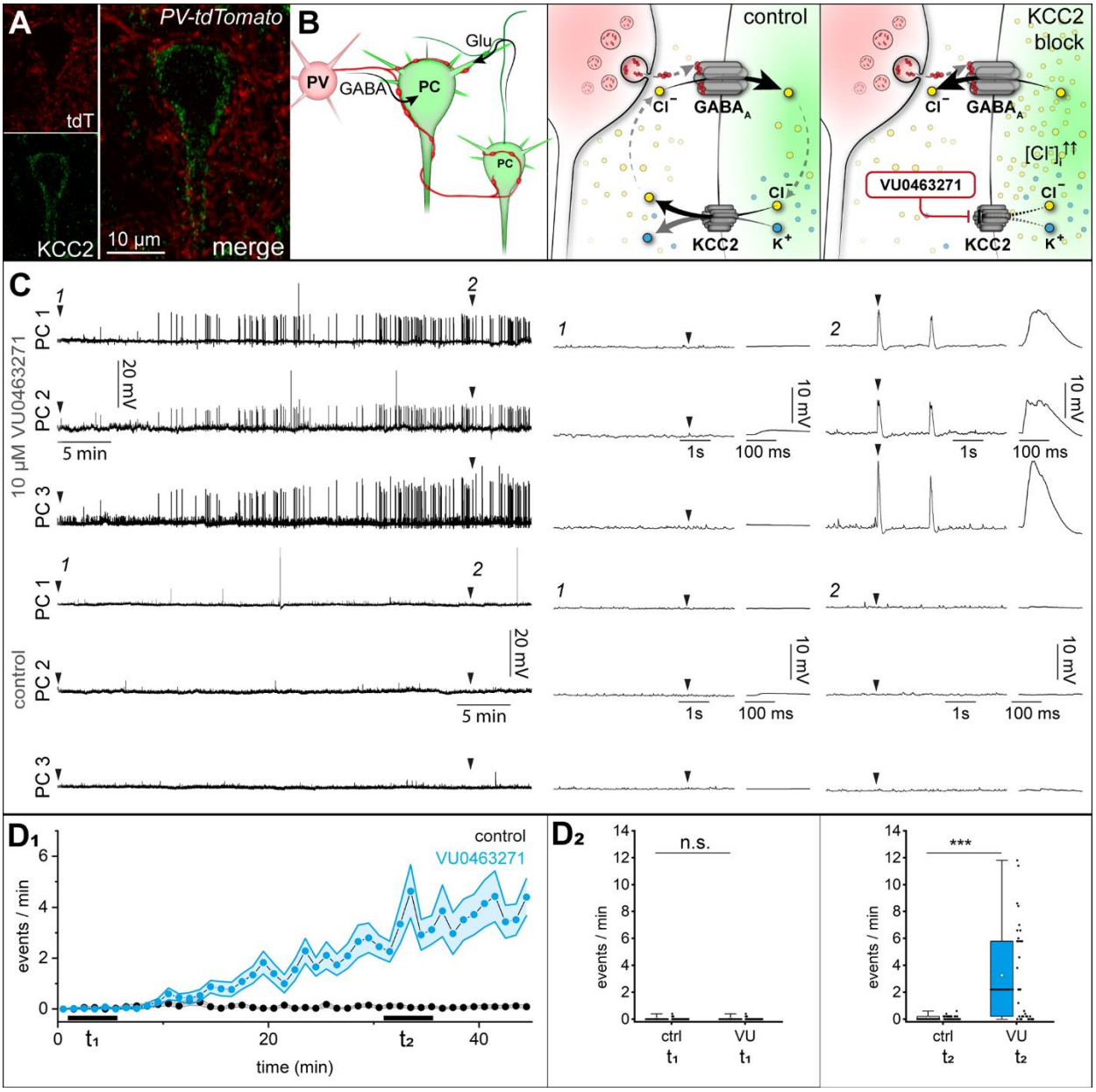
A
PV-tdTomato
tdT
KCC2
10 µm
merge
B
Glu
PV
GABA
PC
PC
control
Cl⁻
GABA_A
Cl⁻
KCC2
K⁺
KCC2 block
Cl⁻
GABA_A
[Cl⁻]_i ↑↑
VU0463271
Cl⁻
KCC2
K⁺
C
10 µM VU0463271
control
PC 1
PC 2
PC 3
20 mV
5 min
1
2
10 mV
1s
100 ms
D1
control
VU0463271
events / min
time (min)
t1
t2
D2
n.s.
***
ctrl
VU
t1
t2

Figure 3.1: Anatomical properties of heterotypic connections
Effects of pharmacological block of KCC2 on population network activity in isolated subicular slices.
A) Confocal image showing tdT^+ terminals (red) surrounding the KCC2-immunoreactive soma (green) and proximal dendrite of a pyramidal cell. Left, the signals for tdT^+ (top) and KCC2 labeling (bottom) are shown separately. Right, overlapped image.
B) Simplified cartoons illustrating the essential circuitry involved in the experiment and its proposed mechanistic explanation (i.e. increase of intracellular chloride concentrations following KCC2 block and change in $GABA_A$ receptor mediated signaling from hyper- to depolarizing). PV, parvalbumin-expressing tdT^+ interneurons; PC, pyramidal cell, $GABA_A$, $GABA_A$ receptor, KCC2, K-Cl cotransporter KCC2.
C) Selective time-dependent development of large-amplitude (>20XSD, see Methods for details) compound excitatory postsynaptic potentials in slices exposed to VU463271 (10 µM, top three traces shown from left to right at different time scales) compared to slices exposed to vehicle (bottom three traces shown from left to right at different time scales). PC1, PC2, and PC3 indicate the activity from different pyramidal cells of the triple recordings. 1 and 2 indicate the expanded sections of the leftmost traces. Notice the presence of large events only in the presence of the drug.
D1) Summary time course plots comparing the frequency of large (>20 X baseline SD) events in the presence (blue circles and light blue band, mean±SE) vs. absence of the blocker (black circles, and light grey band, mean±SE). VU463271 was applied after one minute in drug-free solution and maintained for the rest of the experiment.
D1 and **D2**) Box plots comparing the frequency of large events occurring during the same time windows (t1, t2: black bars in C) in slices exposed (VU) or not exposed to the drug (ctrl). n.s.=not significant, ***=$p<0.001$. Individual data points are shown at the right of the box charts.

pharmacological blockade of KCC2 activity, dialysis would set a low intracellular chloride concentration. However, this effect would not impact the non-recorded neurons of the slice, which would remain fully exposed to the consequences of KCC2 block (Figure 3.2). If our explanation is correct, we predicted that application of VU0463271 would be able to generate supra-threshold events in neurons studied under cell-attached configuration, where dialysis of the cytoplasm does not occur. As expected, when we recorded from n=28 neurons (n=4 triples, n=6 pairs and n=4 singles) in slices pre-incubated with VU0463271 for 40 minutes, we observed synchronous supra-threshold epileptiform activity (Figure 3.2), reminiscent of the one originally described in human epileptic subicular slices. The number of spikes/event was 2.5±1.0 (mean±SD), with an average interspike interval within every epileptiform event of 7.7±2.0 ms (mean±SD), event duration of 14.3±8.2 ms (mean±SD), and interevent interval of 2.9±1.8 s (mean±SD). In a subset of recordings (n=20 cells), we were able to compare the occurrence of supra-threshold events in cell-attached (30±13 events/min, mean±SD) vs whole-cell configuration (0±1 events/min, mean±SD) in the same recorded neurons ($p<0.001$, Wilcoxon signed rank test, two-sided) and thus confirm our hypothesis that whole-cell configuration is the reason for the lack of firing. When recorded under whole-cell conditions from slices similarly pre-exposed to VU0463271, the peak of the collected events was 7.8±3.2 mV, their risetime 10.3±3.1 ms, their half width 41.3±8.1 ms, and their interevent interval 2.1±1.4 s, respectively (mean±SD, n=4 triple, n=4 double and n=6 single recordings for a total of n=26 neurons). These properties (large amplitude and slow kinetics) further corroborate their network-driven origin.

We confirmed and expanded this finding by taking advantage of calcium imaging, which allows the simultaneous monitoring of activity in a larger number of cells compared to

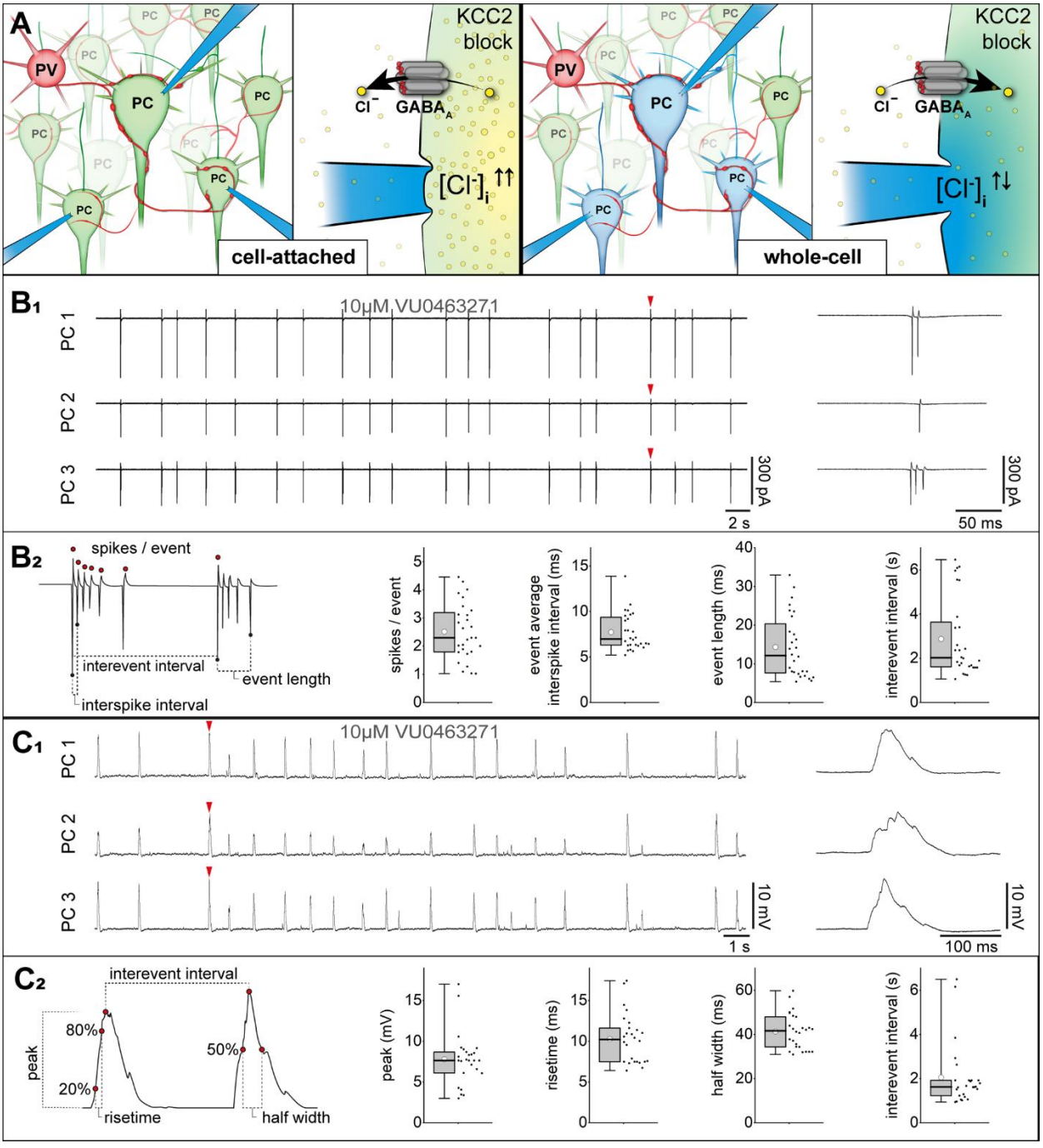
A
PV
PC
KCC2 block
Cl⁻
GABA_A
[Cl⁻]_i ↑↑
cell-attached
[Cl⁻]_i ↑↓
whole-cell
B1
10μM VU0463271
PC 1
PC 2
PC 3
300 pA
2 s
50 ms
B2
spikes / event
interevent interval
event length
interspike interval
spikes / event
event average interspike interval (ms)
event length (ms)
interevent interval (s)
C1
10μM VU0463271
10 mV
1 s
100 ms
C2
interevent interval
peak
80%
20%
50%
risetime
half width
peak (mV)
risetime (ms)
half width (ms)
interevent interval (s)

Figure 3.2: Preserving vs. manipulating the physiological dynamics of intracellular chloride concentration determines whether exposure of slices to VU0463271 triggers supra- or sub-threshold activity in the recorded neurons.
A) Schematic cartoons highlighting the differences imposed by cell-attached (left) vs whole-cell recording configuration (right). Under cell-attached configuration, pharmacological inhibition (KCC2 block) of the KCC2 membrane transporter affects intracellular chloride dynamics leading to an increased internal concentration [Cl^-] in every neuron of the network (including the cells monitored by the electrodes, a triple recording in the example). Physiological dynamics are indicated by the green/yellow color of the cytoplasm. The magnified view of the experimental configuration highlights that, following the elevation of the intracellular [Cl^-], the net current via $GABA_A$ receptors becomes inward (i.e. net movement of chloride ions to the outside, arrow) in resting neurons. In contrast, during whole-cell recordings, the large volume of solution contained in the recording pipette clamps the intracellular [Cl^-] to the same level of the pipette. Under these conditions, the impact of KCC2 inhibition on the intracellular chloride dynamics does not occur in the recorded neurons and the net current via $GABA_A$ receptors remains outward (i.e. net movement of chloride ions to the outside, arrow) at rest. Thus, network events may have opposite contribution of $GABA_A$ receptor activity in the recorded neurons, but not in the remaining cells of the slice.
B1) Example of the spontaneous activity observed under cell-attached recording configuration in a triple recording from a slice pre-exposed (at least 30 min) and still in the presence of VU0463271 (10 μM). PC1, PC2, and PC3 indicate the traces from the different pyramidal neurons. Notice the presence of time locked rhythmical supra-threshold burst events in all the recorded cells (shown at higher temporal magnification in the right inset).
B2) Quantification of VU0463271-induced activity. Left: schematic illustrating the measured parameters. Right: Summary box plots and individual data points for (left to right) the number of spikes/event, event average interspike interval, event length and interevent interval.
C1) As in B1), but in whole-cell configuration. Notice the presence of sub-threshold large amplitude events (shown at higher temporal magnification in the right inset). Notice their complex shape indicative of compound synaptic transmission.
C2) Left, measured parameters. Right, summary graphs for peak amplitude, risetime, half width and interevent interval.

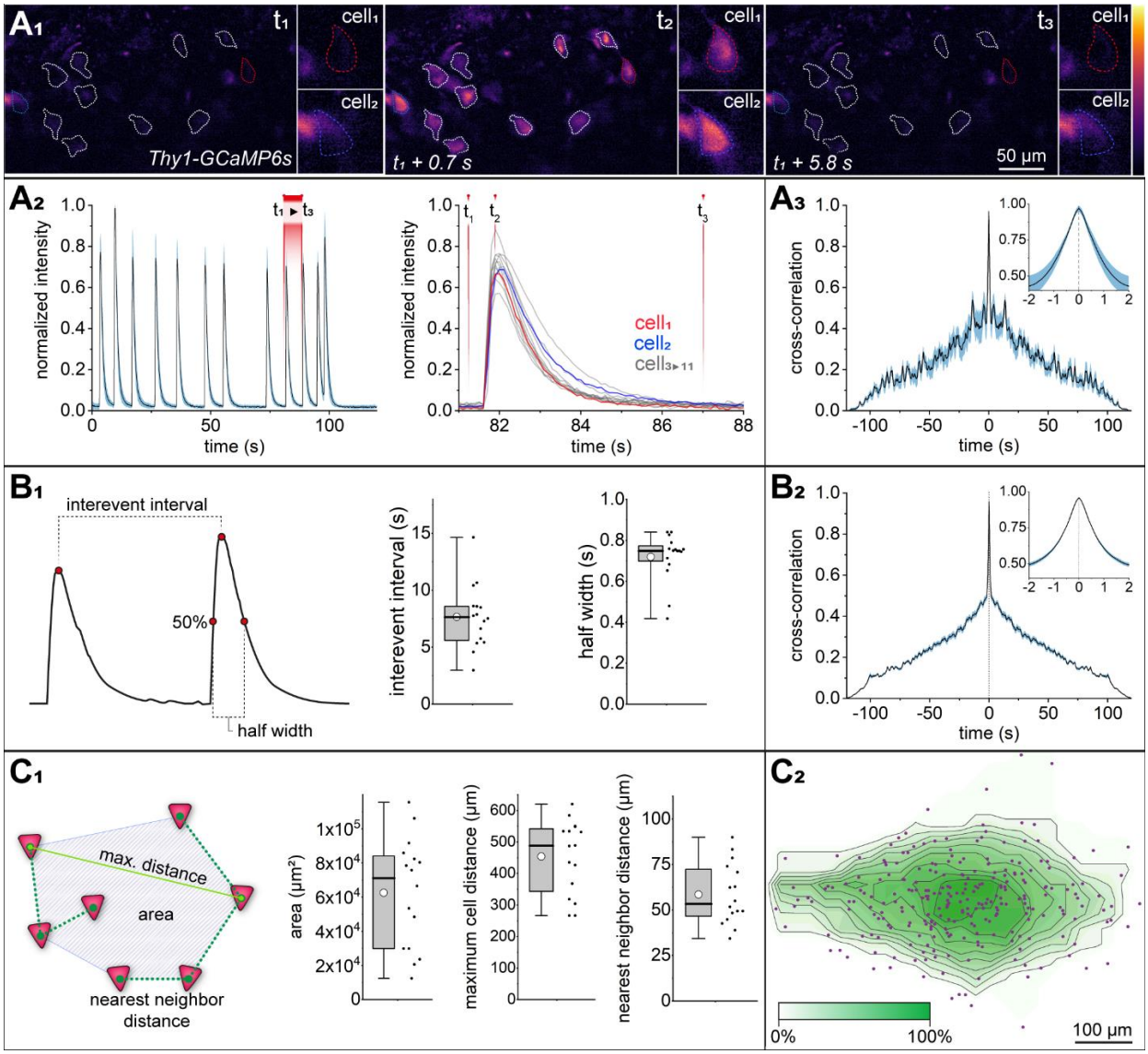
A1
t1
t2
t3
cell1
cell2
Thy1-GCaMP6s
t1 + 0.7 s
t1 + 5.8 s
50 µm
A2
normalized intensity
time (s)
cell1
cell2
cell3▸11
A3
cross-correlation
time (s)
B1
interevent interval
50%
half width
interevent interval (s)
half width (s)
B2
cross-correlation
time (s)
C1
max. distance
area
nearest neighbor distance
area (µm²)
maximum cell distance (µm)
nearest neighbor distance (µm)
C2
0%
100%
100 µm

Figure 3.3: Synchronous calcium transients in clusters of neurons from isolated subicular slices exposed to VU0463271 (10 µM).
A1) Left, pseudo-colored images collected before (t1, left), at the peak (t2, middle) and after return to baseline (t3, right) of the calcium transient. Notice the simultaneous activation of several cells. Insets show two individual cells (cell 1 and cell 2) at increased magnification.
A2) Left, spontaneous rhythmic calcium signal shown as mean±SE of all cells in the cluster of interest. The transient identified by the red bar (between t1 and t2) is shown in more detail to the right for all cells of the measured cluster (cell1 to cell11). Signals from cell 1 and cell 2 (insets of panel A1) are shown in red and blue, respectively. Singals from the remaining cells are in grey.
A3) Mean±SE of all the cross-correlation of each individual cell in the cluster with the average signal. The inset show an expanded view at shorter time lags. Notice the high synchronicity of the events.
B1) Properties of the calcium transients. Left, schematic of the measured indexes. Right, summary plots for interevent intervals and half widths.
B2) Summary graph (mean±SE) of all the averaged cross-correlations for all the imaged slices.
C1) Left, cartoon showing the parameters measured in the cell clusters. Right, Population graphs and indivudal data points for all the quantified indexes in the imaged clusters (area, maximum cell distance and nearest neighbor distance).
C2) Comparison of the density probability of the convex hull area of the imaged cluster (green contour plots) to the density probability of axonal length. The green areas and their borders indicate the probability of including clusters (see Methods for details), the red dotted lines mark the at 50% and 90% limits of the axonal density probability as shown in Figure 2.

electrophysiology and does not interfere with intracellular chloride concentrations. Figure 3.3 shows an example of the local activity of a cluster of eleven pyramidal neurons in an isolated subicular slice prepared from a Thy1-GCaMP6s mouse exposed to 10 µM VU0463271. The peak of the mean cross-correlation of each individual neuron with the average of all the signals was 0.988±0.007 (lag 0.0±0.0 s, n=11 cells), indicating their tight synchrony. The interevent interval was 7.7±2.8 s (mean±SD) and the overall peak cross-correlation and lags were 0.960±0.054, (n=16 clusters), respectively. We defined the spatial properties of clusters of coactive subicular pyramidal cells in n=16 slices by calculating their projected convex hull areas (62567±32114 μm^2, mean±SD), nearest neighbor and maximal cell distances (59±17 µm and 454±117 µm, respectively, mean±SD).

Thus, the functional block of KCC2 activity in isolated subicular networks is sufficient to generate synchronized excitatory events resembling interictal activity. When studied in subicular human tissue from epileptic patients, interictal-like events have a specific pharmacological profile requiring both GABAergic and glutamatergic transmission (Cohen et al., 2002). For comparison, we decided to explore the nature of the synaptic activity underlying VU0463271-induced events revealed by our experimental conditions. As shown in Figure 3.4, blocking either $GABA_A$-type or AMPA-type receptors almost completely suppressed their occurrence. In fact, the addition of the $GABA_A$ receptor antagonist gabazine reduced the frequency of large spontaneous events from 2.8±4.3 events/min (mean±SD) to 0.3±0.4 events/min (n=15 triples and n=1 pair for a total of 47 neurons, $p<0.001$, W=524, Z=4.34709, $d_{Cohen}=1.64$, Wilcoxon signed rank test, two-sided), and the inclusion of the AMPA-type glutamate receptor antagonist NBQX decreased it from 2.7±2.8 events/min to 0.1±0.2 events/min (n=3 triples and n=4 pairs for a total of 17 cells, p=0.001, W=105, Z=3.27245, $d_{Cohen}=2.61$, Wilcoxon signed rank test, two sided). Interestingly, in the

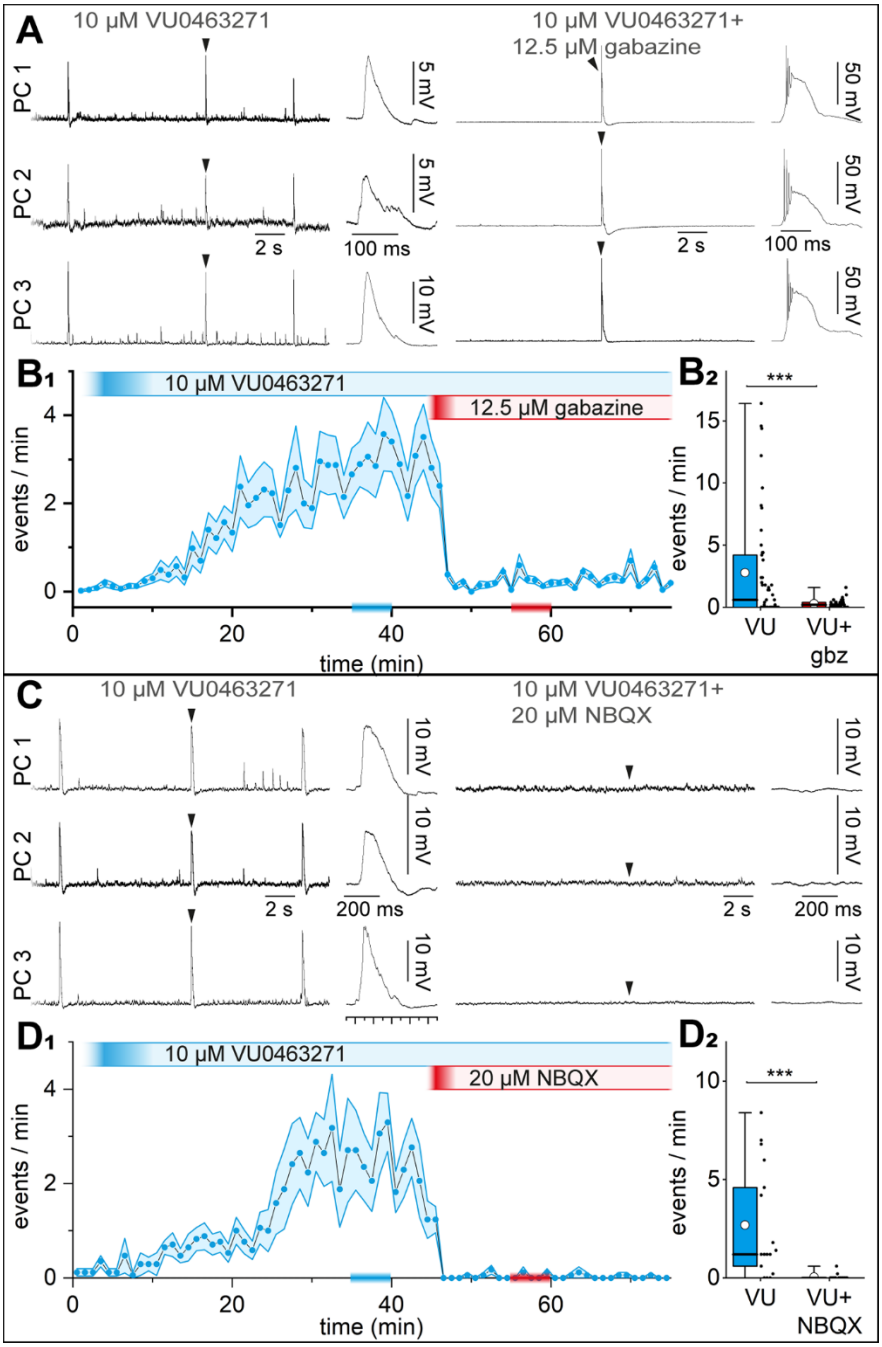
A
10 µM VU0463271
10 µM VU0463271+
12.5 µM gabazine
PC 1
PC 2
PC 3
5 mV
50 mV
10 mV
2 s
100 ms
B1
10 µM VU0463271
12.5 µM gabazine
events / min
time (min)
B2
***
VU
VU+
gbz
C
10 µM VU0463271
10 µM VU0463271+
20 µM NBQX
200 ms
D1
20 µM NBQX
D2
NBQX

Figure 3.4: VU0463271-induced network events require both GABAergic and glutamatergic synaptic transmission.
A) Traces from a triple recording under whole-cell recording conditions in the presence of VU0463271 (10 µM, left) and after the addition of gabazine (12.5 µM). PC1, PC2, and PC3 indicate the different pyramidal cells of the triple. Events indicated by the black arrowhead are shown at magnified temporal scale in the insets. Notice that gabazine dramatically reduced event frequency and transformed the few residual events from sub-threshold EPSPs into bursts.
B1) Summary plot of the time course of several experiments (mean±SE). Notice the slow development of large events similar to Figure 5 and the dramatic decrease in frequency following $GABA_A$ receptor inhibition.
B2) Summary box plots and individual data points comparing the frequency of the events in VU0463271 (VU) and after the addition of gabazine (VU+gbz). ***= $p<0.001$.
C), **D1)** and **D2)** Same organization as in A), B1) and B2), but for experiments testing the effect of blocking glutamatergic synaptic transmission via NBQX (20 µM). Notice the almost complete disappearance of the events.

presence of VU0463271 and gabazine, the very rare residual events became supra-threshold paroxysmal depolarizing shifts, similar to what has been described in isolated subicular preparations exposed to $GABA_A$ and $GABA_B$ receptor antagonists in the absence of VU0463271 (Fiske et al., 2020). In contrast, this transformation was not observed in the presence NBQX.

Taken together, these results suggested that the application of VU0463271 to naïve isolated subicular circuits in vitro is capable of producing spontaneous synchronous events with physiological and pharmacological hallmarks resembling the interictal-like events reported in human epileptic tissue studied in vitro (Cohen et al., 2002). Moreover, the fact that we were able to observe epileptiform activity following exposure of non-epileptic slices to VU0463271 suggests the possibility of taking advantage of this model in vitro to test the role played by specific neuronal types.

In particular, we decided to investigate the involvement of PV^+ interneurons because of their special role in the control of cellular excitability and synchronization (Hu et al., 2014). In order to manipulate PV^+ cells, we took advantage of the PV-cre mouse line established by Hippenmeyer et al. to label this class of interneurons with tdTomato (tdT) and/or control them via excitatory/inhibitory opsins (ChR2 and ArchT mice, respectively, see Methods section for their detailed definitions). However, as off-target recombination has been reported to occur to various degrees in different brain regions (in several commonly used cre-lines, Hu et al., 2013; Müller-Komorowska et al., 2020), we directly validated our experimental conditions and confirmed the specificity and selectivity of our approach for subicular networks. (Figure 3.5). Furthermore, we characterized and quantified the morphofunctional properties of individual subicular PV^+ cells as interneurons with fast-spiking phenotype and spatially-specific axo-dendritic localization (Figures 3.6 and 3.7).

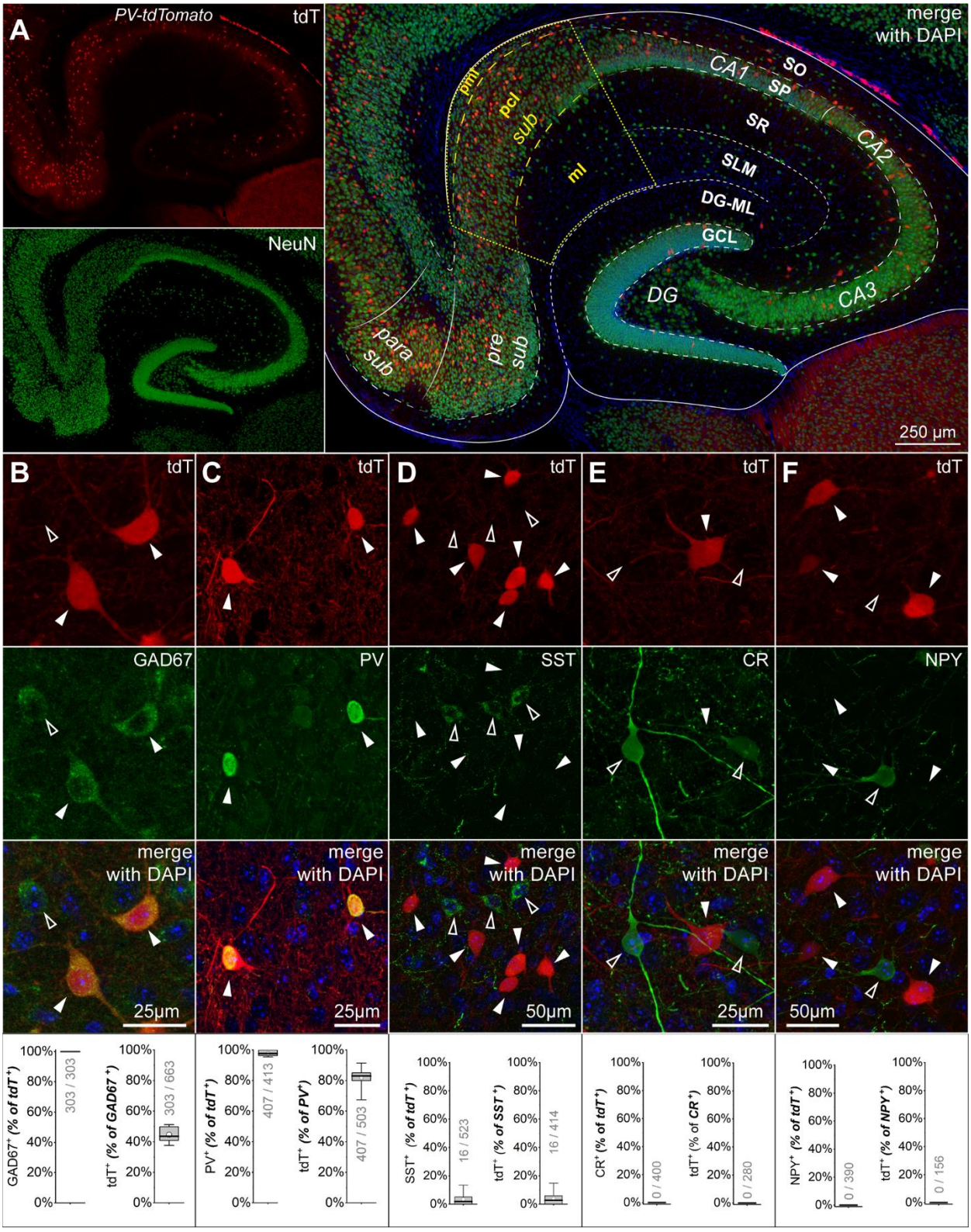
A
PV-tdTomato
tdT
NeuN
merge
with DAPI
CA1
SO
SP
SR
SLM
DG-ML
GCL
CA2
CA3
DG
pml
pcl
sub
ml
para
sub
pre
sub
250 µm
B
C
D
E
F
tdT
GAD67
PV
SST
CR
NPY
merge
with DAPI
25µm
50µm
GAD67+ (% of tdT+)
tdT+ (% of GAD67+)
PV+ (% of tdT+)
tdT+ (% of PV+)
SST+ (% of tdT+)
tdT+ (% of SST+)
CR+ (% of tdT+)
tdT+ (% of CR+)
NPY+ (% of tdT+)
tdT+ (% of NPY+)
303 / 303
303 / 663
407 / 413
407 / 503
16 / 523
16 / 414
0 / 400
0 / 280
0 / 390
0 / 156
100%
80%
60%
40%
20%
0%

Figure 3.5: Validation of the specificity of the PV-tdTomato mouse.
A) Distribution of tdTomato-expressing neurons in the subicular complex and hippocampus. Left, channels showing tdTomato expression (red, tdT), NeuN immunoreactivity (green, NeuN) and DAPI nuclear counterstaining (DAPI, blue). Right, merged image of all the channels detailing the various subregions and layers. Para sub, parasubiculum; pre sub, presubiculum; sub, subiculum; CA1, Cornu Ammonis subfield 1; CA2, Cornu Ammonis subfield 2; CA3, Cornu Ammonis subfield 3; DG, dentate gyrus. Subicular layers in yellow as follows: pml, polymorphic layer; pcl, pyramidal cell layer; ml, molecular layer. Hippocampal layers in white as follows: SO, stratum oriens; SP, sratum pyramidale; SR, stratum radiatum; SLM, stratum lacunosum-moleculare; DG-ML, molecular layer of the dentate gyrus, GCL, granule cell layer. The yellow dotted line indicates the subicular border.
B), C), D), and **F),** Immunohistochemical reactivity of tdT^+ neurons for (left to right) GAD67, parvalbumin (PV), somatostatin (SST), calretinin (CR) and neuropeptide Y (NPY). Top to bottom: tdT fluorescence, reactivity to the specific marker tested, combined images including DAPI nuclear counterstaining and summary boxplots. Filled and empty arrowheads for reference show tdT^+ neurons, and cells immunoreactive to the specific marker tested, respectively. Notice in the summary plot that all tdT+ cells are $GAD67^+$, almost every tdT^+ neuron expresses PV, and only a small fraction of PV^+ does not display tdT immunofluorescence. Also, notice the lack (or minimal in the case of SST) overlap with the other markers.

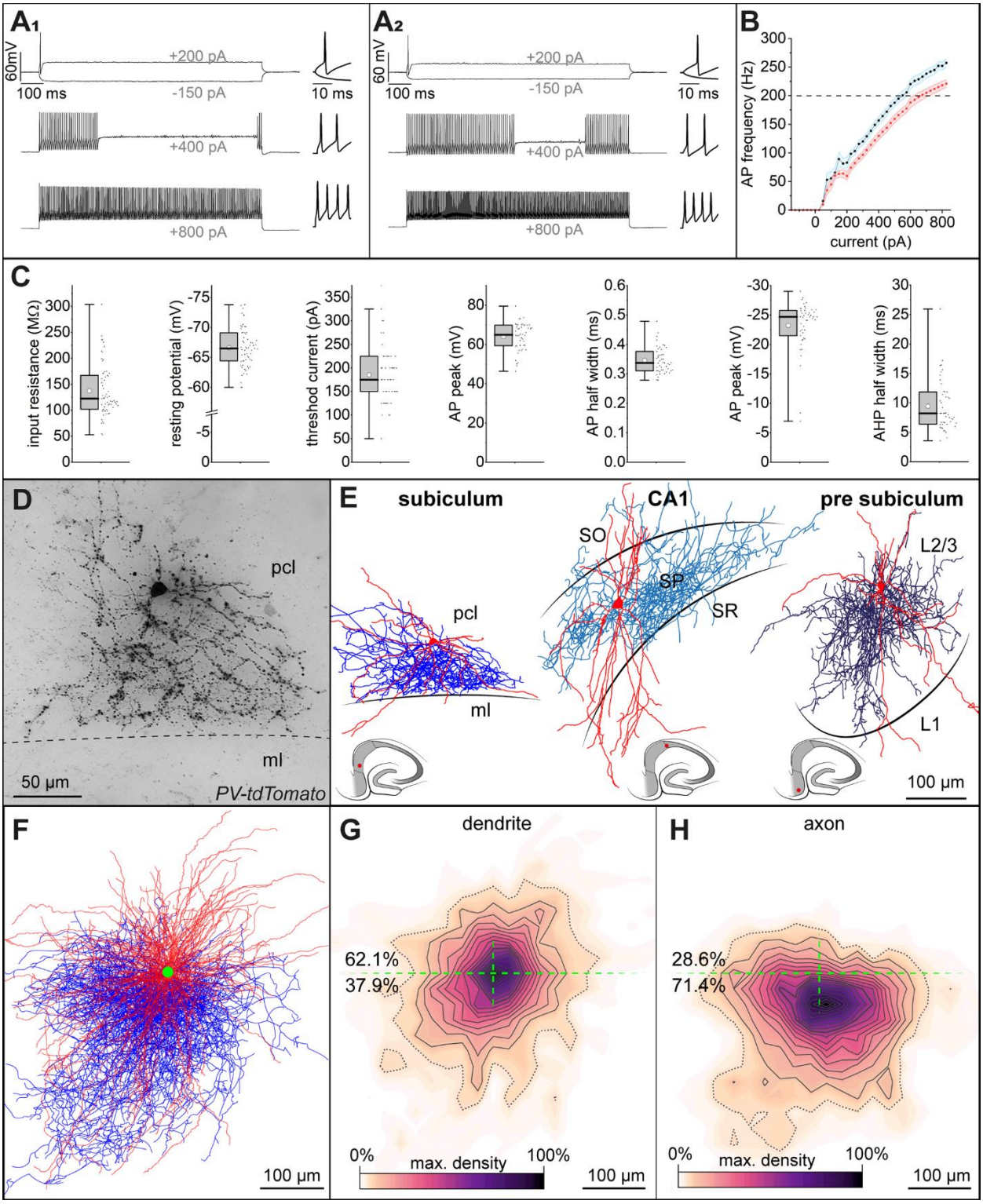
A1
60mV
100 ms
+200 pA
-150 pA
10 ms
+400 pA
+800 pA
A2
60 mV
100 ms
+200 pA
-150 pA
10 ms
+400 pA
+800 pA
B
AP frequency (Hz)
current (pA)
C
input resistance (MΩ)
resting potential (mV)
threshold current (pA)
AP peak (mV)
AP half width (ms)
AP peak (mV)
AHP half width (ms)
D
pcl
ml
50 µm
PV-tdTomato
E
subiculum
CA1
pre subiculum
SO
SP
SR
pcl
ml
L2/3
L1
100 µm
F
100 µm
G
dendrite
62.1%
37.9%
0%
max. density
100%
100 µm
H
axon
28.6%
71.4%
0%
max. density
100%
100 µm

Figure 3.6: Firing patterns, membrane properties and structural characteristics of subicular tdT$^+$ interneurons of the PV-tdTomato mouse.
A1) and **A2)** Typical action potential trains in in response to long (1 s) depolarizing current pulses. Notice the single action potential at threshold current levels and the membrane deflection following a hyperpolarizing current step (top), the stuttering phenotype at intermediate levels (middle) and the rapid firing triggered by larger current steps (bottom). The right insets show the initial part of the traces at a magnified temporal scale. Notice the minimal spike frequency adaptation.
B) Current/frequency plot. The blue and red curves indicate the maximum (blue symbols) and average (red symbols) frequency measured within the train. Bands are ±SE. Notice that in both cases frequencies >200 Hz can be reached.
C) Summary plots of measured basic membrane properties. Left to right: membrane input resistance, resting potential, threshold current, action potential (AP) peak amplitude and half width and afterhyperpolarization (AHP) peak and half width. Box plots and individual data points are illustrated on the left and right side of the graphs, respectively.
D) Micrograph of a recovered biocytin-filled tdT$^+$ cell. Notice the high density of synaptic terminals. Dotted lines indicate the border between the pyramidal cell layer (pcl) and the molecular layer (ml).
E) Reconstructed tdT$^+$ neurons from the subiculum and its adjacent regions, i.e. CA1 hippocampus and pre subiculum. Dendrites in red and axons in blue. Notice the dense axonal arborization in all cases and the larger tangential spread in the case of the CA1 cell. Notice also the multipolar dendritic arborization of the subicular cell (see also Figure 2.1)
F) Overlap of all the reconstructed interneurons aligned on their soma (green circle) and deep/superficial position within the subiculum.
G) and **H)** Summary plots of density probability for dendrites and axons, respectively. Notice the opposite orientation biases with respect to the deeper vs most superficial parts of the region.

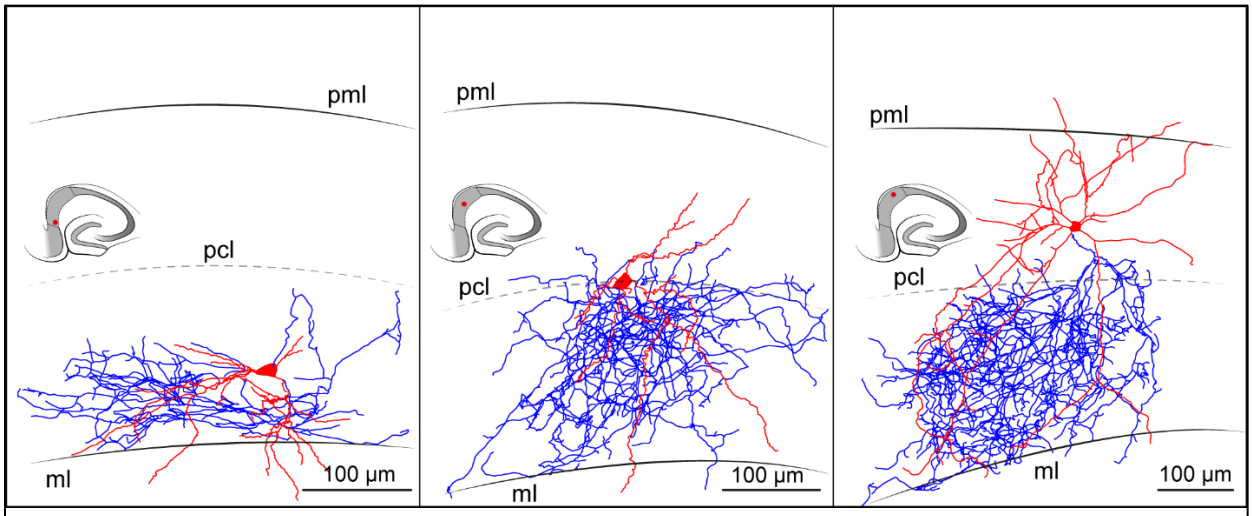

Figure 3.7: Variability of biocytin-filled reconstructed PV⁺ cells. Examples are located in the more superficial (left), middle (middle) and deeper portions of the subicular pyramidal cell layer (pcl). Pml, polymorphus layer; ml, molecular layer. The dotted gray line marks equidistance from the superficial and deeper border of the pyramidal cell. Notice the bias of the axonal arborization to more superficial directions compared to the dendritic arborization.Insets show the position of the specific neruon (red circle) within the slice. Gray areas, principal cell layers of the hippocampal formation.

Given their impact on network function, we paid particular attention in evaluating the synaptic output of PV^+ subicular neurons onto postsynaptic pyramidal cells by performing simultaneous paired recordings (Figure 3.8). This is important to establish the strength of their functional connections and their specific postsynaptic domain targeting. The overall probability of finding a functionally detectable unitary connection was roughly 50%. Unitary inhibitory postsynaptic currents (uIPSCs) recorded in voltage-clamp configuration at a holding potential of +10 mV (n=28 pairs) had a short latency (0.5±0.3 ms, mean±SD), with an amplitude of 252±303 pA (mean±SD). Their measured risetime and half width kinetics were 1.1±0.6 ms (mean±SD) and 12.0±2.8 (mean±SD), respectively. Failures were rare (4±7 %, mean±SD) showing reliability of transmission. Interestingly, latency was correlated with uIPSC risetime (R^2=0.56, $p<0.001$, n=28 pairs), indicating that the faster events were occurring on a target domain close to the presynaptic cell of origin (usually selected within 70±23 µm, mean±SD of the postsynaptic cell soma). Furthermore, the larger amplitude events were also associated with faster risetimes, and originated a typical L-shaped curve, similar to what was reported for uIPSCs in the CA1 hippocampal region.[31] These results suggest that the larger events originate close to the postsynaptic somatic recording site. We decided to investigate this issue by identifying points of close apposition between the pre- and postsynaptic neurons (Figure 3.9), as previously reported for excitatory connections between subicular pyramidal cells (Fiske et al., 2020). In comparison to that study, putative contact sites from PV^+ neurons onto pyramidal cells (total n=64 from n=11 reconstructed pairs) appeared mostly restricted to the perisomatic compartment with a substantial fraction (~38%) located within 50 µm from the soma, ~53% between 50 and 150 µm from it, and a minimal fraction further away. Furthermore, larger events were associated with the presence of at least a single contact site close to the soma. Plotting the peak uIPSC current vs. the minimal distance of

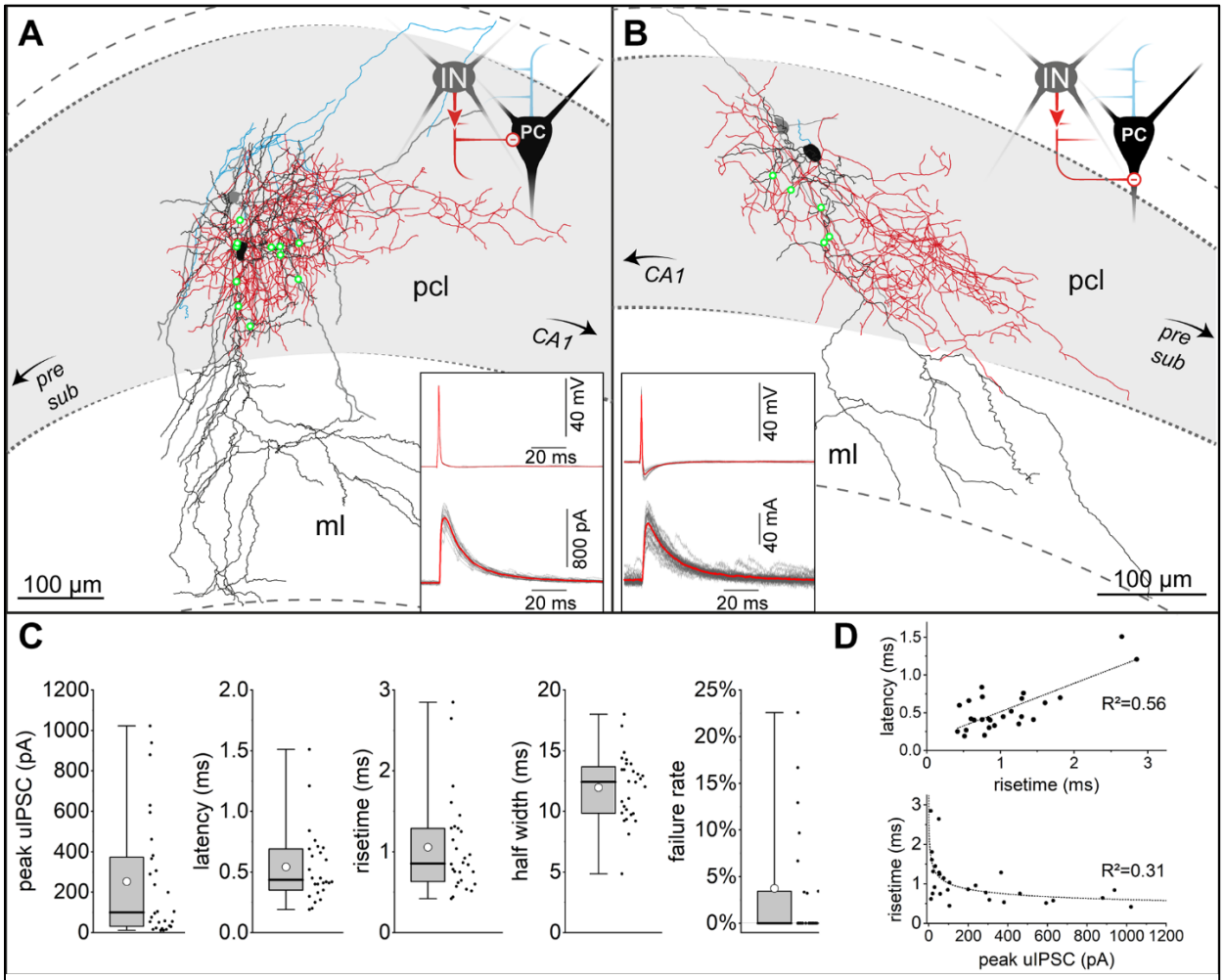

Figure 3.8: Putative contact sites and functional properties of unitary inhibitory postsynaptic currents (uIPSCs) generated by tdT⁺ cells onto pyramidal neurons.

A) and **B)** Examples of reconstructed pairs between a tdT⁺ presynaptic interneuron (IN, dendrites, grey; axon, red) and a postsynaptic pyramidal cell (PC, dendrites, black, axon, blue). Points of close apposition between the presynaptic axon and postsynaptic dendrites are highlighted by green circles. Notice the presence of a putative somatic contact in A). pml, polymorphic layer; pcl, pyramidal cell layer; ml, molecular layer; presub, presubiculum, CA1, CA1 subfield of the hippocampus. Insets show the uIPSCs recorded from the illustrated pairs. The presynaptic action potentials (top) and postsynaptic responses (bottom) are shown in gray and their averages in red, respectively. Notice that the uIPSC from pair B) is of smaller amplitude and slower kinetics, and the lack of putative somatic contact sites in the reconstructed pair.

C) Summary plots of the uIPSC properties measured for all the recorded pairs.

D) Top, linear correlation between risetime and latency suggesting somatic targeting of spatially close postsynaptic target cells. Bottom, relationship between the uIPSC risetime and amplitude. Values included in the graph were measured from averaged uIPSCs. Notice the L-shape of the scatterplot. Fits are indicated by the continuous line (top, linear and bottom, allometric).

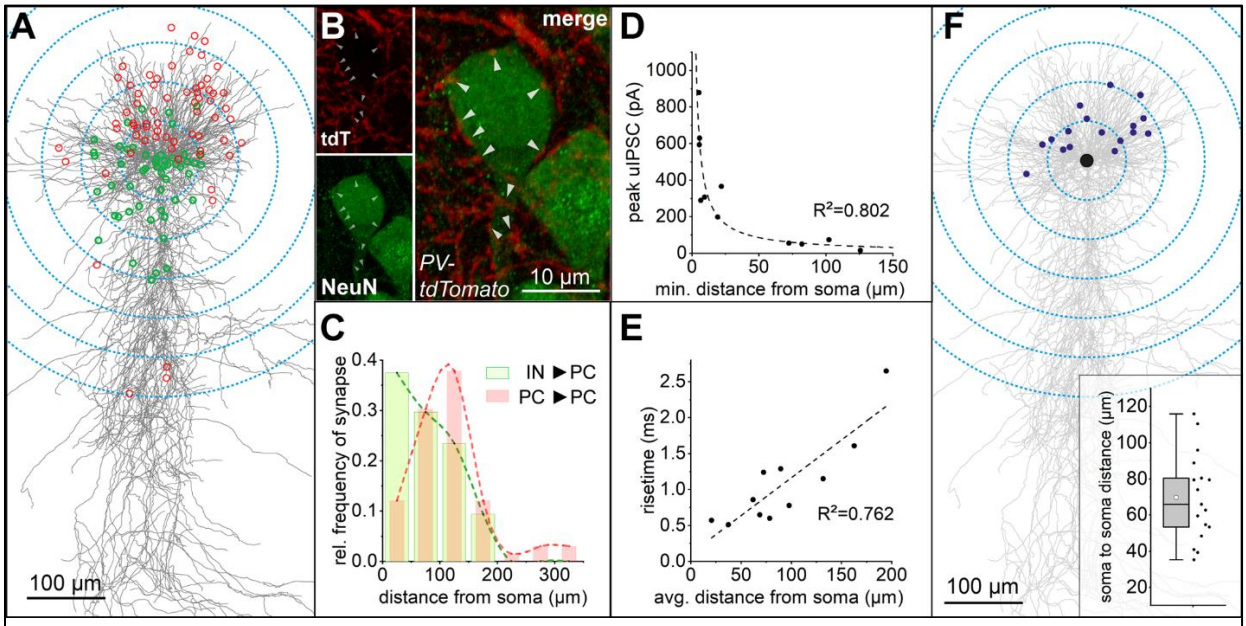

Figure 3.9: Structural analysis of synaptic connections between presynaptic tdT⁺ interneurons and postsynaptic pyramidal cells.

A) Summary plot containing all the reconstructed pyramidal neurons. The putative contact sites originated by tdT⁺ cells are indicated by the green circles. Red circles indicate, for comparison, the location (within the reference provided by the blue concentric dotted circles) of pyramidal to pyramidal cell connections reported by Fiske et al.

B) Example of a confocal image showing basket-like structures formed by tdT⁺ terminals (red) onto a subicular neuron (NeuN, green). The separate channels are shown to the left and the merged image to the right.

C) Comparison of the somatic distances of putative contact sites established by either presynaptic tdT⁺ cells (green bars) or pyramidal neurons (red bar, data from Fiske et al., 2020) with postsynaptic pyramidal cells. Dotted lines connect the centers of the bars. Notice the absence of putative synapses at the more distal dendritic sites in the case of connections originating from tdT⁺ cells.

D) Summary plot relating the shortest distance of putative contact sites to peak uIPSC amplitude. Notice the L-shape of the scatter plot, similar to what is shown in Figure 3.9 D. The fit is indicated by the dotted line

E) Relationship between uIPSC risetime and average distance of putative contact sites from the soma. Linear regression indicated by the dotted line.

F) Summary graph marking the position of the presynaptic tdT⁺ cell (dark small circles) relative to the postsynaptic target (large circle, dendrites are overlapped, grey). Notice the preferential deeper layer location of the presynaptic soma compared to its target. The inset shows a box chart of the intersomatic distances measured in n=17 pairs.

the putative contact site(s) from the postsynaptic soma resulted in an L-shaped plot similar to what was obtained in Figure 3.8, consistent with a dendritic filtering effect that is more prominent at more distal dendritic sites.[32] As expected, the distance from the soma of the putative contact site(s) was correlated to the risetime kinetics of the uIPSC (R^2=0.762, p=0.017, n=11 pairs). The presynaptic interneurons of the connected pairs were located deeper within the stratum pyramidale relative to the postsynaptic pyramidal cell (n=17 pairs). Thus, our data indicate that subicular PV^+ cells predominantly innervate the perisomatic area of postsynaptic pyramidal neurons. As this area is spatially close to the action potential initiation site of subicular pyramidal neurons (Colbert et al., 1996) PV^+ cells would be predicted to influence action potential generation and synchronization in the target population (Cobb et al., 1995; Miles et al., 1996). Therefore, assuming spike-to-spike transmission between pairs of cells, it is possible that a single PV^+ interneuron could drive population activity in clusters. More realistically, we think that, because of the variability in the amplitude of uIPSCs observed in pairs (see Figure 3.8), a few PV^+ cells may actually be required.

If the epileptiform events observed in the presence of VU0463271 truly depended on the activity of a few PV^+ cells, we reasoned that even their limited optogenetic activation should successfully generate similar discharges, whereas their optogenetic inhibition should reduce spontaneous network synchronous activity.

As shown in Figure 3.10, we began by verifying the effectiveness of optogenetic stimulation on PV^+ cells in subicular slices not yet exposed to VU0463271. Under these experimental conditions, we could reliably trigger individual action potentials in PV^+ interneurons either in cell-attached or whole-cell configuration (n=18 cells), but not in pyramidal cells either in cell-attached mode (n=17 cells), or after passing in whole-cell configuration, which produced a

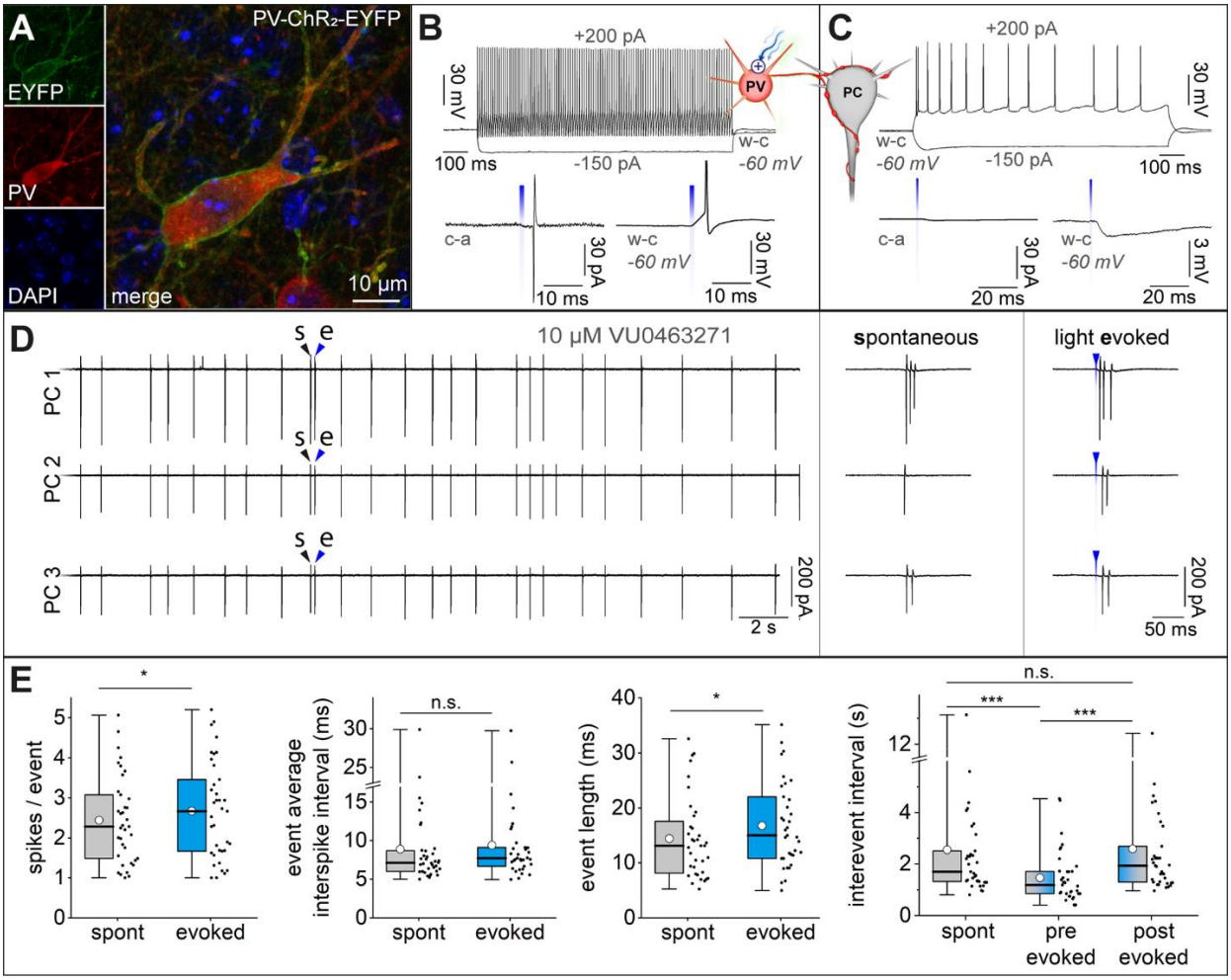
A
EYFP
PV
DAPI
PV-ChR2-EYFP
merge
10 µm
B
+200 pA
30 mV
100 ms
-150 pA
PV
w-c
-60 mV
c-a
30 pA
10 ms
w-c
-60 mV
30 mV
10 ms
C
+200 pA
PC
30 mV
w-c
-60 mV
-150 pA
100 ms
c-a
30 pA
20 ms
w-c
-60 mV
3 mV
20 ms
D
10 µM VU0463271
PC 1
PC 2
PC 3
s
e
200 pA
2 s
spontaneous
light evoked
200 pA
50 ms
E
spikes / event
spont
evoked
*
event average interspike interval (ms)
n.s.
event length (ms)
*
interevent interval (s)
n.s.
***
***
spont
pre evoked
post evoked

Figure 3.10: Optogenetic stimulation of PV^+ interneurons in the absence and in the presence of VU0463271 generates different responses.
A) Left, confocal images showing separate signals for ChR2-EYFP expression (top), PV immunoreactivity (middle) and DAPI counterstain (bottom) in a subicular interneuron. Right, same neuron with all signals merged.
B) Control experiment showing that optogenetic stimulation (blue arrowed waves and plus sign) triggers single spikes in fast-spiking PV^+ subicular interneurons (PV) in slices not exposed to the drug. Top, typical fast-spiking firing pattern and membrane response to a hyperpolarizing current step of a cell selected for optogenetic stimulation. Bottom, a 1 ms blue light flash triggers a single action potential both in cell-attached (c-a, left) and whole-cell (w-c, right) configuration.
C) No supra-threshold activity is observed (same experimental conditions as in B) when recording from a pyramidal cell (PC). Top, Notice the different firing pattern and membrane properties compared to B) and the lack of firing under either cell-attached or whole-cell recording conditions (bottom).
D) Optogenetic stimulation of PV^+ subicular interneurons in slices exposed to VU0463271 (10 μM) and cell-attached recording from three pyramidal neurons (PC 1, PC 2 and PC 3). The black and blue arrowheads indicate the spontaneous (s) and light-evoked (e) events, which are displayed to the right at higher temporal resolution to the right. Notice their similarity.
E) Summary plots comparing the properties of spontaneous vs. light evoked (spikes/event, interspike interval and event length). Evoked events show minor but significant differences in spikes/event and event length. *=$p<0.05$. The last plot compares the average baseline interevent interval before light stimulation (spont) with the intervals between the light-evoked event and the one preceding (pre evoked) or following it (post evoked). Notice the difference between the spontaneous vs. “pre evoked” intervals indicating the temporal randomness of stimulation and the return to similar values (spont vs. post evoked) showing the reset of the timing of the network event generator. ***=$p<0.001$.

response of 0.4±1.0 mV (mean±SD, n=17 cells). However, when the same experiment was performed on slices pre-exposed to VU0463271 (for at least 30 minutes) and showing the typical epileptiform activity, the same light stimulation was capable of evoking supra-threshold burst events in pyramidal cells, which were reminiscent of spontaneous discharges. A comparison of the properties of spontaneous vs. light-triggered events revealed differences in the number of action potential/event (2.5±1.1 vs 2.7±1.2, mean±SD, n=7 triples, n=6 pairs and n=4 single cells, for a total of 37 neurons, p=0.011, W=171, Z=-2.53726, d_{Cohen}=0.92, Wilcoxon signed rank test, two-sided) and in the event durations (14.4±7.5 ms vs 16.8±7.8 ms, mean±SD, n=5 triples, n=8 pairs and 4 single cells, for a total of 35 neurons, p=0.007, W=150, Z=-2.69437, d_{Cohen}=1.02, Wilcoxon signed rank test, two-sided, two cells of two separate triple recordings produced only single-spike events, so durations could not be measured). No changes, however, were detected in the interspike intervals within the event (8.9±5.2 ms vs 9.4±5.2 ms, mean±SD, n=5 triples, n=7 pairs and 4 single cells, for a total of 35 neurons, p=0.075, W=206, Z=-1.77714, d_{Cohen}=0.63, Wilcoxon signed rank test, two-sided). We interpret these differences as a result of the artificial nature of channelrhodopsin stimulation. Optogenetic stimulation is likely to drive highly synchronous firing in several PV^+ cells, probably in excess of how many are needed to generate spontaneous events, hence the stronger events (longer and with more spikes). However, most importantly, the average spontaneous baseline interevent interval (spont, 2.6±2.3 s, mean±SD, n=7 triples, n=6 pairs and n=4 single cells, for a total of 37 neurons) measured before delivering the light flash was indistinguishable from the specific interevent interval measured between the light-evoked event and the next spontaneous discharge in the same cells (post evoked, 2.6±2.2 s, mean±SD, p=1.0, t=0.52, DF=72, repeated measures ANOVA on ranks with Bonferroni post-hoc adjustment). This argues for a “reset” of the network timing. In fact, light stimulation was timed randomly relative

to the spontaneous events, as indicated by the difference between the baseline interevent interval (spont) and the one occurring between the last spontaneous discharge before the one evoked by the flash (pre evoked, 1.5±1.0 s, mean±SD, n=7 triples, n=6 pairs and n=4 single cells, for a total of 37 neurons, $p<0.001$, $t=10.11$, $DF=72$, repeated measures ANOVA on ranks with Bonferroni post-hoc adjustment). In fact, the "pre evoked" interevent interval was also different from the one measured after the reset of network timing (post evoked, $p<0.001$, =7 triples, n=6 pairs and n=4 single cells, for a total of 37 neurons, $p<0.001$, $t=10.63$, $DF=72$, repeated measures ANOVA on ranks with Bonferroni post-hoc adjustment). We think that the optogenetic-triggered reset of network timing is strong evidence for a mechanistic involvement of PV^+ cells in the generation of epileptiform events.

We decided to reinforce this conclusion by testing the effects of optogenetic inhibition of PV^+ interneurons on VU0463271-dependent activity (Figure 3.11). Before performing this experiment, we confirmed that, in the absence of the drug, activation of ArchT effectively hyperpolarized fast-spiking interneurons (-2.9±1.5 mV, mean±SD, n=11 cells) in slices prepared from PV-ArchT mice. In the presence of VU0463271, when a flash of 15 s duration was delivered, the most prominent observation was a marked decrease in the frequency of spontaneously occurring discharges (from 2.3±0.9 events/15 sec to 1.0±0.9 events/15 sec, mean±SD, n=3 triples, n=6 pairs and n=4 single cells, for a total of 25 cells, $p<0.001$, $W=297$, $Z=4.18849$, $d_{Cohen}=3.07$, Wilcoxon signed rank test, two-sided). In agreement with our previous interpretation, this result confirms that the activity of PV^+ interneurons is a crucial determinant of epileptiform activity triggered by KCC2 loss-of-function. Additional changes, albeit minor, were detected in the number of spikes per event (from 4.3±2.3 to 4.4±2.3, mean±SD, n=3 triples, n=5 pairs and n=2 single cells, for a total of 21 neurons, $p<0.028$, $W=150$, $Z=2.1932$, $d_{Cohen}=1.09$, Wilcoxon signed rank test,

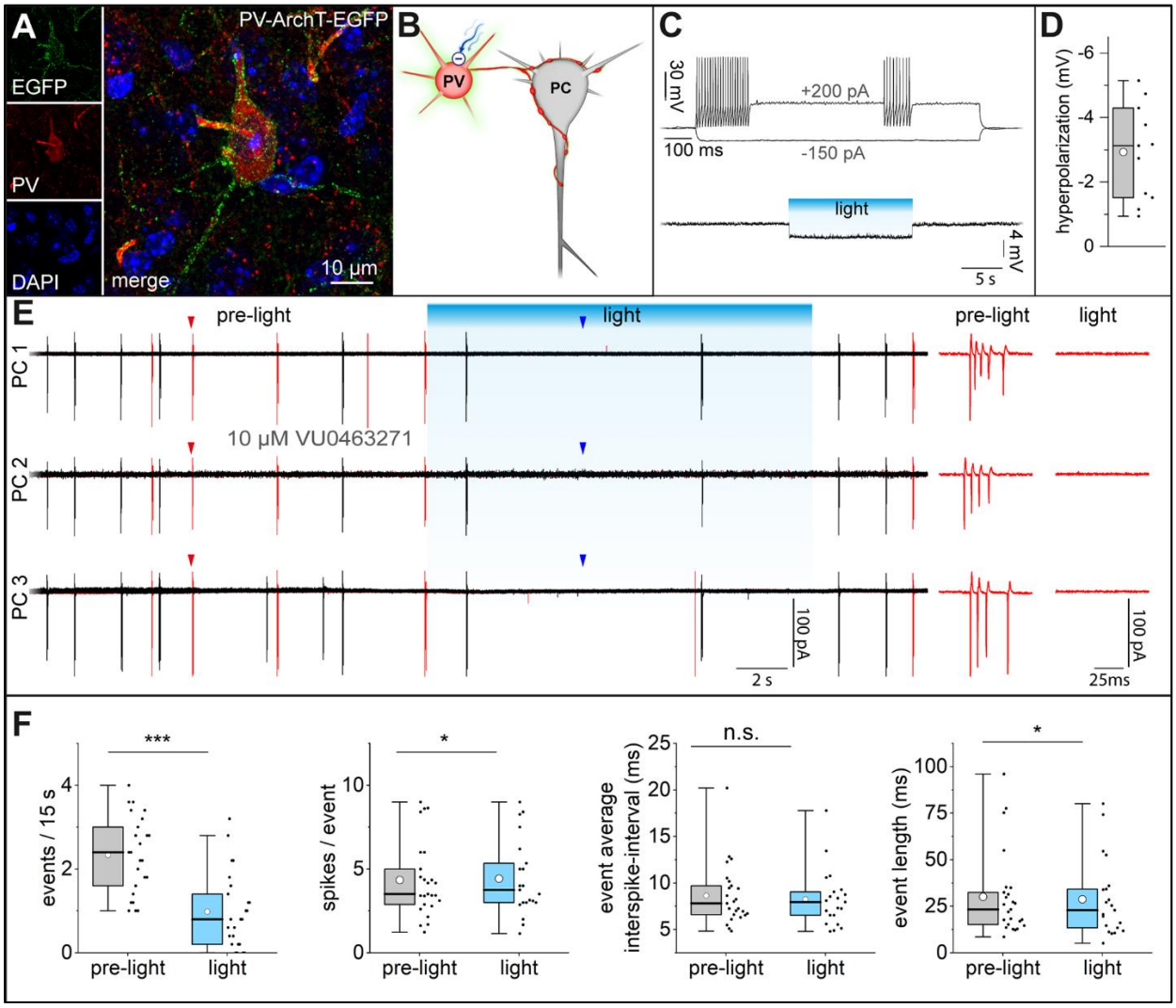
A
EGFP
PV
DAPI
PV-ArchT-EGFP
merge
10 µm
B
PV
PC
C
30 mV
+200 pA
100 ms
-150 pA
light
4 mV
5 s
D
hyperpolarization (mV)
E
pre-light
light
PC 1
10 µM VU0463271
PC 2
PC 3
100 pA
2 s
25ms
F
events / 15 s
***
pre-light
light
spikes / event
*
event average interspike-interval (ms)
n.s.
event length (ms)

Figure 3.11: Optogenetic inhibition of PV^+ subicular interneurons reduces VU0463271-dependent network bursts.
A) Left, confocal images of ArchT-EGFP fluorescence (top, EGFP), PV immunoreactivity (middle, PV) and DAPI nuclear counterstain (bottom, DAPI) of a subicular interneuron. Right, same cell with all signals superimposed.
B) Cartoon showing the stimulation experimental setup. A flash of light (blue arrowed wave and minus sign) inhibits PV^+ interneurons (PV) connected to pyramidal cells (PC).
C) Light activation of ArchT in PV^+ interneurons: notice the typical electrophysiological signature of fast-spiking cells (top) and the hyperpolarization of the membrane potential caused by the light flash (blue bar).
D) Summary box plot for ArchT-induced hyperpolarization in n=11 cells.
E) Example of a simultaneous cell-attached recording from three pyramidal neurons (PC 1, PC 2 and PC 3) in the presence of VU0463271 (10 µM). Three sweeps are superimposed, and events from a single sweep are highlighted in red. Notice the synchronous activity and the reduced occurrence of events in the presence of the light (blue bar). An expanded view of selected bursts (red arrowhead) is shown to the right (pre-light). The blue arrowheads indicate the region of the trace in the presence of the light expanded to the right (light).
F) Summary graphs and individual data points of the properties of the events in the absence vs. presence of light stimulation. Left to right: event frequency (events/15 s), spikes/event, interspike interval and event length. Notice the large suppression in the occurrence of network bursts during the flash and the minor changes in spikes/event and event length. *=$p<0.05$, ***=$p<0.001$.

two-sided, the overall number of recordings is lower than what reported for event frequency because in n=4 cells no events could be observed in the presence of the light) and in the event duration (from 30.1±22.5 ms to 28.7±20.8 ms mean±SD, n=3 triples, n=5 pairs and n=2 single cells, for a total of 21 neurons, $p<0.037$, $W=176$, $Z=2.08546$, $d_{Cohen}=1.02$, Wilcoxon signed rank test, two-sided). No differences were found in the average interspike interval within an event (from 8.6±3.3 ms to 8.3±3.1 ms, mean±SD, n=3 triples, n=5 pairs and n=2 single cells, for a total of 21 neurons, $p<0.082$, $W=166$, $Z=1.73788$, $d_{Cohen}=0.82$, Wilcoxon signed rank test, two-sided). We think that the changes measured in the properties of the events (number of spikes and event duration) were probably due to reduced inactivation of voltage-gated sodium/calcium channels because of both membrane hyperpolarization and the reduced occurrence of events during the light flash. Taken together, the results of these experiments provide compelling evidence that excitatory signaling from PV^+ interneurons is mechanistically involved in subicular epileptiform activity induced by KCC2 loss of function and may act as a cellular trigger for epileptiform activity.

Discussion

Our work is a novel and original attempt to model and study what has been proposed to be a critical epileptogenic step of TLE (in a reduced preparation in vitro) and provides compelling mechanistic evidence for the involvement of PV^+ interneurons in the generation of epileptiform activity similar to what has been described in human epileptic tissue.

A "model of subicular-specific epileptogenesis" in vitro?

Strictly speaking, "epileptogenesis" refers to the process that converts the brain from a healthy state to a chronic condition suffering from spontaneous seizures, i.e. epilepsy (Pitkanen et al., 2015). This, of course, cannot occur in a reduced preparation in vitro. Hence, by "model of epileptogenesis in vitro" we refer to a reduced experimental setup that can generate epileptiform activity when challenged by what *in vivo* studies have proposed to be a key epileptogenic step. In our case, this would be the specific decreased expression of KCC2 in the deafferented subiculum (Huberfeld et al., 2011). The strength and usefulness of our simplified model rests on its ability to disentangle causal factors from mechanistically unrelated epiphenomena. This goal may be difficult to achieve when working with tissue obtained from epileptic animals or human patients. For example, one the most compelling structural alterations long assumed to be epileptogenic in TLE (mossy fiber sprouting in the dentate gyrus) may actually turn out to be just an epiphenomenon (Heng et al., 2013).

Another important point to discuss is that altered chloride homeostasis in human epileptic tissue seems to occur only in fraction of subicular pyramidal neurons (Huberfeld et al 2007). Interestingly, bath application of VU0463271 (at the same concentration used here) in

hippocampal slices was reported to generate $GABA_A$ receptor-mediated excitation only in a subset of pyramidal cells (Otsu et al., 2020). This would explain similarity between the spontaneous activity recorded here and the interictal discharges observed in the subiculum of the sclerotic hippocampal formation of patients suffering from TLE (Cohen et al., 2002; Reyes-Garcia et al., 2018).

KCC2 model of "epileptogenesis in vitro": interictal- and ictal-like electrical activity

Under our experimental conditions, we observed interictal-like discharges, but never events reminiscent of long-lasting ictal-like activity. We offer the following potential explanations.

First, under our experimental conditions in vitro, subicular networks have a decreased number of neurons and reduced connectivity compared to the intact situation in vivo. This may be the root of our failure to observe full-blown ictal-like events, which may require a larger critical mass. However, other possibilities, related to synaptic or intrinsic plasticity, may also be relevant. In fact, Huberfeld et al. 2011 suggested that ictal discharges are driven by pre-ictal events that depend critically on NMDA receptor-dependent synaptic plasticity. NMDA receptor-dependent long-term potentiation was directly observed in cultured rodent slices when epileptiform activity was maintained for several hours (Abegg et al., 2004). It is therefore possible that our experiments did not last long enough to allow for the sufficient development of this type (or of other forms) of synaptic plasticity. A third limit may be the loss of subcortical dynamic neuromodulatory inputs, which may be directly required to generate ictal-like even (for example, acetylcholine; D'Antuono et al., 2007) or indirectly favor plasticity (Palacios-Filardo et al., 2019). Additionally, human epileptic tissue shows hyper-innervation of pyramidal neurons by PV^+ terminals (Muñoz et al., 2007), which may increase the impact of PV^+ cells on the network, but this is not present under

our experimental conditions. Lastly, we should consider that the reported deafferentation of the subiculum regards primarily CA1 inputs (Huberfeld et al., 2015), and that the combination of intrinsically-generated rhythms with direct external inputs from the entorhinal cortex may be required to detonate an ictal-like event (Herrington et al., 2015). In fact, in order to limit the effect of VU exclusively to local subicular circuits, we were forced to use a preparation disconnected from any external input, including the entorhinal cortex. The actual relevance of some of these hypotheses can be tested experimentally. For example: (i) longer exposure to VU0463271 may be attempted to trigger various forms of plasticity, (ii) neuro-modulation may be simulated by exogenous application of specific pharmacological agonists, and (iii) the impact of entorhinal afferent by optogenetic stimulation (Suh et al., 2011) even in a reduced subicular slice.

Contribution of PV^+ interneurons to epileptiform activity

The role(s) played by cortical GABAergic interneurons in the epileptic brain are increasingly being recognized as complex (Magloire et al., 2015; Lévesque et al., 2019; Jiang et al., 2016). In addition to their remarkable morphofunctional diversity (reviewed by Tremblay et al. in the cortex and by Pelkey et al. in the hippocampus), it is important to consider the specific type of activity investigated (inter-ictal, pre-ictal or ictal), the area of interest (inside/outside epileptic focus) and the temporal stage considered during the natural history of the disease. After neuronal loss in the CA1 subfield (Huberfeld et al., 2015), a fraction of the pyramidal cells of the subiculum of TLE patients have been shown to regress to a state lacking KCC2 expression, which perturbs intracellular chloride homeostasis (Cohen et al., 2002; Hubferfeld et al., 2007). Our study suggests that, at this stage, reduced KCC2 function in subicular circuits may trigger epileptiform discharges that are dependent on PV^+ interneurons. Our most parsimonious explanation is that the

natural tendency of local subicular excitatory circuits to generate epileptiform activity (Fiske et al., 2020) cannot be suppressed by $GABA_A$ receptor-mediated signaling under conditions of impaired KCC2 functions. Comparing the epileptiform activity recorded by Fiske et al. in the complete absence of inhibition with the data presented here in the presence of VU0463271 reveals remarkable differences suggesting a more complex scenario. In the complete absence of inhibition, spontaneous epileptiform events originated much more rarely than events resulting from KCC2 inhibition (by about two orders of magnitude). Therefore, we suggest that subicular population bursts are likely to be initiated by the random firing of pyramidal neurons interconnected by a positive synaptic feedback system (Fiske et al., 2020; Böhm et al., 2017) , similar to what has been proposed to occur in the hippocampus (Traub et al., 1991). In contrast, the more frequent occurrence of epileptiform events in the presence of VU0463271-altered GABAergic input might be predominantly initiated by fast signaling devices such as PV^+ interneurons themselves (Jonas et al., 2004). The contribution of PV^+ interneurons appears especially relevant given the proximity of their postsynaptic target domains to the action potential initiation site of pyramidal cells Colbert et al., 1996). In addition, PV^+ interneurons are endowed with a dense axonal arborization, which controls a large number of target cells (Cobb et al., 1995; Miles et al., 1996), as also suggested here by the higher probability of finding connections from PV^+ to pyramidal cells when compared to connections between pyramidal neurons (about one order of magnitude higher, this work compared to Fiske et al. 2020 and Böhm et al. 2017).

Conclusions

In summary, our work has taken a direct and quantitative approach to study the mechanistic role of subicular interneurons in the generation of epileptiform network activity in a key region

involved in TLE, the subiculum. Our results are consistent with the "KCC2 down-regulation" theory of epileptogenesis and suggest that the powerful perisomatic input of PV^+ cells, when altered by reductions in KCC2 activity, is sufficient to produce network hyper-excitability and hyper-synchronization, which is reminiscent of epileptic interictal-like activity. Our model may provide the opportunity to study additional factors potentially involved in interictal-ictal transition such as synaptic and/or intrinsic plasticity, the strength of neuro-modulation and, finally, the role of entorhinal afferents.

Chapter 4. General Discussion

The past two chapters have expanded our knowledge on the cell-specific connectivity of subicular microcircuits, the potential of the subiculum to initiate epileptiform activity under different conditions, and the contribution of specific cell-types to these events. Chapter 2 detailed the first morphofunctional study of local excitatory subicular pyramidal cell circuits and revealed that 1) pyramidal cells in this region, classified by objective methods, are non-randomly connected, 2) connections between pyramidal cells are mediated mostly by synapses formed on basal dendrites, and 3) cell-type specific epileptiform events emerge when GABAergic signaling is blocked. Chapter 3 summarized the role that subicular PV+ interneurons have in a subicular network where KCC2 function is inhibited, a proposed step of epileptogenesis. We found that 1) PV+ interneurons form synapses primarily on perisomatic locations and form powerful inhibitory connections with pyramidal cells, 2) inhibiting KCC2 function in the subiculum induces synchronized epileptiform bursts and 3) PV+ drive the epileptiform bursts induced by KCC2 block.

Tissue specific differences in neuronal network and epilepsy research

Using animal models to study how neuronal networks function and the role these networks have in human diseases is a common approach in neuroscience. Nevertheless, recognizing important differences between human and mouse systems is essential for proper interpretation of any experimental results. An important question that my thesis sought to address was how interconnected the pyramidal neurons in the subiculum are, as the answer to this question is highly relevant to the role that this region plays in generating activity linked to epilepsy. In fact, our connectivity estimate of ~5% might be substantially lower than what would be found if the experiment here was conducted in human tissue. Multi-electrode patch clamp experiments using

human tissue found that the degree of connectivity in human excitatory neurons in the cortex is at least 2.5 times greater than in homologous sections of mouse cortex (Seeman et al., 2018; Molnar et al., 2008; Peng et al., 2019). An increased degree of connectivity between excitatory neurons might presumably require an equally increased number of connections with interneurons to regulate excitation within the network. The spontaneous, synchronous activity I have shown in the isolated subiculum when GABAergic inhibition is blocked might be more dramatic in human tissue. Likewise, the KCC2 blockade-dependent activity described in chapter 3 would potentially be stronger if a higher degree of connectivity exists between interneurons. In this case, activity resulting from manipulations in our mouse model might underestimate the effect that would happen in a human network.

The use of human epileptic tissue to study the molecular underpinnings of epileptogenesis and ictogenesis is a valuable approach. Findings from human epileptic tissue would be more directly applicable to the disease and would not be confused with unrelated phenomena occurring in animal models. However, human tissue is not without its drawbacks. Satisfactory control tissue for comparison is nearly impossible to acquire, as healthy brain tissue is never voluntarily removed. Additionally, similar to slices from rodents, potentially important connections with other brain regions are cut during slicing, limiting how accurately the network recapitulates an epileptic brain. A final complication arises from the effect previous treatments had on the tissue. By the time surgical resection is necessary, numerous drug regimens have likely been tried, and treatment could potentially alter ion channel dynamics in a way that do not reflect “pristine” epileptic tissue. Thus, findings from human tissue should always be compared to findings from rodent models through these lenses.

In general, no animal model fully reproduces the features of human TLE. Chemoconvulsant models are popular systems in which to model TLE (Lévesque et al., 2016). Although they do not perfectly recapitulate the disease, they share many histopathological changes, develop chronic seizures after a latent period, and are arguably more convenient than other epilepsy models (Lévesque et al., 2013; Curia et al., 2008). *Status epilepticus* (SE) refers to a life threatening period where seizure activity lasts for at least 30 minutes without full recovery of consciousness. Administration of either systemic pilocarpine or kanic acid induce status epilepticus within 1 hour, with chronic seizures beginning ~2 weeks later. Mortality tends to be more significant in the pilocarpine model (30-40% vs 5-30%), although SE can be cut short to standardize the duration by administration of benzodiazepines. Whether kainic acid or pilocarpine models more closely reflect actual TLE is an important question. The latent period, where a variety of molecular and structural changes are thought to take place leading to chronic epilepsy, is much shorter in these models (days to weeks) than in TLE (possibly months to years). Therefore, the epileptogenic changes that are thought to potentially be key to understanding epilepsy are occurring in a condensed timeframe. It is possible this is beneficial, as it allows scientists to study key changes without waiting years for them to develop, but the alacrity with which they occur also means they might not encompass all the suspected epileptogenic changes. Likewise, the changes that do occur might be unrelated epiphenomena that are not connected to chronic seizures. For example, both pilocarpine and kainic acid models are characterized by mossy fiber sprouting and subsequent recurrent connection formation, a structural seen in TLE patents as well. However, studies demonstrating that these recurrent connections are not contributing to pathological activity have been published (Buckmaster, 2014), and instead the sprouting of mossy fibers might be a characteristic of a brain that has undergone SE, but not a causative factor.

Network implications of burst firing neurons

This thesis work corroborates numerous previous studies that burst firing neurons are present in large numbers within the subiculum when defined by their intrinsic properties in an *in vitro* slice. As a firing modality, burst firing is interesting in several aspects. From a biophysical standpoint, the mechanisms underlying burst firing are thought to be driven by calcium channels (Jung et al., 2001; Metz et al., 2005). During the rising phase of an action potential, voltage gated sodium channels drive the neuron's membrane potential to depolarized voltages. At a high enough voltage, high voltage gated calcium channels become activated. However, due to their relatively slower kinetics, the channel does not fully open until after voltage dependent potassium channels have started to return the membrane potential to a more negative potential. At this point, the driving force for calcium through these channels, defined as the difference between the current membrane potential and the equilibrium potential, is large, and this calcium tail current induces an afterdepolarization that leads to burst firing. The identity of the specific calcium channel type responsible for driving the ADP required for bursting is still not entirely resolved. Initially, R-type calcium channels were thought to primarily be responsible, but recent evidence using a newly developed specific antagonist of T-type calcium channels has challenged this notion (Joksimovic et al., 2017). T-type channels can be downregulated by the neuromodulator serotonin (Petersen et al., 2017), and serotonergic terminals are abundant in the subiculum (Oleskevich and Descarries, 1990). Therefore, I find it plausible that serotonin might be a major regulator of burst firing *in vivo*.

Burst firing has significant relevance for plasticity in subicular networks as well. In general, burst firing increases the reliability of unreliable synapses. The EPSP amplitude of connections

between subicular pyramidal neurons was relatively weak and failed to elicit an action potential nearly 50% of the time. However, these responses were the result of single action potentials. When an action potential arrives at a synaptic terminal, calcium enters via voltage gated calcium channels, triggering neurotransmitter release through synaptic vesicles. If additional action potentials arrive before calcium is removed from the terminal, the residual calcium combined with a new influx through voltage gated channels can result in a release of larger amounts of synaptic vesicles, eliciting a stronger response in the post-synaptic neuron. Therefore, even though intra-subicular connections are small, connections in which burst-firing neurons are the pre-synaptic partner might be strengthened through this short term facilitation. Even though my data showed that type 2 to type 1 connections are the least common, I believe the overall effect of these connections in the network might be more impactful since the pre-synaptic neuron is bursting. Burst firing also has implications for long term plasticity in the subiculum. Spike timing dependent plasticity (STDP) is a mechanism by which a back-propagating action potential and an EPSP triggered in a dendrite can result in synaptic plasticity at nearby synapses (Caporale and Dan, 2008). Either LTP or LTD can result depending on the time the back propagating action potential arrives relative to the EPSP. Canonical instances of STDP are characterized by LTD when the pre-synaptic neuron fires after the post-synaptic neuron, and the strength of the LTD increases as this timing difference becomes smaller. Conversely, LTP results from the pre-synaptic neuron firing before the post-synaptic neuron, with the strength again modulated by the absolute difference in timing. Recent experiments have demonstrated that the STDP rules are reversed in weak burst firing neurons (this study separated “weak” burst firing neurons and “strong” burst firing neurons) and requires back propagating bursts of action potentials rather than single spikes (Pandey and Sikdar, et al., 2014). The authors used local stimulation to trigger pre-synaptic spikes,

and although they specifically mention these rules in reference to CA1-subiculum synapses, it is possible their local stimulation might be impacting intra-subicular connections as well. Their stimulating electrode was typically located towards the apical dendrites of the recorded neuron, but stimulating in this region will inevitably effect local subicular axons, as our data shows a preference for pre-synaptic subicular neurons in this general region.

An abundance of burst firing neurons is one proposed characteristic that might predispose neural networks to epileptiform activity (Traub and Miles, 1991; Jensen and Yaari, 1997; Yaari and Beck, 2002). The entorhinal cortex, amygdala, and subiculum have all been implicated in initiating epileptiform activity, and each region contains neurons that can be classified as bursting (EC: Hamam et al., 2000; Amygdala: Duvarci and Pare, 2014). While the exact ratios sometimes differ, estimates of bursting and regular spiking neurons usually favor a larger population of bursting neurons in the mouse and rat subiculum (Knopp et al., 2005; Chung et al., 2015). This imbalance of burst firing neurons can become even more exaggerated in both the pilocarpine and kainic acid models of TLE. Shortly after status epilepticus, the level of burst firing neurons increases in both models (Wellmer et al., 2002; Chung et al., 2015). While the exact mechanism for this increase is unclear, it could potentially result from downregulation of K+ channels or increased Ca2+ currents following status epilepticus. Additionally, local interneurons exhibit stronger inhibitory control of bursting neurons than regular spiking neurons (Menendez de la Prida 2003; Panuccio et al., 2012). Death of PV+ interneurons and other inhibitory inputs (human tissue: Andrioli et al., 2007; kainic acid model: Drexel et al., 2012; pilocarpine: Knopp et al., 2008; Dinocourt et al., 2003) might enhance bursting activity, resulting in the subiculum initiating epileptiform activity. Increased bursting might also potentiate local excitatory synapses that inevitably lead to pathological activity. Our data supports this, as blockade of GABAergic

signaling specifically in the subiculum was sufficient to generate synchronous bursts. Activity that might be considered on par with seizures, however, was notably absent. My opinion is that extra subicular inputs are necessary for transforming spontaneous epileptiform activity generated locally in the subiculum to a more widespread, seizure like event. This idea is supported by experiments where PV+ interneurons were permanently silenced in the subiculum using viral vectors encoding tetanus light chain (Drexel et al., 2017). With extra subicular inputs intact, recurrent spontaneous limbic seizures emerged in mice after PV+ were essentially excluded from the network. Ultimately, increased bursting might prime the network for pathological activity, and excitatory inputs coupled with local subicular activity are what pushes the network over the edge.

Neuromodulators and their role in epilepsy

Neuromodulators can exert powerful control on the activity of neurons, and several different neuromodulators are known to be involved in epilepsy. A deeper examination of the mechanisms through which these neuromodulators might mediate their effect can potentially deepen our understanding of the molecular changes at the heart of epilepsy. Serotonin has repeatedly been shown to have anti-epileptic effects (Petrucci et al., 2020). Blocking serotonin reuptake suppresses seizures in animal models of epilepsy (Prendiville and Gale, 1993; Yan et al., 1994; Bagdy et al., 2007; Buchanan et al., 2014). Conversely, decreasing its concentration throughout the brain pharmacologically or genetically promotes seizures (Wenger et al., 1973; Maynert et al., 1975; Lazarova et al., 1983; Applegate and Tecott, 1998; Upton et al., 1998). Throughout the hippocampus, pyramidal cell activity is modulated by serotonin released via en passant synapses (Amaral and Lavenex, 2007), but the serotonergic terminal density is the highest in the subiculum (Oleskevich and Descarries, 1990). Recently, serotonin was shown to suppress bursting in

subicular pyramidal neurons via inhibition of T-type calcium channels, a channel that carries the calcium current responsible for driving bursts (Petersen et al., 2017). As discussed previously, bursting neurons are strongly linked to epilepsy, and decreasing their burst propensity through serotonergic modulation might explain the antiepileptic effect of this neuromodulator. TLE is characterized by regional atrophy in the hippocampus. It is possible that this regional atrophy caused by chronic seizures might include serotonergic fibers, consequently lowering the extracellular tonic concentration and allowing more pyramidal neurons to begin bursting.

Other neuromodulators have interesting effects on the subiculum as well. The adrenergic system is critical for LTP at CA1-subiculum synapses. Specifically, synapses at which CA1 innervates bursting neurons undergo a presynaptic form of LTP when adrenergic receptors are activated (Wójtowicz et al., 2010). The potentiation of these synapses decreases in the pilocarpine model of epilepsy (Grosser et al., 2015; Grosser et al., 2020), but the effect that this decrease in LTP has on network activity and epilepsy is unclear. A weakening of these synapses would arguably decrease seizure susceptibility since bursting cells would then receive less excitation. However, CA1 experiences substantial cell loss in TLE patients, so weakened CA1-bursting neuron synapses might not be an epileptogenic network change. LTP at CA1-subiculum synapses is thought to contribute to learning and memory, and it is possible that this change might explain the hippocampus dependent memory impairments seen in TLE patients rather than be a source of pathological network activity.

Cholinergic signaling in the subiculum is another mechanism by which network activity in the subiculum can be regulated. Activation of muscarinic acetylcholine receptors in conjunction with metabotropic glutamate receptors enhances burst activity of subicular bursting neurons (Moore et al., 2009; Graves et al., 2012). The involvement of the subiculum in learning and

memory might involve specific tuning of bursting neurons through cholinergic signaling (Solari and Hangya, 2018). Interestingly, levels of acetylcholine are thought to increase during status epilepticus (Jope et al., 1986; Jope et al., 1987; Hillert et al, 2014). This might trigger two potentially epileptogenic changes. The first is an increase in bursting from hippocampal neurons, including subicular neurons. The second is a potentiation of CA1-subiculum synapses, although the potentiation is specific to LTP at CA1-regular spiking neuron synapses. However, regular-to-bursting excitatory connections are the most prevalent intra-subicular connectivity motif, and potentiation of CA1-regular spiking neurons might still have a strong impact on network activity if the excitation is propagated further to bursting neurons.

When is the subiculum relevant to epilepsy?

An open question in epilepsy research is when do specific regions drive epileptiform activity. From studies using human epileptic tissue, it is clear that the subiculum generates spontaneous activity on its own. However, a majority of patients who undergo temporal lobe resection as an adult were diagnosed with TLE before the age of 18. Therefore, it is possible that the subiculum is not the network driving aberrant activity early on in the disease. Hippocampal sclerosis is regularly seen in autopsies of TLE patients, with the hilus, CA1, and CA3 experiencing the most significant neuron loss. In addition to the subiculum, granule cells of the DG remain relatively resistant. These neurons have also been shown to sprout mossy fibers in both human tissue and animal models of TLE, and these newly sprouted fibers form recurrent connections with other granule cells. This sprouting is also thought to be concurrent with the latent period of epilepsy (Buckmaster, 2012). Therefore, one plausible situation is one in that granule cells, which can powerfully activate CA3, might be the neuronal population that initiates epileptiform activity early on. The activity then

spreads throughout the hippocampus, over time resulting in excitotoxicity of CA3 pyramidal neurons, which are thought to be sensitive to metabolic challenges resulting from excessive activity. Later, the subiculum might begin to initiate seizures after changes in KCC2 expression owing to deafferentation following CA1 pyramidal neuron degeneration. However, the role of mossy fiber sprouting in epilepsy is not clear, with evidence that it is pro-epileptogenic (Tauck and Nadler, 1985), anti-epileptogenic (Sloviter, 1992), and an epiphenomenon (Heng et al., 2013).

A more general change in inhibition might explain which region initiates seizures. Interneuron loss within CA3 and CA1 also occurs in the brains of patients with TLE and in animal models. Importantly, in animal models, the degeneration within these areas happens before chronic seizures begin. A general decrease in inhibition in these networks could prime the region for synchronous activity. Furthermore, the interneurons that do survive might form additional synapses in a compensatory manner and have been shown to become more synchronous prior to ictal events (Grasse et al., 2013; Toyoda et al., 2015). Sustained, synchronous interneuron firing could lead to 1) rebound excitation in pyramidal neurons following depolarization block, 2) an excessive accumulation of extracellular potassium, or 3) excitatory GABAergic currents due to the accumulation of chloride in pyramidal neurons. All of these mechanisms might result in synchronous excitatory neuron firing, which could either initiate seizure activity, or lead to other epileptogenic changes.

Ultimately, though, the subiculum does appear to inherit the role of seizure initiating region. Exactly what makes this region so resistant to neurodegeneration is not known. CA2 is also moderately unaffected by neuronal death, potentially due to increased levels of calcium binding proteins (Solviter, 1989). A similar mechanism might protect subicular pyramidal neurons. Their reliance on calcium currents to burst might also require a higher degree of calcium binding

proteins, resulting in their protection from excitotoxicity (Fujise et al., 1995). Additionally, with bursting comes increased extracellular glutamate concentrations. Expression of excitatory amino acid transporters, which work to remove glutamate from the synaptic cleft, at increased levels in the subiculum might provide a level of protection as well. A final mechanism might be expression of AMPA receptor subunits that render the channels less permeable to calcium. The projections of the subiculum are exquisitely suited, then, to allow for epileptiform activity generated in this region to spread widely throughout the brain, a requirement for generalized convulsions.

Future experiments

This thesis has shed light on the properties of excitatory connections between subicular pyramidal cells and their ability to generate synchronous activity. However, several important questions can be asked based on this data. One of the most interesting points involves the finding that our manipulations of the subicular network never generated any activity reminiscent of a seizure. A likely explanation is that the subiculum does not generate full ictal events on its own, requiring extra subicular inputs to add on to the spontaneous activity it can generate. One area that projects heavily to the subiculum is the entorhinal cortex. A mouse line that expresses cre recombinase (pOxr1-cre) specifically in medial entorhinal cortex neurons was developed by the Tonegawa lab (Suh et al., 2011), potentially allowing us to ask an important question: would activation of these inputs in conjunction with either GABA antagonists or KCC2 blockers be sufficient to exacerbate the resulting spontaneous activity? Isolating the subiculum would cut off these inputs, and by crossing the pOxr1-cre line with a floxed channelrhodopsin mouse would allow us to activate the axons that remain in the subiculum after it is isolated. I could then apply the GABA receptor antagonists or the KCC2 blocker, wait for the resulting activity, and using an event detector, trigger

optogenetic activation of the inputs during spontaneous activity to see if the activity changes in strength or duration.

Plasticity at synapses between subicular pyramidal neurons is a potentially important aspect of this network that has yet to be explored. Investigating the mechanisms of plasticity between pyramidal neurons would be vital for understanding the normal function of the subiculum and might potentially answer questions related to the mechanism of interictal activity as well. Paired recordings between connected pyramidal neurons where the pre-synaptic neuron is in current clamp and the post-synaptic neuron is in voltage clamp (at +40 mV) would allow us to determine the presence of NMDA receptors at these synapses. The emergence of interictal activity is thought to depend on synaptic plasticity, as blockade of NMDA receptors in human tissue from patients with epilepsy inhibits any sort of interictal activity and subsequent ictal-like events. It is possible that plasticity at pyramidal to pyramidal neuron synapses is necessary for interictal activity to develop. If the VU0463271 dependent activity is a model of inter-ictal events, an interesting question is whether the synchronous activity following KCC2 blockade requires potentiation of pyramidal neuron synapses to develop. If pre-treatment of subicular slices with NMDA receptor antagonists prevents the emergence of VU0463271 dependent activity, it would suggest that NMDA mediated plasticity at pyramidal-pyramidal synapses is an important step in the epileptogenic process. Determining how the AMPA/NMDA ratio changes in connected pairs in control ACSF compared to VU0463271 would indicate if these synapses are potentiated by blockade of KCC2.

Another open question that my work raises is if bursting and regular spiking pyramidal neurons contribute equally to network events that result from GABA receptor antagonism or from KCC2 blockade. Until somewhat recently, this would have been a difficult question to answer

since no specific markers of regular spiking or burst-spiking neurons had been described. However, recent work by the Schmitz lab provided evidence that VGLUT2 is a specific marker for bursting neurons in the subiculum, and they developed a VGLUT2-cre mouse that can allow for cell specific control of bursting neuron activity via channelrhodopsin or archaerhodopsin (Wozny et al., 2018). An intriguing experiment would be to stimulate or inhibit bursting neurons in an isolated subiculum in the presence of GABA antagonists or VU0463271. If activation of bursting neurons via channelrhodopsin was sufficient to trigger events that were similar to the spontaneous events, it would suggest that bursting neurons have the ability to initiate these events and perhaps the occasional firing of bursting neurons is the trigger for the events.

References

Abegg MH, Savic N, Ehrengruber MU, McKinney RA, Gähwiler BH, (2004). Epileptiform activity in rat hippocampus strengthens excitatory synapses. J Physiol 554:439-448.

Aggleton JP, Christiansen K (2015). The subiculum: the heart of the extended hippocampal system. Progress in brain research 219:65-82.

Alvarado-Rojas C, Huberfeld G, Baulac M, Clemenceau S, Charpier S, Miles R, de la Prida LM, Le Van Quyen M (2015). Different mechanisms of ripple-like oscillations in the human epileptic subiculum. Ann Neurol 77:281-290.

Amaral DG (1993). Emerging principles of intrinsic hippocampal organization. Current opinion in neurobiology 3:225-229.

Amaral DG, Dolorfo C, Alvarez-Royo P (1991). Organization of CA1 projections to the subiculum: a PHA-L analysis in the rat. Hippocampus 1:415-435.

Amaral D, Lavenex P (2007). Hippocampal neuroanatomy. In The Hippocampus Book, ed. Andersen P, Morris R, Amaral D, Bliss T, O'Keefe J, pp. 37–114. Oxford University Press, New York, NY.

Amaral DG, Scharfman HE, Lavenex P (2007). The dentate gyrus: fundamental neuroanatomical organization (dentate gyrus for dummies). Progress in brain research 163:3-22.

Amaral DG, Witter MP (1989). The three-dimensional organization of the hippocampal formation: a review of anatomical data. Neuroscience 31:571-591.

Andersen P., Bliss T. V., Skrede K. K. (1971). Lamellar organization of hippocampal pathways. Exp. Brain Res. 13, 222–238

Andersen P, Soleng AF, Raastad M. The hippocampal lamella hypothesis revisited. Brain Res. 2000 Dec 15;886(1-2):165-171

Andrioli A, Alonso-Nanclares L, Arellano JI, DeFelipe J (2007).Quantitative analysis of parvalbumin-immunoreactive cells in the human epileptic hippocampus. Neuroscience 149(1):131-43.

Aniksztejn L, Demarque M, Morozov Y, Ben-Ari Y, Represa A (2001). Recurrent CA1 collateral axons in developing rat hippocampus. Brain research 913:195-200.

Applegate CD, Tecott LH (1998). Global increases in seizure susceptibility in mice lacking 5-HT2C receptors: a behavioral analysis. Experimental neurology 154:522-530.

Avoli M, Louvel J, Pumain R, Köhling R (2005). Cellular and molecular mechanisms of epilepsy in the human brain. Progress in neurobiology 77:166-200.

Bagdy G, Kecskemeti V, Riba P, Jakus R (2007). Serotonin and epilepsy. Journal of neurochemistry 100:857-873.

Bains JS, Longacher JM, Staley KJ (1999). Reciprocal interactions between CA3 network activity and strength of recurrent collateral synapses. Nat Neurosci 2:720-726.

Barker BS, Nigam A, Ottolini M, Gaykema RP, Hargus NJ, Patel MK (2017). Pro-excitatory alterations in sodium channel activity facilitate subiculum neuron hyperexcitability in temporal lobe epilepsy. Neurobiology of disease 108:183-194.

Barnes CA, McNaughton BL, Mizumori SJ, Leonard BW, Lin LH (1990). Comparison of spatial and temporal characteristics of neuronal activity in sequential stages of hippocampal processing. Progress in brain research 83:287-300.

Bartsch JC, Behr J (2020). Noncanonical, Dopamine-Dependent Long-Term Potentiation at Hippocampal Output Synapses in a Rodent Model of First-Episode Psychosis. Frontiers in molecular neuroscience 13:55.

Behr J, Empson RM, Schmitz D, Gloveli T, Heinemann U (1996). Electrophysiological properties of rat subicular neurons in vitro. Neuroscience letters 220:41-44.

Ben-Ari Y (2002). Excitatory actions of gaba during development: the nature of the nurture. Nat Rev Neurosci 3:728-739.

Benini R, Avoli M (2005). Rat subicular networks gate hippocampal output activity in an in vitro model of limbic seizures. The Journal of physiology 566:885-900.

Biedenkapp JC, Rudy JW (2009). Hippocampal and extrahippocampal systems compete for control of contextual fear: role of ventral subiculum and amygdala. Learning and memory (Cold Spring Harbor, NY).16:38-45.

Bilkey DK, Schwartzkroin PA, (1990). Variation in electrophysiology and morphology of hippocampal CA3 pyramidal cells. 514(1):77-83.

Bliss TV, Lomo T (1973). Long-lasting potentiation of synaptic transmission in the dentate area of the anaesthetized rabbit following stimulation of the perforant path. The Journal of physiology 232:331-356.

Blumcke I, Spreafico R, Haaker G, Coras R, Kobow K, Bien CG, Pfäfflin M, Elger C, et al. (2017). Histopathological Findings in Brain Tissue Obtained during Epilepsy Surgery. The New England journal of medicine 377:1648-1656.

Blümcke I, Vinters HV, Armstrong D, Aronica E, Thom M, Spreafico R (2009). Malformations of cortical development and epilepsies: neuropathological findings with emphasis on focal cortical dysplasia. Epileptic disorders : international epilepsy journal with videotape 11:181-193.

Böhm C, Peng Y, Maier N, Winterer J, Poulet JF, Geiger JR, Schmitz D (2015). Functional Diversity of Subicular Principal Cells during Hippocampal Ripples. J Neurosci 35:13608-13618.

Bormann J, Hamill OP, Sakmann B (1987). Mechanism of anion permeation through channels gated by glycine and gamma-aminobutyric acid in mouse cultured spinal neurones. The Journal of physiology 385:243-286.

Buchanan GF, Murray NM, Hajek MA, Richerson GB (2014). Serotonin neurones have anti-convulsant effects and reduce seizure-induced mortality. The Journal of physiology 592:4395-4410.

Buchin A, Chizhov A, Huberfeld G, Miles R, Gutkin BS (2016). Reduced Efficacy of the KCC2 Cotransporter Promotes Epileptic Oscillations in a Subiculum Network Model. J Neurosci 36:11619-11633.

Buckmaster PS (2014). Does mossy fiber sprouting give rise to the epileptic state? Advances in experimental medicine and biology 813:161-168.

Buzsáki G, Moser EI (2013). Memory, navigation and theta rhythm in the hippocampal-entorhinal system. Nat Neurosci 16:130-138.

Cammarota M, Losi G, Chiavegato A, Zonta M, Carmignoto G (2013). Fast spiking interneuron control of seizure propagation in a cortical slice model of focal epilepsy. The Journal of physiology 591:807-822.

Canteras NS, Swanson LW (1992). Projections of the ventral subiculum to the amygdala, septum, and hypothalamus: a PHAL anterograde tract-tracing study in the rat. J Comp Neurol 324:180-194.

Caporale N, Dan Y (2008).Spike timing-dependent plasticity: a Hebbian learning rule. Annu Rev Neurosci 31:25-46.

Cembrowski MS, Phillips MG, DiLisio SF, Shields BC, Winnubst J, Chandrashekar J, Bas E, Spruston N (2018). Dissociable Structural and Functional Hippocampal Outputs via Distinct Subiculum Cell Classes. Cell 173:1280-1292.e1218.

Cembrowski MS, Spruston N (2019). Heterogeneity within classical cell types is the rule: lessons from hippocampal pyramidal neurons. Nat Rev Neurosci 20:193-204.

Cembrowski MS, Wang L, Lemire AL, Copeland M, DiLisio SF, Clements J, Spruston N (2018). The subiculum is a patchwork of discrete subregions. eLife 7.

Cenquizca LA, Swanson LW (2007). Spatial organization of direct hippocampal field CA1 axonal projections to the rest of the cerebral cortex. Brain research reviews 56:1-26.

Chamma I, Chevy Q, Poncer JC, Lévi S (2012). Role of the neuronal K-Cl co-transporter KCC2 in inhibitory and excitatory neurotransmission. Front Cell Neurosci 6:5.

Chen LY, Lévesque M, Avoli M, (2019). KCC2 antagonism increases neuronal network excitability but disrupts ictogenesis in vitro. J Neurophysiol. 122(3):1163-1173.

Chizhov AV, Amakhin DV, Zaitsev AV (2019). Mathematical model of Na-K-Cl homeostasis in ictal and interictal discharges. PLoS One 14:e0213904.

Chung S, Spruston N, Koh S (2015). Age-dependent changes in intrinsic neuronal excitability in subiculum after status epilepticus. PLoS One 10:e0119411.

Cobb SR, Buhl EH, Halasy K, Paulsen O, Somogyi P (1995). Synchronization of neuronal activity in hippocampus by individual GABAergic interneurons. Nature 378:75-78.

Cohen I, Navarro V, Clemenceau S, Baulac M, Miles R (2002). On the origin of interictal activity in human temporal lobe epilepsy in vitro. Science 298:1418-1421.

Cooper DC, Chung S, Spruston N (2005). Output-mode transitions are controlled by prolonged inactivation of sodium channels in pyramidal neurons of subiculum. PLoS Biol 3:e175.

Cooper DC, Moore SJ, Staff NP, Spruston N (2003). Psychostimulant-induced plasticity of intrinsic neuronal excitability in ventral subiculum. J Neurosci 23:9937-9946.

Curia G, Longo D, Biagini G, Jones RS, Avoli M (2008). The pilocarpine model of temporal lobe epilepsy. Journal of neuroscience methods 172:143-157.

D'Antuono M, Kawasaki H, Palmieri C, Curia G, Biagini G, Avoli M (2007). Antiepileptic drugs and muscarinic receptor-dependent excitation in the rat subiculum. Neuropharmacology 52(5):1291-302.

Delpire E, Baranczak A, Waterson AG, Kim K, Kett N, Morrison RD, Daniels JS, Weaver CD, et al. (2012). Further optimization of the K-Cl cotransporter KCC2 antagonist ML077: development of a highly selective and more potent in vitro probe. Bioorganic and medicinal chemistry letters 22:4532-4535.

Deshpande A, Bergami M, Ghanem A, Conzelmann KK, Lepier A, Götz M, Berninger B (2013). Retrograde monosynaptic tracing reveals the temporal evolution of inputs onto new neurons in the adult dentate gyrus and olfactory bulb. Proceedings of the National Academy of Sciences of the United States of America 110:E1152-1161.

Deuchars J, Thomson AM (1996). CA1 pyramid-pyramid connections in rat hippocampus in vitro: dual intracellular recordings with biocytin filling. Neuroscience 74:1009-1018.

Devinsky O, Vezzani A, O'Brien TJ, Jette N, Scheffer IE, de Curtis M, Perucca P (2018). Epilepsy. Nature reviews Disease primers 4:18024.

Ding SL (2013). Comparative anatomy of the prosubiculum, subiculum, presubiculum, postsubiculum, and parasubiculum in human, monkey, and rodent. J Comp Neurol 521:4145-4162.

Dinocourt C, Petanjek Z, Freund TF, Ben-Ari Y, Esclapez M (2003). Loss of interneurons innervating pyramidal cell dendrites and axon initial segments in the CA1 region of the hippocampus following pilocarpine-induced seizures. J Comp Neurol 459(4):407-25.

Dong HW, Swanson LW, Chen L, Fanselow MS, Toga AW (2009). Genomic-anatomic evidence for distinct functional domains in hippocampal field CA1. Proceedings of the National Academy of Sciences of the United States of America 106:11794-11799.

Drexel M, Preidt AP, Sperk G (2012). Sequel of spontaneous seizures after kainic acid-induced status epilepticus and associated neuropathological changes in the subiculum and entorhinal cortex. Neuropharmacology 63:806-817.

Drexel M, Romanov RA, Wood J, Weger S, Heilbronn R, Wulff P, Tasan RO, Harkany T, et al. (2017). Selective Silencing of Hippocampal Parvalbumin Interneurons Induces Development of Recurrent Spontaneous Limbic Seizures in Mice. J Neurosci 37:8166-8179.

Duvarci S, Pare D (2014). Amygdala microcircuits controlling learned fear. Neuron 82:966-980.

Elahian B, Lado NE, Mankin E, Vangala S, Misra A, Moxon K, Fried I, Sharan A, et al. (2018). Low-voltage fast seizures in humans begin with increased interneuron firing. Ann Neurol 84:588-600.

Engel J, Jr. (2001). Classification of epileptic disorders. Epilepsia 42:316.

Engel J, Jr. (2006). Report of the ILAE classification core group. Epilepsia 47:1558-1568.

Fisher RS (1989). Animal models of the epilepsies. Brain research Brain research reviews 14:245-278.

Fiske MP, Anstötz M, Welty LJ, Maccaferri G (2020). The intrinsic cell type-specific excitatory connectivity of the developing mouse subiculum is sufficient to generate synchronous epileptiform activity. The Journal of physiology 598:1965-1985.

Fricker D, Verheugen JA, Miles R (1999). Cell-attached measurements of the firing threshold of rat hippocampal neurones. The Journal of physiology 517 (Pt 3):791-804.

Fujise N, Hunziker W, Heizmann CW, Kosaka T (1995). Distribution of the calcium binding proteins, calbindin D-28K and parvalbumin, in the subicular complex of the adult mouse. Neuroscience research 22:89-107.

Fujita S, Toyoda I, Thamattoor AK, Buckmaster PS (2014). Preictal activity of subicular, CA1, and dentate gyrus principal neurons in the dorsal hippocampus before spontaneous seizures in a rat model of temporal lobe epilepsy. J Neurosci 34:16671-16687.

Gigg J (2006). Constraints on hippocampal processing imposed by the connectivity between CA1, subiculum and subicular targets. Behavioural brain research 174:265-271.

Goldberg EM, Coulter DA (2013). Mechanisms of epileptogenesis: a convergence on neural circuit dysfunction. Nat Rev Neurosci 14:337-349.

Grasse DW, Karunakaran S, Moxon KA (2013). Neuronal synchrony and the transition to spontaneous seizures. Experimental neurology 248:72-84.

Graves AR, Moore SJ, Bloss EB, Mensh BD, Kath WL, Spruston N (2012). Hippocampal pyramidal neurons comprise two distinct cell types that are countermodulated by metabotropic receptors. Neuron 76:776-789.

Greene JR, Lin H, Mason AJ, Johnson LR, Totterdell S (1997). Differential expression of NADPH-diaphorase between electrophysiologically-defined classes of pyramidal neurons in rat ventral subiculum, in vitro. Neuroscience 80:95-104.

Greene JR, Totterdell S (1997). Morphology and distribution of electrophysiologically defined classes of pyramidal and nonpyramidal neurons in rat ventral subiculum in vitro. J Comp Neurol 380:395-408.

Greenfield JG, Love S, Louis DN, Ellison D (2008). Greenfield's neuropathology. 8th ed London: Hodder Arnold;. pp. 198–9; 535–9; 1340–2.

Grillner S, Graybiel AM (2006). Microcircuits : the Interface Between Neurons and Global Brain Function. Cambridge, Mass: MIT Press in cooperation with Dahlem University Press.

Groenewegen HJ, Vermeulen-Van der Zee E, te Kortschot A, Witter MP (1987). Organization of the projections from the subiculum to the ventral striatum in the rat. A study using anterograde transport of Phaseolus vulgaris leucoagglutinin. Neuroscience 23:103-120.

Grosser S, Buck N, Braunewell KH, Gilling KE, Wozny C, Fidzinski P, Behr J (2020). Loss of Long-Term Potentiation at Hippocampal Output Synapses in Experimental Temporal Lobe Epilepsy. Frontiers in molecular neuroscience 13:143.

Grosser S, Hollnagel JO, Gilling KE, Bartsch JC, Heinemann U, Behr J (2015). Gating of hippocampal output by β-adrenergic receptor activation in the pilocarpine model of epilepsy. Neuroscience 286:325-337.

Grundy D (2015). Principles and standards for reporting animal experiments in The Journal of Physiology and Experimental Physiology. The Journal of physiology 593:2547-2549.

Guzman SJ, Schlögl A, Frotscher M, Jonas P (2016). Synaptic mechanisms of pattern completion in the hippocampal CA3 network. Science 353:1117-1123.

Hamam BN, Kennedy TE, Alonso A, Amaral DG (2000). Morphological and electrophysiological characteristics of layer V neurons of the rat medial entorhinal cortex. J Comp Neurol 418:457-472.

Hamidi S, Avoli M, (2015). KCC2 function modulates in vitro ictogenesis. Neurobiolgy of Disease 79:51-8

Harris E, Witter MP, Weinstein G, Stewart M (2001). Intrinsic connectivity of the rat subiculum: I. Dendritic morphology and patterns of axonal arborization by pyramidal neurons. J Comp Neurol 435:490-505.

Harris KD, Hirase H, Leinekugel X, Henze DA, Buzsáki G (2001). Temporal interaction between single spikes and complex spike bursts in hippocampal pyramidal cells. Neuron 32:141-149.

Hartigan JA (1975). Clustering Algorithms. John Wiley and Sons, Inc., New York, NY.

Hauser WA, Hesdorffer DC (1990). Epilepsy: Frequency, causes, and consequences. Epilepsy Foundation of America; Landover, MD:

Häusser M, Spruston N, Stuart GJ (2000). Diversity and dynamics of dendritic signaling. Science 290:739-744.

Hendricks WD, Westbrook GL, Schnell E (2019). Early detonation by sprouted mossy fibers enables aberrant dentate network activity. Proceedings of the National Academy of Sciences of the United States of America 116:10994-10999.

Heng K, Haney MM, Buckmaster PS (2013). High-dose rapamycin blocks mossy fiber sprouting but not seizures in a mouse model of temporal lobe epilepsy. Epilepsia 54:1535-1541.

Herman JP, Dolgas CM, Carlson SL (1998). Ventral subiculum regulates hypothalamo-pituitary-adrenocortical and behavioural responses to cognitive stressors. Neuroscience 86:449-459.

Herrington R, Lévesque M, Avoli M (2015). Subiculum-entorhinal cortex interactions during in vitro ictogenesis. Seizure 31:33-40.

Hille B (2001). Ion Channels of Excitable Membranes. Sinauer, Sunderland, MA.

Hillert MH, Imran I, Zimmermann M, Lau H, Weinfurter S, Klein J (2014). Dynamics of hippocampal acetylcholine release during lithium-pilocarpine-induced status epilepticus in rats. Journal of neurochemistry 131:42-52.

Hu H, Gan J, Jonas P, (2014). Interneurons. Fast-spiking, parvalbumin^{+} GABAergic interneurons: from cellular design to microcircuit function. Science. 345(6196):1255263.

Huberfeld G, Blauwblomme T, Miles R (2015). Hippocampus and epilepsy: Findings from human tissues. Revue neurologique 171:236-251.

Huberfeld G, Menendez de la Prida L, Pallud J, Cohen I, Le Van Quyen M, Adam C, Clemenceau S, Baulac M, et al. (2011). Glutamatergic pre-ictal discharges emerge at the transition to seizure in human epilepsy. Nat Neurosci 14:627-634.

Huberfeld G, Wittner L, Clemenceau S, Baulac M, Kaila K, Miles R, Rivera C (2007). Perturbed chloride homeostasis and GABAergic signaling in human temporal lobe epilepsy. J Neurosci 27:9866-9873.

Hübner CA, Holthoff K (2013). Anion transport and GABA signaling. Front Cell Neurosci 7:177.

Ishihara Y, Fukuda T (2016). Immunohistochemical investigation of the internal structure of the mouse subiculum. Neuroscience 337:242-266.

Ishizuka N, Weber J, Amaral DG (1990). Organization of intrahippocampal projections originating from CA3 pyramidal cells in the rat. J Comp Neurol 295:580-623.

Jarsky T, Mady R, Kennedy B, Spruston N (2008). Distribution of bursting neurons in the CA1 region and the subiculum of the rat hippocampus. J Comp Neurol 506:535-547.

Jensen MS, Yaari Y (1997). Role of intrinsic burst firing, potassium accumulation, and electrical coupling in the elevated potassium model of hippocampal epilepsy. J Neurophysiol 77(3):1224-33.

Jiang X, Lachance M, Rossignol E (2016). Involvement of cortical fast-spiking parvalbumin-positive basket cells in epilepsy. Prog Brain Res 226:81-126.

Joksimovic SM, Eggan P, Izumi Y, Joksimovic SL, Tesic V, Dietz RM, Orfila JE, DiGruccio MR, et al. (2017). The role of T-type calcium channels in the subiculum: to burst or not to burst? The Journal of physiology 595:6327-6348.

Joksimovic SM, Izumi Y, Joksimovic SL, Tesic V, Krishnan K, Asnake B, Jevtovic-Todorovic V, Covey DF, et al. (2019). Novel neurosteroid hypnotic blocks T-type calcium channel-dependent rebound burst firing and suppresses long-term potentiation in the rat subiculum. British journal of anaesthesia 122:643-651.

Joliffe IT (1986). Principal Component Analysis. Springer, New York, NY

Jonas P, Major G, Sakmann B (1993). Quantal components of unitary EPSCs at the mossy fibre synapse on CA3 pyramidal cells of rat hippocampus. The Journal of physiology 472:615-663.

Jope RS, Morrisett RA, Snead OC (1986). Characterization of lithium potentiation of pilocarpine-induced status epilepticus in rats. Experimental neurology 91:471-480.

Jope RS, Simonato M, Lally K (1987). Acetylcholine content in rat brain is elevated by status epilepticus induced by lithium and pilocarpine. Journal of neurochemistry 49:944-951.

Jung HY, Staff NP, Spruston N (2001). Action potential bursting in subicular pyramidal neurons is driven by a calcium tail current. J Neurosci 21:3312-3321.

Kampa BM, Stuart GJ (2006). Calcium spikes in basal dendrites of layer 5 pyramidal neurons during action potential bursts. J Neurosci 26:7424-7432.

Kandel ER, Schwartz JH, Jessel TM, Siegelbaum SA, Hudspeth AJ (2012). Principles of Neural Science, 5th edn. McGraw-Hill, New York, NY.

Karadsheh MF, Delpire E (2001). Neuronal restrictive silencing element is found in the KCC2 gene: molecular basis for KCC2-specific expression in neurons. Journal of neurophysiology 85:995-997.

Kelley MR, Deeb TZ, Brandon NJ, Dunlop J, Davies PA, Moss SJ (2016). Compromising KCC2 transporter activity enhances the development of continuous seizure activity. Neuropharmacology 108:103-110.

Kim HK, Gschwind T, Nguyen TM, Bui AD, Felong S, Ampig K, Suh D, Ciernia AV, et al. (2020). Optogenetic intervention of seizures improves spatial memory in a mouse model of chronic temporal lobe epilepsy. Epilepsia 61:561-571.

Kim SM, Ganguli S, Frank LM (2012). Spatial information outflow from the hippocampal circuit: distributed spatial coding and phase precession in the subiculum. J Neurosci 32:11539-11558.

Kim Y, Spruston N (2012). Target-specific output patterns are predicted by the distribution of regular-spiking and bursting pyramidal neurons in the subiculum. Hippocampus 22:693-706.

Klausberger T, Somogyi P (2008). Neuronal diversity and temporal dynamics: the unity of hippocampal circuit operations. Science 321:53-57.

Knopp A, Frahm C, Fidzinski P, Witte OW, Behr J (2008). Loss of GABAergic neurons in the subiculum and its functional implications in temporal lobe epilepsy. Brain : a journal of neurology 131:1516-1527.

Knopp A, Kivi A, Wozny C, Heinemann U, Behr J (2005). Cellular and network properties of the subiculum in the pilocarpine model of temporal lobe epilepsy. J Comp Neurol 483:476-488.

Kostyuk PG, Krishtal OA, Pidoplichko VI (1981). Calcium inward current and related charge movements in the membrane of snail neurones. The Journal of physiology 310:403-421.

Krieger P, de Kock CPJ, Frick A (2017). Calcium Dynamics in Basal Dendrites of Layer 5A and 5B Pyramidal Neurons Is Tuned to the Cell-Type Specific Physiological Action Potential Discharge. Front Cell Neurosci 11:194.

Krook-Magnuson E, Armstrong C, Oijala M, Soltesz I (2013). On-demand optogenetic control of spontaneous seizures in temporal lobe epilepsy. Nature communications 4:1376.

Larkum ME, Zhu JJ, Sakmann B (1999). A new cellular mechanism for coupling inputs arriving at different cortical layers. Nature 398:338-341.

Lazarova M, Bendotti C, Samanin R (1983). Studies on the role of serotonin in different regions of the rat central nervous system on pentylenetetrazol-induced seizures and the effect of di-n-propylacetate. Naunyn-Schmiedeberg's archives of pharmacology 322:147-152.

Le Duigou C, Bouilleret V, Miles R (2008). Epileptiform activities in slices of hippocampus from mice after intra-hippocampal injection of kainic acid. The Journal of physiology 586:4891-4904.

Lee S, Lee C, Woo C, Kang SJ, Shin KS (2019). Chronic social defeat stress increases burst firing of nucleus accumbens-projecting ventral subicular neurons in stress-susceptible mice. Biochemical and biophysical research communications 515:468-473.

Lévesque M, Avoli M (2013). The kainic acid model of temporal lobe epilepsy. Neuroscience and biobehavioral reviews 37:2887-2899.

Lévesque M, Avoli M, Bernard C (2016). Animal models of temporal lobe epilepsy following systemic chemoconvulsant administration. Journal of neuroscience methods 260:45-52.

Lévesque M, Avoli, M The subiculum and its role in focal epileptic disorders. Rev Neurosci, in press

Lisman JE (1997). Bursts as a unit of neural information: making unreliable synapses reliable. Trends in neurosciences 20:38-43.

Lowry CA (2002). Functional subsets of serotonergic neurones: implications for control of the hypothalamic-pituitary-adrenal axis. Journal of neuroendocrinology 14:911-923.

Magloire V, Cornford J, Lieb A, Kullmann DM, Pavlov I (2019). KCC2 overexpression prevents the paradoxical seizure-promoting action of somatic inhibition. Nat Commun 10:1225.

Maglóczky Z, Freund TF (2005). Impaired and repaired inhibitory circuits in the epileptic human hippocampus. Trends in neurosciences 28:334-340.

Martin RC, Bortz JJ, Snyder P, (2006). Epilepsy and Nonepileptic Seizure Disorders. In P. J. Snyder, P. D. Nussbaum, & D. L. Robins (Eds.). Clinical neuropsychology: A pocket handbook for assessment (p. 318–350). American Psychological Association.

Mason A (1993). Electrophysiology and burst-firing of rat subicular pyramidal neurons in vitro: a comparison with area CA1. Brain research 600:174-178.

Masukawa LM, Benardo LS, Prince DA (1982). Variations in electrophysiological properties of hippocampal neurons in different subfields. Brain research 242:341-344.

Mattia D, Hwa GG, Avoli M (1993). Membrane properties of rat subicular neurons in vitro. Journal of neurophysiology 70:1244-1248.

Mattia D, Kawasaki H, Avoli M (1997). In vitro electrophysiology of rat subicular bursting neurons. Hippocampus 7:48-57.

Maynert EW, Marczynski TJ, Browning RA (1975). The role of the neurotransmitters in the epilepsies. Advances in neurology 13:79-147.

Menendez de la Prida L (2003). Control of bursting by local inhibition in the rat subiculum in vitro. The Journal of physiology 549:219-230.

Menendez de la Prida L (2006). Functional features of the rat subicular microcircuits studied in vitro. Behavioural brain research 174:198-205.

Menendez de la Prida L, Suarez F, Pozo MA (2003). Electrophysiological and morphological diversity of neurons from the rat subicular complex in vitro. Hippocampus 13:728-744.

Metz AE, Jarsky T, Martina M, Spruston N (2005). R-type calcium channels contribute to afterdepolarization and bursting in hippocampal CA1 pyramidal neurons. J Neurosci 25:5763-5773.

Miles R, Wong RK (1983). Single neurones can initiate synchronized population discharge in the hippocampus. Nature 306:371-373.

Miles R, Wong RK (1986). Excitatory synaptic interactions between CA3 neurones in the guinea-pig hippocampus. The Journal of physiology 373:397-418.

Miles R, Tóth K, Gulyás AI, Hájos N, Freund TF (1996). Differences between somatic and dendritic inhibition in the hippocampus. Neuron 16:815-823.

Miri ML, Vinck M, Pant R, Cardin JA (2018). Altered hippocampal interneuron activity precedes ictal onset. eLife 7.

Molnár G, Oláh S, Komlósi G, Füle M, Szabadics J, Varga C, Barzó P, Tamás G (2008). Complex events initiated by individual spikes in the human cerebral cortex. PLoS Biology 6:e222

Moore SJ, Cooper DC, Spruston N (2009). Plasticity of burst firing induced by synergistic activation of metabotropic glutamate and acetylcholine receptors. Neuron 61:287-300.

Morris RG, Schenk F, Tweedie F, Jarrard LE (1990). Ibotenate Lesions of Hippocampus and/or Subiculum: Dissociating Components of Allocentric Spatial Learning. The European journal of neuroscience 2:1016-1028.

Muñoz A, Méndez P, DeFelipe J, Alvarez-Leefmans FJ (2007). Cation-chloride cotransporters and GABA-ergic innervation in the human epileptic hippocampus. Epilepsia 48:663-73.

Naber PA, Lopes da Silva FH, Witter MP (2001). Reciprocal connections between the entorhinal cortex and hippocampal fields CA1 and the subiculum are in register with the projections from CA1 to the subiculum. Hippocampus 11:99-104.

Naber PA, Witter MP (1998). Subicular efferents are organized mostly as parallel projections: a double-labeling, retrograde-tracing study in the rat. J Comp Neurol 393:284-297.

Namura S, Takada M, Kikuchi H, Mizuno N (1994). Topographical organization of subicular neurons projecting to subcortical regions. Brain research bulletin 35:221-231.

Noebels JL, Avoli M, Rogawski MA, Olsen RW, Delgado-Escueta AV, eds (2012). Jasper's basic mechanisms of the epilepsies (National Center for Biotechnology Information, Bethesda, MD). ed 4.

Oleskevich S, Descarries L (1990). Quantified distribution of the serotonin innervation in adult rat hippocampus. Neuroscience 34:19-33.

Olson JM, Tongprasearth K, Nitz DA (2017). Subiculum neurons map the current axis of travel. Nat Neurosci 20:170-172.

O'Keefe J, Nadel L. (1978). The hippocampus as a cognitive map. Oxford University Press

O'Mara SM, Commins S, Anderson M, Gigg J (2001). The subiculum: a review of form, physiology and function. Progress in neurobiology 64:129-155.

O'Mara SM, Sanchez-Vives MV, Brotons-Mas JR, O'Hare E (2009). Roles for the subiculum in spatial information processing, memory, motivation and the temporal control of behaviour. Progress in neuro-psychopharmacology and biological psychiatry 33:782-790.

Otsu Y, Donneger F, Schwartz EJ, Poncer JC (2020). Cation-chloride cotransporters and the polarity of GABA signalling in mouse hippocampal parvalbumin interneurons. J Physiol 598:1865-1880.

Palacios-Filardo J, Mellor JR, (2019). Neuromodulation of hippocampal long-term synaptic plasticity. Curr Opin Neurobiol 54:37-43.

Palma E, Amici M, Sobrero F, Spinelli G, Di Angelantonio S, Ragozzino D, Mascia A, Scoppetta C, et al. (2006). Anomalous levels of Cl- transporters in the hippocampal subiculum from temporal lobe epilepsy patients make GABA excitatory. Proceedings of the National Academy of Sciences of the United States of America 103:8465-8468.

Pandey A, Sikdar SK (2014). Depression biased non-Hebbian spike-timing-dependent synaptic plasticity in the rat subiculum. The Journal of physiology 592:3537-3557.

Panuccio G, Vicini S, Avoli M (2012). Cell type-specific properties of subicular GABAergic currents shape hippocampal output firing mode. PLoS One 7:e50241.

Payne JA, Rivera C, Voipio J, Kaila K (2003). Cation-chloride co-transporters in neuronal communication, development and trauma. Trends in neurosciences 26:199-206.

Paz JT, Huguenard JR (2015). Microcircuits and their interactions in epilepsy: is the focus out of focus? Nat Neurosci 18:351-359.

Pelkey KA, Chittajallu R, Craig MT, Tricoire L, Wester JC, McBain CJ (2017). Hippocampal GABAergic Inhibitory Interneurons. Physiological reviews 97:1619-1747.

Peng Y, Mittermaier FX, Planert H, Schneider UC, Alle H, Geiger JRP (2019). High-throughput microcircuit analysis of individual human brains through next-generation multineuron patch-clamp. Elife 8:e48178.

Petersen AV, Jensen CS, Crépel V, Falkerslev M, Perrier JF (2017). Serotonin Regulates the Firing of Principal Cells of the Subiculum by Inhibiting a T-type Ca(2+).Current. Front Cell Neurosci 11:60.

Petrucci AN, Joyal KG, Purnell BS, Buchanan GF (2020). Serotonin and sudden unexpected death in epilepsy. Experimental neurology 325:113145.

Pitkänen A, Lukasiuk K, Dudek FE, Staley KJ, (2015). Epileptogenesis. Cold Spring Harb Perspect Med 5(10):a022822.

Prendiville S, Gale K (1993). Anticonvulsant effect of fluoxetine on focally evoked limbic motor seizures in rats. Epilepsia 34:381-384.

Rall W (1977). Core conductor theory and cable properties of neurons. In Handbook of Physiology, ed. Kandel E and Geiger S, pp. 39–97. American Physiological Society, Washington, DC.

Reyes-Garcia SZ, Scorza CA, Araújo NS, Ortiz-Villatoro NN, Jardim AP, Centeno R, Yacubian EMT, Faber J, Cavalheiro EA, (2018). Different patterns of epileptiform-like activity are generated

in the sclerotic hippocampus from patients with drug-resistant temporal lobe epilepsy. Sci Rep 8:7116.

Santos VR, Melo IS, Pacheco ALD, Castro OW (2019). Life and death in the hippocampus: What's bad? Epilepsy and behavior : EB:106595.

Schenk F, Morris RG (1985). Dissociation between components of spatial memory in rats after recovery from the effects of retrohippocampal lesions. Experimental brain research 58:11-28.

Schiller J, Major G, Koester HJ, Schiller Y (2000). NMDA spikes in basal dendrites of cortical pyramidal neurons. Nature 404:285-289.

Schwartz G (1978). Estimating the dimension of a model. Ann Stat 6, 461–464.

Schwartzkroin PA, Prince DA (1978). Cellular and field potential properties of epileptogenic hippocampal slices. Brain research 147:117-130.

Seress L, Abrahám H, Lin H, Totterdell S (2002). Nitric oxide-containing pyramidal neurons of the subiculum innervate the CA1 area. Experimental brain research 147:38-44.

Seeman SC, Campagnola L, Davoudian PA, Hoggarth A, Hage TA, Bosma-Moody A, Baker CA, Lee JH, Mihalas S, Teeter C, Ko AL, Ojemann JG, Gwinn RP, Silbergeld DL, Cobbs C, Phillips

J, Lein E, Murphy G, Koch C, Zeng H, Jarsky T (2018).Sparse recurrent excitatory connectivity in the microcircuit of the adult mouse and human cortex. Elife 26;7:e37349.

Sessolo M, Marcon I, Bovetti S, Losi G, Cammarota M, Ratto GM, Fellin T, Carmignoto G (2015). Parvalbumin-Positive Inhibitory Interneurons Oppose Propagation But Favor Generation of Focal Epileptiform Activity. J Neurosci 35:9544-9557.

Sharp PE (1997). Subicular cells generate similar spatial firing patterns in two geometrically and visually distinctive environments: comparison with hippocampal place cells. Behavioural brain research 85:71-92.

Sharp PE (1999). Subicular place cells expand or contract their spatial firing pattern to fit the size of the environment in an open field but not in the presence of barriers: comparison with hippocampal place cells. Behavioral neuroscience 113:643-662.

Simonnet J, Brecht M (2019). Burst Firing and Spatial Coding in Subicular Principal Cells. J Neurosci 39:3651-3662.

Sivakumaran S, Cardarelli RA, Maguire J, Kelley MR, Silayeva L, Morrow DH, Mukherjee J, Moore YE, et al. (2015). Selective inhibition of KCC2 leads to hyperexcitability and epileptiform discharges in hippocampal slices and in vivo. J Neurosci 35:8291-8296.

Sloviter RS (1989). Calcium-binding protein (calbindin-D28k).and parvalbumin immunocytochemistry: localization in the rat hippocampus with specific reference to the selective vulnerability of hippocampal neurons to seizure activity. J Comp Neurol 280:183-196.

Sloviter RS (1992). Possible functional consequences of synaptic reorganization in the dentate gyrus of kainate-treated rats. Neuroscience letters 137:91-96.

Solari N, Hangya B (2018). Cholinergic modulation of spatial learning, memory and navigation. The European journal of neuroscience 48:2199-2230.

Somogyi P, Tamás G, Lujan R, Buhl EH (1998). Salient features of synaptic organisation in the cerebral cortex. Brain research Brain research reviews 26:113-135.

Spruston N (2008). Pyramidal neurons: dendritic structure and synaptic integration. Nat Rev Neurosci 9:206-221.

Spruston N, Jaffe DB, Johnston D (1994). Dendritic attenuation of synaptic potentials and currents: the role of passive membrane properties. Trends in neurosciences 17:161-166.

Squire LR, Stark CE, Clark RE (2004). The medial temporal lobe. Annual review of neuroscience 27:279-306.

Staff NP, Jung HY, Thiagarajan T, Yao M, Spruston N (2000). Resting and active properties of pyramidal neurons in subiculum and CA1 of rat hippocampus. Journal of neurophysiology 84:2398-2408.

Stewart M (1997). Antidromic and orthodromic responses by subicular neurons in rat brain slices. Brain research 769:71-85.

Stewart M, Wong RK (1993). Intrinsic properties and evoked responses of guinea pig subicular neurons in vitro. Journal of neurophysiology 70:232-245.

Suh J, Rivest AJ, Nakashiba T, Tominaga T, Tonegawa S (2011). Entorhinal cortex layer III input to the hippocampus is crucial for temporal association memory. Science 334:1415-1420.

Sulis Sato S, Artoni P, Landi S, Cozzolino O, Parra R, Pracucci E, Trovato F, Szczurkowska J, et al. (2017). Simultaneous two-photon imaging of intracellular chloride concentration and pH in mouse pyramidal neurons in vivo. Proceedings of the National Academy of Sciences of the United States of America 114:E8770-e8779.

Szirmai I, Buzsáki G, Kamondi A (2012). 120 years of hippocampal Schaffer collaterals. Hippocampus 22:1508-1516.

Tamamaki N, Nojyo Y (1995). Preservation of topography in the connections between the subiculum, field CA1, and the entorhinal cortex in rats. J Comp Neurol 353:379-390.

Taube JS (1993). Electrophysiological properties of neurons in the rat subiculum in vitro. Experimental brain research 96:304-318.

Tauck DL, Nadler JV (1985). Evidence of functional mossy fiber sprouting in hippocampal formation of kainic acid-treated rats. J Neurosci 5:1016-1022.

Toyoda I, Bower MR, Leyva F, Buckmaster PS (2013). Early activation of ventral hippocampus and subiculum during spontaneous seizures in a rat model of temporal lobe epilepsy. J Neurosci 33:11100-11115.

Toyoda I, Fujita S, Thamattoor AK, Buckmaster PS (2015). Unit Activity of Hippocampal Interneurons before Spontaneous Seizures in an Animal Model of Temporal Lobe Epilepsy. J Neurosci 35:6600-6618.

Traub RD, Miles R (1991). Neuronal Networks of the Hippocampus. Cambridge University Press, New York, NY.

Upton N, Stean T, Middlemiss D, Blackburn T, Kennett G (1998). Studies on the role of 5-HT2C and 5-HT2B receptors in regulating generalised seizure threshold in rodents. European journal of pharmacology 359:33-40.

Urban NN, Henze DA, Barrionuevo G (2001). Revisiting the role of the hippocampal mossy fiber synapse. Hippocampus 11:408-417.

Vreugdenhil M, Hoogland G, van Veelen CW, Wadman WJ (2004). Persistent sodium current in subicular neurons isolated from patients with temporal lobe epilepsy. The European journal of neuroscience 19:2769-2778.

Wang Y, Xu C, Xu Z, Ji C, Liang J, Wang Y, Chen B, Wu X, et al. (2017). Depolarized GABAergic Signaling in Subicular Microcircuits Mediates Generalized Seizure in Temporal Lobe Epilepsy. Neuron 95:92-105.e105.

Wellmer J, Su H, Beck H, Yaari Y (2002). Long-lasting modification of intrinsic discharge properties in subicular neurons following status epilepticus. The European journal of neuroscience 16:259-266.j

Wenger GR, Stitzel RE, Craig CR (1973). The role of biogenic amines in the reserpine-induced alteration of minimal electroshock seizure thresholds in the mouse. Neuropharmacology 12:693-703.

Wieser HG (2004). ILAE Commission Report. Mesial temporal lobe epilepsy with hippocampal sclerosis. Epilepsia 45:695-714.

Witter MP (2006). Connections of the subiculum of the rat: topography in relation to columnar and laminar organization. Behavioural brain research 174:251-264.

Witter MP, Groenewegen HJ (1990). The subiculum: cytoarchitectonically a simple structure, but hodologically complex. Progress in brain research 83:47-58.

Wójtowicz AM, Fidzinski P, Heinemann U, Behr J (2010). Beta-adrenergic receptor activation induces long-lasting potentiation in burst-spiking but not regular-spiking cells at CA1-subiculum synapses. Neuroscience 171:367-372.

Wong RK, Prince DA (1978). Participation of calcium spikes during intrinsic burst firing in hippocampal neurons. Brain research 159:385-390.

Wong RK, Traub RD (1983). Synchronized burst discharge in disinhibited hippocampal slice. I. Initiation in CA2-CA3 region. Journal of neurophysiology 49:442-458.

Wozny C, Beed P, Nitzan N, Pössnecker Y, Rost BR, Schmitz D (2018). VGLUT2 Functions as a Differential Marker for Hippocampal Output Neurons. Front Cell Neurosci 12:337.

Wozny C, Kivi A, Lehmann TN, Dehnicke C, Heinemann U, Behr J (2003). Comment on "On the origin of interictal activity in human temporal lobe epilepsy in vitro". Science 301:463; author reply 463.

Wozny C, Knopp A, Lehmann TN, Heinemann U, Behr J (2005). The subiculum: a potential site of ictogenesis in human temporal lobe epilepsy. Epilepsia 46 Suppl 5:17-21.

Wright R, Raimondo JV, Akerman CJ (2011). Spatial and temporal dynamics in the ionic driving force for GABA(A) receptors. Neural plasticity 2011:728395.

Yaari Y, Beck H (2002). "Epileptic neurons" in temporal lobe epilepsy. Brain Pathol. 12(2):234-9.

Yan QS, Jobe PC, Cheong JH, Ko KH, Dailey JW (1994). Role of serotonin in the anticonvulsant effect of fluoxetine in genetically epilepsy-prone rats. Naunyn-Schmiedeberg's archives of pharmacology 350:149-152.

Yekhlef L, Breschi GL, Lagostena L, Russo G, Taverna S (2015). Selective activation of parvalbumin- or somatostatin-expressing interneurons triggers epileptic seizurelike activity in mouse medial entorhinal cortex. Journal of neurophysiology 113:1616-1630.